

AD-779 945

ATMOSPHERIC TRANSMISSION OF 1.06
MICRON LASER RADIATION: APPLICATION
TO STANDOFF MISSILE PERFORMANCE

Charles H. Coolidge, Jr.

Air Force Institute of Technology
Wright-Patterson Air Force Base, Ohio

March 1974

DISTRIBUTED BY:

NTIS

National Technical Information Service
U. S. DEPARTMENT OF COMMERCE
5285 Port Royal Road, Springfield Va. 22151

Unclassified

SECURITY CLASSIFICATION OF THIS PAGE(When Data Entered)

Abstract (Continued)

Total attenuation is the sum of the separate attenuating mechanisms: aerosols, molecules, rain, fog, and clouds. Aerosol coefficient calculations are based on Mie Theory computations using indices of refraction and a particle size distribution typical of Central Europe. Molecular absorption calculations were made using line by line computations using molecular absorption line parameters compiled by Air Force Cambridge Research Laboratories. Rain, fog, and cloud computations assume homogeneity of these media.

All coefficients are related to atmospheric observables or mean seasonal conditions. The maximum laser lock-on range may then be determined as a function of various meteorological conditions. Tables and equations are provided for ease in use of the model.

1a

Unclassified

SECURITY CLASSIFICATION OF THIS PAGE(When Data Entered)

100-100000
100-100000
100-100000

✓ ATMOSPHERIC TRANSMISSION OF 1.06 MICRON
LASER RADIATION: APPLICATION TO
STAND-OFF MISSILE PERFORMANCE

THESIS

β

GEP/PH/74-4

CHARLES H. COOLIDGE, JR.
CAPTAIN USAF

Approved for public release; distribution unlimited

ib

ATMOSPHERIC TRANSMISSION OF
1.06 MICRON LASER RADIATION:
APPLICATION TO STAND-OFF
MISSILE PERFORMANCE

THESIS

Presented to the Faculty of the School of Engineering
of the Air Force Institute of Technology
Air University
in Partial Fulfillment of the
Requirements for the Degree of
Master of Science

by

Charles H. Coolidge, Jr., BS
Captain USAF

Graduate Engineering Physics

March 1974

Approved for public release; distribution unlimited

Preface

This topic was researched at the request of the Operations Evaluation Group, Assistant Chief of Staff, Studies and Analysis, USAF. The performance of a laser guided stand-off missile in the close-air-support mission is dependent on a complex interdependent set of factors including laser design, target characteristics, receiver design, and atmospheric conditions. Although the relationship among all these factors is developed, this work addresses in detail only the problem of atmospheric transmission in determining maximum missile lock-on range. An applied approach is taken in which factors affecting atmospheric transmission are discussed, these factors are then related to atmospheric observables, and these observables are then related to an atmospheric transmission. An attempt is made to utilize existing atmospheric models and widely accepted concepts to apply to this important operational problem. Where model theories are not supported by measurements, sensitivity analyses are undertaken. It has become obvious to the author in the course of this investigation that the model predictions when compared to actual measurements are still inexact due to the inaccuracies in the measurement and reporting of meteorological conditions, the difficulty of measuring aerosol composition, size, and distribution, and the many approximations which must be made to reasonably calculate the atmospheric transmission.

I would like to express my sincere appreciation to the many people without whose assistance such an indepth investigation could never have been accomplished in the allotted time period. In particular,

I would like to thank Colonel Ed Battle who sponsored this work and who provided continued support throughout the entire effort. A special debt of gratitude is owed to Major Paul Try of Headquarters, Air Weather Service, for his hours of assistance and consultation throughout this project and in particular for his providing the initial Mie Theory computer program and expert advice as to changes that could be made in the program. Many interesting discussions on various approaches to the problem were held with Captain Neil McQuage, Staff Meteorologist, Air Force Avionics Laboratory. Mr. Paul Markley and Mr. Phil Miller of Aeronautical Systems Division and Mr. Frank McCann of the Avionics Laboratory provided valuable literature sources.

I also thank Doctors Louis Elterman, Robert Fenn, Robert McClatchey, Erik Shettle, and Frederic Volz of Air Force Cambridge Research Laboratory for their expert guidance and the valuable information they provided. Without their detailed and candid advice about shortcomings of present models and without results of the most recent of their investigations (some of it unpublished), this work would have been considerably limited. In addition, appreciation goes to the following at Air Force Environmental Technical Applications Center who provided climatological data and advice for this project: Majors Tom Stanton and David Lydon, Captain Ken Nozaki, and Lt Gerald Riley. Major Carl Case, my thesis advisor at Air Force Institute of Technology, provided valuable insight and direction that enabled me to clarify the problem. My wife, Bonnie, and son, Charles, have given their unselfish support and understanding throughout the days necessary to complete this work.

Charles H. Coolidge, Jr.
Captain, USAF

Contents

	<u>Page</u>
Preface	ii
List of Figures	vi
List of Tables	viii
Abstract	x
I. Introduction	1
Background	1
Purpose of the Report	3
Scope of Report	4
Assumptions	5
Development of the Report	5
II. Development of the Atmosphere-Free Laser Lock-on Range Equation	7
Energy from Laser	7
Energy Loss at Target	8
III. Atmospheric Attenuation of Laser Radiation	23
Atmospheric Effects on Laser Radiation	24
Atmospheric Effects on Reflected Laser Radiation	25
Atmospheric Extinction Coefficient	27
IV. Molecular Absorption and Scattering	30
Molecular (Rayleigh) Scattering	30
Molecular Absorption	32
Distribution of Molecular Absorbers	36
Distribution Data	42
Comparison of Distributions	44
Wavelength Dependence of Absorption	47
Absorption at 1.063μ	49
Calculation of the Absorption Coefficient	49
V. Atmospheric Aerosol	51
Aerosol Attenuation	51
Formation and Removal of Particles in the Atmosphere	54
Particle Size and Size Distribution (General)	55
Particle Size and Size Distribution (Specific)	58
Particle Composition	60

	<u>Page</u>
Complex Index of Refraction	65
Particle Growth	65
Vertical Distribution	71
 VI. Aerosol Attenuation for Horizontal Path at Ground Level	 73
Particle Size Distribution	73
Analysis of Size Distributions	76
Analysis of Refractive Index	84
Aerosol Model	87
Effect of Relative Humidity on Model Attenuation from Meteorological Observables	 91
Use of the Model	95
Other Models	96
Model Limitations/Assumptions	99
 VII. Aerosol Attenuation for a Slant Path	 101
Particle Size Distribution (Function of Altitude) .101	
Total Particle Concentration (Function of Altitude)	 102
Mixing Depth Concept	104
AFCRL Vertical Aerosol Model	106
Latest Attenuation Measurements	107
Average Aerosol Profiles	110
Vertical Aerosol Model	111
Boundary (Mixing) Layer Depth	114
Aerosol Model and Use	117
 VIII. Other Atmospheric Attenuating Mechanisms: Clouds, Fog and Precipitation	 120
Attenuation by Rain	120
Meteorological Parameters for Rain Attenuation. . .124	
Attenuation by Fog	126
Attenuation by Clouds	128
Other Attenuating Mechanisms	130
Backscatter	130
Use of Attenuation Coefficients in Model	131
 IX. Conclusions and Recommendations	 134
 Bibliography	 141
 Appendix A: Molecular Absorption Calculations and Tables . . .147	
Appendix B: Summary of Mie Theory and Calculations155	
Appendix C: Use of the Model	162
 Vita	 167

List of Figures

<u>Figure</u>		<u>Page</u>
1	Receiver Oriented at More than 90° from Perpendicular to Target	9
2	Receiver Located Along Normal to Reflecting Surface .	10
3	Target-Receiver Geometry	13
4	Sun-Target-Receiver Geometry	17
5	Water Vapor Concentration as a Function of Temperature and Relative Humidity	43
6	Size Ranges of Aerosols	52
7	Particle Size Distribution Shift due to Coagulation .	70
8	Typical Experimental Scattering Coefficient Curves .	74
9	Attenuation Coefficient Curves of Aerosol Size Distributions	80
10	Effect of Changing Power Law on Slopes of Attenuation Curves	82
11	Particle Growth with Change in Relative Humidity and Wavelength Dependence of Growth	90
12	Graphical Solution to Allard's Law	94
13	<u>Electro-Optical Handbook</u> Attenuation Coefficient Curves for Various Meteorological Ranges	98
14	Experimental Curves of Attenuation Coefficient for Various Meteorological Ranges	98
15	Average Vertical Aerosol Concentrations with Altitude	103
16	Comparison of Vertical Aerosol Distribution Models. .	105
17	Family of Exponential Scaling Factors Used by Elterman	107
18	Measured Vertical Profiles over Germany	109
19	Mean Theoretical Mixing Heights for Stuttgart, Germany	113

<u>Figure</u>		<u>Page</u>
20	Pasquill Stability Categories	115
21	Rain Attenuation Curves	123
22	Deirmendjian Cl Cloud Distribution	123
23	Absorption Line Intensities 9385 cm^{-1} to 9415 cm^{-1} . .	149
24	Attenuation Efficiency Factor as a Function of Size Parameter	160

List of Tables

<u>Table</u>	<u>Page</u>
I. Concentrations of Uniformly Mixed Gases	39
II. Vertical Profiles of Midlatitude Summer, Midlatitude Winter, and 1962 U.S. Standard Atmospheres: Surface to 500 mb	45
III. Average Monthly/Seasonal Profiles of Relative Humidity and Temperature for Germany: Surface to 500 mb	46
IV. Estimates of Particle Formation	62
V. Possible Atmospheric Gases from which Particles May be Formed	64
VI. Table of Refractive Indices	66
VII. Particle Growth with Relative Humidity as a Function of Size	69
VIII. Indices of Refraction Assumed for Calculations	77
IX. Aerosol Size Distributions	78
X. Sensitivity Analyses on Effect of Changing Limits of Integration	83
XI. Effect of Changing Imaginary Part of Refractive Index	84
XII. Per-Particle Aerosol Attenuation Coefficients	86
XIII. Ratios of 1.0636 μ Attenuation Coefficient to .55 μ Attenuation Coefficient for Several Aerosol Distributions	88
XIV. Typical Median Rain Droplet Sizes as a Function of Source Mechanism	124
XV. Meteorological Rainfall Categories	126
XVI. Attenuation Coefficients for Rain	126
XVII. Cloud and Fog Attenuation Coefficients	129
XVIII. Representative Values for Backscatter Coefficient	132
IXX. Vibration Partition Functions	148

<u>Table</u>	<u>Page</u>
XX. Absorption Line Parameters	148
XXI. Molecular Absorption Coefficients for 9389.6714 cm^{-1} .	151
XXII. Molecular Absorption Coefficients for 9398.220 cm^{-1} .	151
XXIII. Molecular Absorption Coefficients for 9398.4962 cm^{-1} .	152
XXIV. Molecular Absorption Coefficients for 9401.760 cm^{-1} .	152
XXV. Molecular Absorption Coefficients for 9403.857 cm^{-1} .	153
XXVI. Molecular Absorption Coefficients for 9388.98 cm^{-1} . .	153
XXVII. Molecular Absorption Coefficients for 9407.07 cm^{-1} . .	154
XXVIII. Aerosol Attenuation Coefficients for Vertical Clear Air Background	164

Abstract

Laser designator characteristics, target composition and size, laser designator-target-receiver geometry, receiver characteristics, and atmospheric conditions limit the maximum range at which a laser target designator system may lock-on and track a target. This report shows the relationship of these factors and develops a model for the prediction of maximum lock-on range for a 1.06μ laser target designator system where atmospheric attenuation is the limiting system factor.

A transcendental lock-on range equation is developed which is a function only of atmospheric conditions and the designator-target-receiver geometry. Several qualifying assumptions are made in the derivation of this equation: (1) the typical military target is a diffuse Lambertian surface with ten percent reflectivity; (2) the laser energy is reflected only from the target surface; and (3) the reflected radiation is entirely within the field of view of the receiver.

This report assumes the validity of the Beer-Lambert Law for describing atmospheric transmission of laser radiation. The determination of atmospheric attenuation is reduced to a calculation of the attenuation due to aerosol scattering and absorption, molecular scattering, molecular absorption, and scattering by fogs, clouds, and rain. Theoretical calculations of the attenuation coefficients demonstrate that fogs, clouds, and rain are the largest atmospheric attenuators. For dry atmospheric conditions, the chief attenuating mechanism of 1.06μ laser radiation is the aerosol. Molecular absorption proves to be of lesser importance while molecular (Rayleigh)

scattering is negligible.

Theoretical calculations of molecular absorption coefficients are made using atmospheric absorption line intensities compiled by Air Force Cambridge Research Laboratories. Molecular absorption coefficients, which are a function of temperature, pressure and relative humidity, are related to mean seasonal atmospheric profiles. Calculations of the aerosol attenuation coefficient are made using Mie Theory; these calculations are limited to single scattering theory. The calculations are based on a continental aerosol model using refractive indices typical of those reported for Central Europe, although sensitivity analyses are conducted using other models. Aerosol attenuation is related to ground level horizontal visibility. A boundary (mixed) layer concept is used to describe the vertical distribution of aerosols.

Mie Theory calculations are also made to determine the attenuation coefficient for clouds where clouds are assumed to be homogeneous. Attenuation coefficients for rain are calculated using the geometrical approximation for Mie Theory where rain showers are assumed to be homogeneous and monodisperse. Rain attenuation coefficients are related to rain rates reported by the meteorologist. Attenuation coefficients for fog are related to visibility and are those used in a previous Monte Carlo study.

Equations and Tables are provided for ease in determining attenuation coefficients as a function of meteorological observables. These coefficients may then be used to solve the maximum lock-on range equation for various tactical scenarios. The model is specifically

designed for use in variable laser-target-receiver geometry and slant path calculations.

ATMOSPHERIC TRANSMISSION OF 1.06 MICRON LASER RADIATION:
APPLICATION TO STAND-OFF MISSILE PERFORMANCE

1. Introduction

Background

Laser target designator systems locate targets using the same basic principles used by conventional radar; that is, the system detects radiation reflected from an object (target). The purpose of the laser target designator system, however, is to designate where the target is located relative to the receiver rather than to measure the range. The laser transmitter, also called designator or illuminator, illuminates the target with pulses of radiant energy in a narrow beam and the receiver detector discerns (in its relatively wide field of view) where the laser energy is being reflected, thereby locating the target (Ref 24:13-6).

The receiver detector for the laser target designator system detects the narrow-band reflected laser radiation. Once the radiation is detected by the receiver sensor, then tracking is accomplished by one of two methods. The receiver may track the "one brightest spot in the field of view" or may track the "centroid of entire illumination in the field of view" (Ref 52:23). This detection and tracking scheme of the laser designator receiver system is then unlike the broad-band detection systems which detect target-background contrast. These broad-band detection systems generally use a high-resolution TV imaging system which provides a target image on the TV screen. The system operator then must place a tracking gate over the display to begin

receiver tracking.

The laser target designator system, on the other hand, requires that the target be initially acquired by some other means. This implies that the target must have been recognized by the system operator using some means (usually visual) other than the designator system. The laser designator may then be directed at the target (object). Once the laser is illuminating the target, then receiver lock-on and tracking is possible.

Several factors determine the maximum range at which the receiver may acquire and track a target once the target has been illuminated. These factors include: detector sensitivity and design, target geometry and size, laser transmitter (illuminator) power and beam geometry and positions of the receiver and illuminator relative to the target. The last factor is complicated by the fact that the target must be initially acquired by means other than the designator system. Because the laser target designator requires acquisition of the target by other means, many tactical system uses have evolved. Possible uses include: (1) the receiver and transmitter are co-located on the same aircraft; (2) the receiver and transmitter are located on separate aircraft; and (3) the transmitter is ground-based, but the receiver is an aircraft. Thus, the laser radiation may traverse two completely different paths. This report addresses this general two path problem. The co-location of source and receiver then is a simplification of this more general case.

An additional complicating factor is atmospheric attenuation of the laser radiation. The laser radiation is scattered and absorbed

by atmospheric aerosols and molecules. Other atmospheric phenomena such as clouds, fog, and precipitation also scatter and absorb laser radiation. In fact, this atmospheric attenuation is a serious system limiting factor in the effective operational use of a laser target designator system.

The determination of atmospheric effects on the laser radiation may be reduced to a determination of the effects of the separate attenuating mechanisms. These mechanisms--molecular scattering, molecular absorption and aerosol scattering and absorption--are then related to meteorological observables. Using these relationships, one can determine the total atmospheric attenuation of radiation as a function of radiation path and the meteorological observables. Similar relationships may be used to determine the attenuation of laser radiation due to the other attenuating mechanisms: clouds, fog, and precipitation.

Purpose of the Report

The purpose of this report is to investigate the atmospheric attenuation of laser radiation and to determine methods for prediction of laser target designator system lock-on ranges. This involves investigating the various attenuation factors and then associating these factors with measurable atmospheric quantities. This report includes the investigation of several different atmospheric attenuation models to determine the assumptions of each. The models also are compared with each other and with results of flight test data.

Scope of Report

Since atmospheric attenuation of radiation is sensitive to the wavelength of the laser radiation, then it is necessary to limit the frequencies for which the atmospheric attenuation is determined. This report, therefore, investigates the attenuation of laser radiation for one wavelength, 1.06μ . In addition, this investigation is limited to atmospheric attenuation models which predict laser target designator system performance in a continental geographical area such as Germany. It is also limited to vertical models of the lowest 20,000 feet of the troposphere.

The report compares various models for the prediction of atmospheric attenuation. An attempt is made to utilize existing models whenever possible. Where existing models are unsatisfactory for this particular tactical application, then they are modified to conform with recent measurements. The report discusses in detail the attenuating mechanisms and the relationship of these mechanisms to the attenuation models.

It does not, however, examine the details of the various sensor systems. For an assumed sensor design, this report determines the maximum system lock-on range where atmospheric attenuation is the limiting system factor. In addition, two atmospheric related factors not included in this investigation are: (1) beamspreading due to turbulence; and (2) change in the refractive index of air with change in altitude.

The first of the two factors is not investigated because several references indicated that small pockets of air rising and falling in

the path of the beam would cause local defocusing of the beam but that the energy reflected by the target will not fluctuate significantly (Ref 6 and Ref 52). For the tactical problem being considered, then, turbulence is a negligible factor; for other systems, especially communication systems, turbulence is not necessarily negligible (Ref 56:B-9).

The change in the refractive index of air with altitude is not discussed due to the negligible effect that this refraction has on laser radiation at these altitudes. This factor only becomes significant for long slant paths when the angle between the receiver and the vertical is larger than 80° (Ref 14:42).

Assumptions

When modeling something as complex as the atmosphere, certain assumptions must be made. These assumptions are too numerous and too lengthy to enumerate at this point. The assumptions will be pointed out in the discussion of each of the separate models. Two important assumptions, however, are worth mention. One is that the laser radiation is assumed to be monochromatic. The other is that the beam geometry is neglected and the attenuation of radiation in the atmosphere is then a function only of the attenuating mechanisms.

Development of the Report

In Chapter II, the variables that determine maximum lock-on range in an atmosphere-free environment are discussed. An atmosphere-free laser lock-on range equation is developed. Chapter III discusses atmospheric effects on laser radiation and modifies the laser lock-on

range equation to include atmospheric effects. In Chapter IV, the atmospheric attenuation of laser radiation due to molecular scattering and absorption is discussed in detail. Chapter V describes atmospheric aerosol in general. This general knowledge is then applied in Chapters VI and VII in the development of the model for prediction of scattering and absorption due to atmospheric aerosol. Chapter VI discusses the ground level aerosol attenuation while Chapter VII investigates the vertical aerosol distribution.

Chapter VIII presents methods for predicting attenuation in clouds, rain, and fog. The use of the model is described in Appendix C. The conclusions and recommendations are presented in Chapter IX.

II. Development of the Atmosphere-Free Laser

Lock-on Range Equation

An understanding of the many variables that determine the maximum range at which a laser guided receiver can acquire and track the target (lock-on range) is essential prior to an investigation of atmospheric attenuation. Excluding the atmosphere, factors which affect the maximum lock-on range and which must be discussed are: (1) laser designator characteristics, (2) target size and composition, and (3) receiver characteristics. In tracing the path of laser energy from the laser to receiver, one must successively investigate the laser, the target, and receiver--all of which may limit detection range.

Energy From Laser. First, one must know peak laser power, pulse duration, transmitter optics, beam profile and beam width in order to determine the power density within the beam. If there is no intervening medium, then the radiant power or radiant flux of the beam is conserved. The radiant intensity, the power per unit solid angle, will change due to the change in beam geometry, and it may not be equal across the beam to begin with depending on whether beam profile is gaussian or constant average distribution. Nevertheless, total power is conserved. The radiant power arriving at the target then is the peak laser power transmitted through the designator optics system

$$P_t = P_p T_d \quad (1)$$

where P_t is the peak power transmitted,

P_p is the peak power of the laser,

and T_d is the transmittance of the designator optics.

Actually, the beam loses some of its energy due to scattering and absorption by the atmosphere. For purposes of our present discussion, however, all of the power arrives at the target area.

Energy Loss at Target. In this simplification, the target becomes the first loss of energy. Target size, geometry, orientation, and reflective characteristics determine the total radiant power reflected into the direction of the receiver. If the beam size at the target site is larger than the target, then the problem becomes more complicated. In this event, the beam will intersect the background and reflect from these surfaces as well as from the target. This is a serious laser designator problem for now the receiver may lock-on the background in lieu of the target depending on the various compositions of the target and background. This problem is most clearly illustrated with the following example. Suppose that the target were a long narrow boat on the open water. The boat might be narrower than the beam, and therefore part of the beam might "spillover" into the background which in this case is water. The water being highly reflective or at least more reflective than the vessel might cause the receiver to be guided to the background, thereby missing the target. Although this problem of beam geometry versus target size is a serious system limitation, it will be assumed for the purpose of this work that the target is larger than the laser beam intersecting it. The beam, then, is reflected only from the target.

The direction and amount of this reflected radiation is extremely important if the detector is to receive as much of it as possible. Most military targets do not have highly reflective surfaces

but absorb and diffuse the radiant laser energy. Moreover, their surfaces are usually highly irregular, often with edges and often at many different angles to the incoming laser beam. Thus, in the operational use, the amount and direction of reflected radiation will vary widely depending on the illuminated target surfaces, edges, and composition and the relative positions of the designator and receiver. The following illustrations may place this difficult problem in better perspective. Consider the relative positions of the designator and receiver with respect to the thatched target as shown in Figure 1.

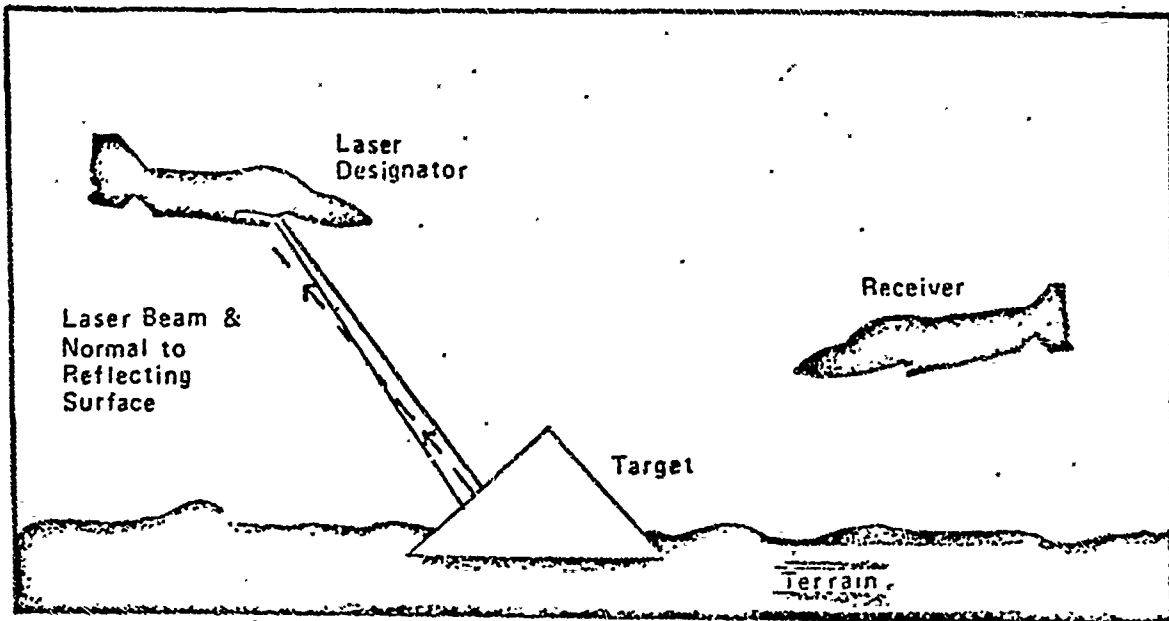


Fig. 1. Receiver Oriented at more than 90° from Perpendicular to Target Reflecting Surface

The receiver detects no laser radiation because the detector is oriented at more than 90 degrees from the perpendicular to the surface. If this same target were oriented as in Figure 2, then the receiver might see more of the projected spot size than the illuminator.

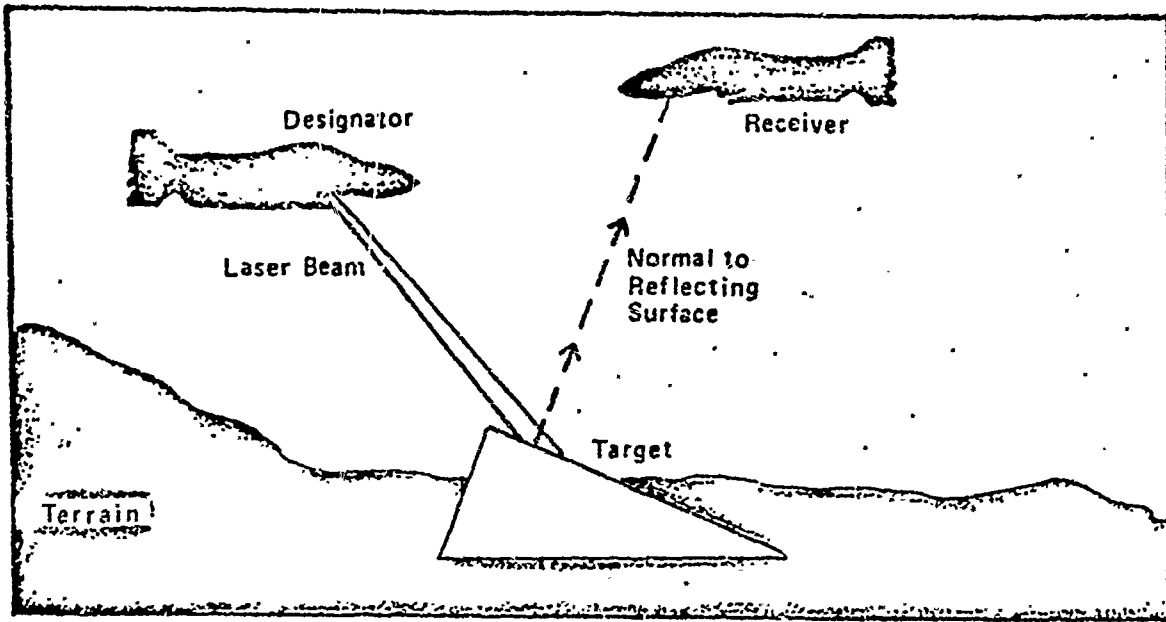


Fig. 2. Receiver Located Along Normal to Reflecting Surface.

If the targets were not the flat surfaces as shown in Figures 1 and 2, but were highly irregular surfaces, then only a small amount of the laser radiation might be reflected into the viewing angle of the receiver. The problem is further complicated by relative positions of the designator and receiver or by their co-location.

The evaluation of the bi-directional reflectance, the ratio of radiant power (or radiant flux as it is often called) reflected into a particular solid angle to the radiant power incident from a specific solid angle, is extremely complex. This reflection is often a specular reflection from a hard surface and the reflected radiation is usually orders of magnitude less in all other directions (Ref 5). The Target Signature Analysis Center (TSAC), University of Michigan, has investigated the bi-directional reflectance of many materials of tactical interest. TSAC's mathematical model for bi-directional

reflectances consists of weighted sums of diffuse reflection from a hard surface, specular reflection from a hard surface and multiple diffuse volume reflection from a thin volume of scattering dielectrics on the surface (Ref 52:15). The three parts of the model are weighted according to experimental results. In order to address the reflectance problem at length, then a maximum lock-on range would have to be calculated for each target of tactical importance.

Although the bi-directional reflectance problem is extremely complicated, certain assumptions may be made. TSAC has published the 1.06 micron laser reflective characteristics of targets of military significance. Variations in reflective properties were found for new and old olive drab paints, surface conditions (wet, dry or dusty), and target composition. Reflectances of 2.9% to 12.1% from clean surfaces of a military jeep were reported by Mardis (Ref 52:19). Dusty surfaces had reflectances as high as 60%. These targets, in addition, exhibited less specular reflectance than many other non-military targets and background materials. For the purpose of this report, a reasonable assumption for the target reflective characteristics is that the target is a perfectly diffusing reflector of incident energy, a Lambertian emitter or reflector, with a reflectance of 10%. This assumption compares favorably with those made by others (Ref 24:13-8).

Briefly, a Lambert source emits radiation completely randomly and this radiation propagates in all directions, from the source with equal radiance, N . Then for the Lambert surface, the bi-directional reflectance, ρ_b , summed over all solid angles yields the total reflectance, ρ_t , given by

$$\rho_t = \int \rho_b d\Omega = \rho_b \int d\Omega \quad (2)$$

where $d\Omega$ is a differential solid angle. The reflectance into the solid angle subtended by the receiver then is

$$\rho_b = \frac{\rho_t}{\pi} \cos \theta_t \Omega \quad (3)$$

where Ω is the receiver solid angle and θ_t is the angle between a normal to the reflecting surface and a line connecting the surface to the receiver as shown in Figure 3. The solid angle subtended by the receiver at a distance R_r is

$$\Omega = \frac{A_r \cos \phi_r}{R_r^2} \quad (4)$$

where A_r is the area of the receiver optics. The area of the receiver optics, $A_r = \frac{\pi d_r^2}{4}$, where d_r is the diameter of the receiver, is multiplied by $\cos \phi_r$. The angle ϕ_r is the angle between the line connecting the receiver and reflecting target surface and the normal to the receiver surface as shown in Figure 3. The factor, $\cos \phi_r$, then is included for those occasions when the receiver is not looking directly at the target surface.

For the tactical application considered in this report, the receiver, in general, views the Lambert reflective surface (target) as a point source (Ref 42). The receiver, then being a long distance from the target, effectively sees the entire surface and this surface subtends a very small angle in the receiver's relatively wide field of view.

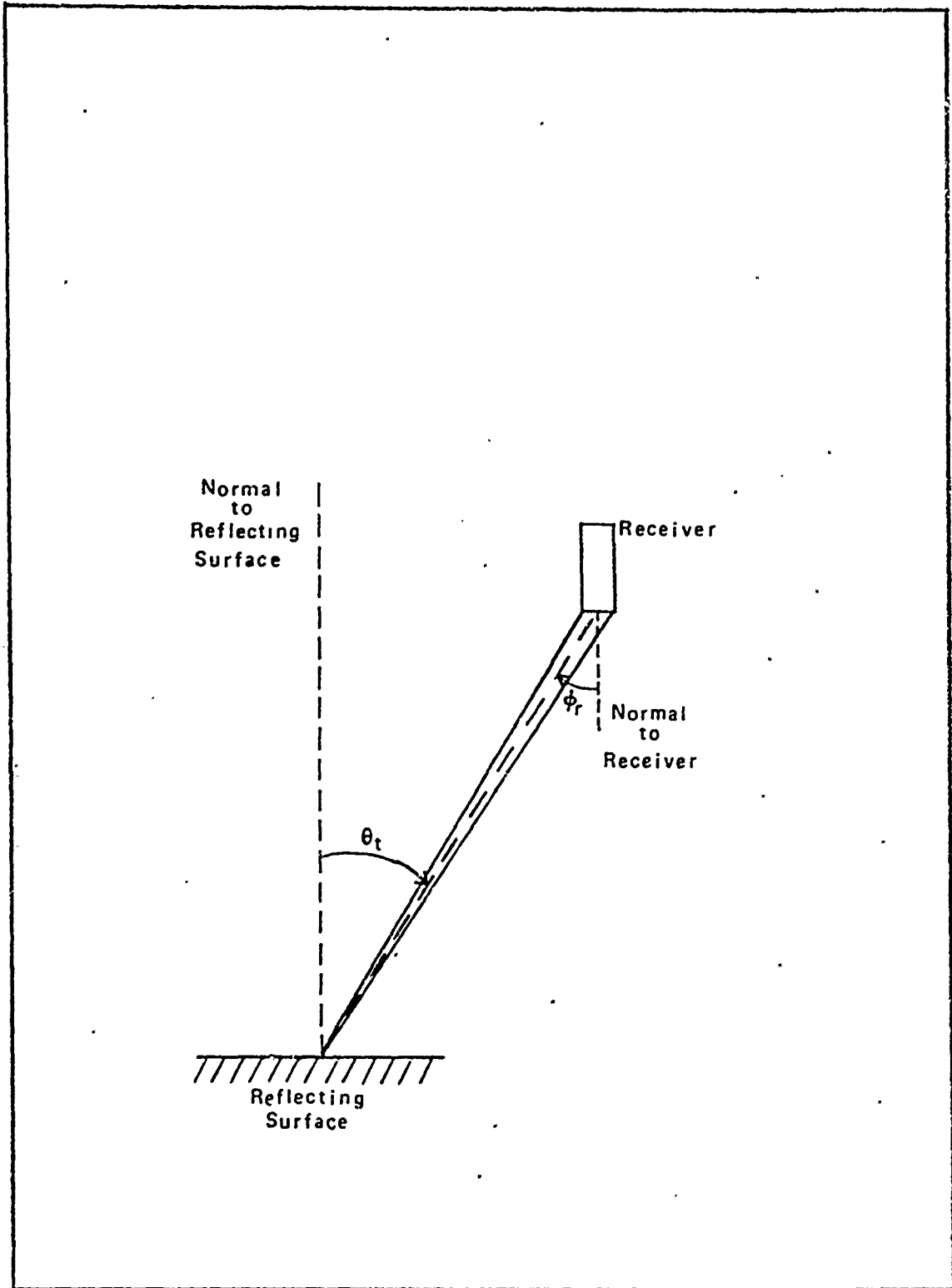


Fig. 3. Target-Receiver Geometry

Combining Eqs (1), (3) and (4), then the power or radiant flux incident on the receiver optics, P'_r , is

$$P'_r = \frac{P_p T_d \rho_t \cos \theta_t A_r \cos \phi_r}{\pi R_r^2} \quad (5)$$

This radiant flux is further reduced by the receiver optics. Hence, the radiant flux received by the sensor, P_r , is given by

$$P_r = \frac{P_p T_d \rho_t \cos \theta_t A_r \cos \phi_r T_r}{\pi R_r^2} \quad (6)$$

where T_r is the transmission of the receiver optics. This expression gives the power detected by the receiver in an atmosphere-free environment from a laser of peak power P_p reflected from a Lambertian surface of reflectivity ρ_t . As it has been developed, this expression is valid for the condition that the laser is the sole emitter of this radiation in the viewing angle of the receiver.

Unfortunately, there are other sources of 1.06μ radiation within the receiver's field of view. This causes the receiver to detect a background signal of 1.06μ radiation. The strength of this background signal and the design characteristics of the receiver detector determine the minimum detectable power at the receiver. This is usually described by a signal-to-noise ratio (Ref 24:13-9) given by

$$\frac{S}{N} = \frac{\beta^2 P_r^2 R_x^2 G^2}{2eB(\beta P_b + I_d) R_x^2 G^2 + 2FKTB} \quad (7)$$

where S/N is the peak signal-to-root-mean-square noise ratio of the receiver detector for one pulse,

B is the bandwidth of the receiver (Hz),

β is the responsivity of the photodetector (amp/watt),

e is the charge on an electron (1.6×10^{-19} coul),

F is the noise factor of the receiver,

G is the internal gain of the photodetector,

I_d is the detector dark current (amp),

K is Boltzmann's constant (1.38×10^{-23} J/°K),

P_r is the peak power received,

P_b is the power received from background radiation (watt),

R_L is the detector load resistance,

and T is the Absolute Temperature of the detector (°K).

The radiant flux from the background radiation, P_b , is found to vary depending on the viewing angle of the detector. The reflected laser power received is essentially monochromatic, but the background power received is much broader spectrally, on the order of 100 to 200 Angstroms with current detector filters in use. Thus, we must investigate the power of background sources over the broader spectral region. We shall discuss the broader range using 100 Angstroms (Å) as an example.

One background source of 1.059 μ to 1.069 μ radiation is the sun. The sun is obviously a background source problem only during daylight hours, but the problem is worthy of discussion. Radiation from the sun incident on the earth's atmosphere is scattered and absorbed by the atmospheric aerosols and molecules. The solar irradiance at the mean

earth-sun distance incident on the earth's atmospheric layer is approximately 6.44 watts/m^2 in the spectral region 1.059μ to 1.069μ (Ref 51:16-6, 16-8) (Ref 58:7). The flux density of the solar radiation at any point in the atmosphere is a complicated function of the path traveled by that radiation. That is, the atmosphere's radiance at the point of observation (detection) is a function of the sun's zenith angle and the receiver's altitude and azimuthal and zenith angles (which together determine the length of the radiance path), the number and kinds of scatterers in the path, and the number and kinds of absorbers in the path. The geometry of this problem is given in Figure 4.

There is no significant atmospheric absorption of the sun's broadband (1.059μ to 1.069μ) radiation (Ref:48). In addition, the emission of radiation by the atmosphere, and in particular by clouds, is an important factor only for detectors that utilize the electromagnetic spectrum beyond approximately 4 microns (Ref 3:1314). Thus, the problem is reduced to determining how much of the sun's radiation is incident on the detector or is scattered into the receiver's field of view.

There are three sources of background solar radiation that may be detected: (1) strongly forward scattered solar radiation when the sun is within the viewing angle of the detector, (2) solar radiation multiply scattered into the receiver's viewing (look) angle, and (3) reflected radiation from the target or target background within the receiver field of view. The first of the three methods is the largest background radiation source and a most important laser receiver problem.

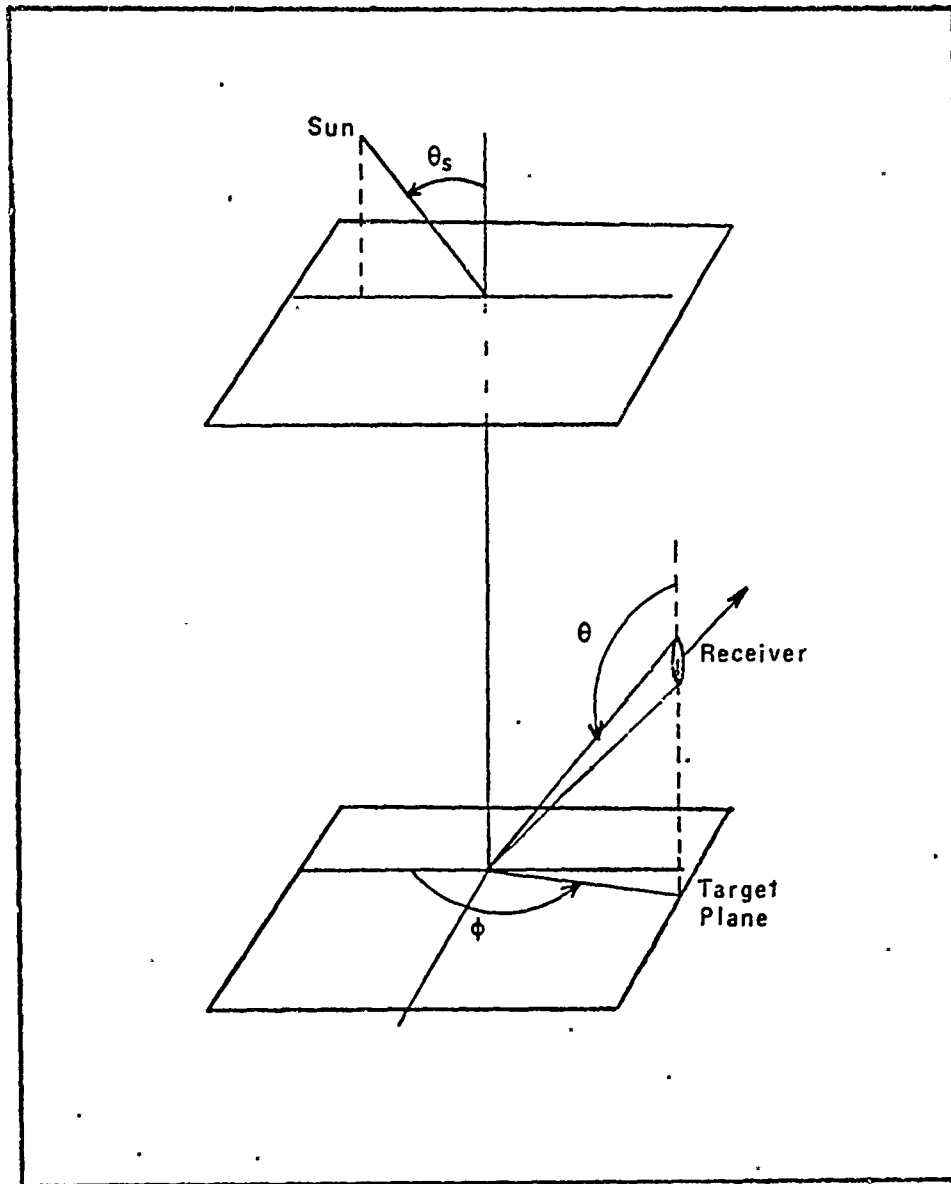


Fig. 4. Sun-Target-Receiver Geometry where θ_s is Sun's Zenith Angle, θ is Receiver's Zenith Angle, ϕ is Receiver's Azimuthal Angle

In general, our system receiver will be viewing a target located on the ground. If the receiver is at a high zenith angle and the sun is likewise at a high zenith angle, then the receiver views only solar radiation that has been scattered into its field of view or reflected from the target area. Although the radiation from the sun is most intense when the sun is near zenith due to the shorter path through the atmosphere, the amount received is greatly reduced by the receiver's viewing angle and direction of viewing. A significant problem exists, however, in the event that the sun and receiver zenith angles approach a maximum and the azimuthal angle of the receiver is such that the receiver opposes (faces) the sun. Even though the amount of solar radiation is a minimum due to its longer path through the atmosphere, this solar radiance with a strong forward scatter component is incident approximately normally on the detector surface.

According to Reference 61, the irradiance of the sun at a zenith angle of 78.5° is 4 watts/m^2 at sea level. Many factors affect the magnitude of this irradiance such as cloud cover, temperature, precipitable water vapor in the air, pressure, number of particles in the air, but this reported value is representative. Such irradiance, which is nearly normally incident on the receiver, results in a serious system limitation especially if the receiver detector is otherwise capable of detecting on the order of 10^{-6} to $10^{-9} \text{ watts/m}^2$. This problem is complicated by the fact that receivers have a wide field of view and therefore subtend a significant portion of this radiation (current detectors' field of view is on the order of 4° to 5°). Reduction of the field of view is a method of alleviating this problem,

but this method exacts a large cost in target acquisition probability.

Elimination of this system deficiency may be accomplished by restricting the tactical use of the weapon system such that during periods of low sun angles the receiver approaches the target in such a manner as to subtend the smallest receiver view angle intersection with the forward scatter component of the solar irradiance. This method means the receiver would be restricted to use only in the quadrants nearest the sun (receiver's back to the sun) and to high angle deliveries--a condition unacceptable in a hostile tactical environment. Another method of eliminating the solar background radiance is designing the receiver logic such that it discriminates against continuous returns as opposed to pulsed receptions. The design of system logic to eliminate sensitivity to extended returns would also eliminate the problem of detection of solar reflected radiation from the target and target background since this radiation is detected as a steady state background component.

Other possible sources of 1.059μ to 1.069μ radiation are the moon, stars, and hot surfaces within the field of view of the detector. The spectral irradiance of the night sky in this region is on the order of 10^{-12} less than the day sky equivalent, although this figure is affected by the phases of the moon (Ref 24:6-9). The laser designator system in the absence of scattered solar radiation, then may detect nanowatts of laser designator energy even without internal system logic. On the other hand, any object within the field of view of the detector could be a significant emitter of this radiation if it were extremely hot. Spectral curves for blackbodies appear in

References 24 and 33 which indicate that objects with temperatures in excess of 500°K emit significant radiation in the 1.059μ to 1.069μ region. This too may be eliminated by the design logic; but in the event no logic utilized, this might be a system limitation.

For the duration of this report, the problem of background signal will be assumed to have been eliminated through the design logic system which discriminates the extended return from the pulsed return. If this assumption were not possible then the more difficult problem of determining the background signal for various receiver and sun zenith angles must be addressed at length. This problem is more commonly known as the radiative transfer problem. This is a much more complex problem and one that has only recently been addressed for the visible region (Ref 19).

In the absence of a background signal reaching the receiver, the Johnson noise term ($2FKTB$) and the dark current term ($2eBI_d R_e G^2$) are the only remaining terms in the denominator of Eq (7). The design specifications of the receiver then uniquely determine the minimum power, P_{mr} , that can be detected by the receiver for a given signal-to-root-mean-square noise ratio. This value of P_{mr} is the minimum detectable laser signal. When this power is equal to the power at the receiver, P_r , computed in Eq (6), then this determines the maximum lock-on range of the laser target designator system in an atmosphere-free environment. Further, if it is assumed that the receiver looks directly at the target ($\cos\phi_r = 1$), then Eq (6) becomes

$$R_r^2 = \frac{P_p T_d \rho_t \cos\theta_t A_r T_r}{\pi P_r} \quad (8)$$

which is the atmosphere-free lock-on range equation.

Unfortunately the signal-to-noise ratio is not constant but varies with temperature for the non-cooled detector heads currently in use. A realistic signal-to-noise ratio (SNR) may be computed, however, based on typical mission profiles and temperatures.

It is not the intent of this report to explore the characteristics of various receivers and lasers. A typical laser peak power and designator optics transmission value are assumed. The target is assumed to be a Lambert emitter with reflectivity of 10%. Further, if typically achievable values are assumed for the receiver transmittance, T_r , and area of the receiver optics, A_r , then the right hand side of Eq (8) is reduced to a constant if one assumes that the receiver views the target normally ($\cos \theta_t = 1$), an optimum condition. Using the design parameters from Reference 24, then the right hand side of Eq (8) is reduced to $6.7 \times 10^9 \text{m}^2$ (Ref 24:13-14). It is important to recognize that this value is for one particular set of design parameters; another set of parameters will yield a different value, but the method of solution is the same and Eq (8) is a general result (for the atmosphere-free lock-on range).

In summary, we have discussed the laser, the target reflective characteristics, and the receiver characteristics and their relationships to the maximum lock-on range. In the development of the range equation, we have assumed: (1) there is no loss of laser power to the atmosphere, (2) the beam at the target is smaller than the target and is reflected only from it and not the background, (3) the target is a perfectly diffuse Lambertian reflector with reflectivity of 10%, (4) the receiver

is so designed so as to discriminate against continuous background returns, and (5) that the target is entirely within the field of view of the receiver.

III. Atmospheric Attenuation of Laser Radiation

As the maximum lock-on range equation was developed in Chapter II, two important laser energy losses were ignored--both of them the result of atmospheric attenuation. As the radiant power travels through the atmosphere, some of it is scattered out of the path to the target or receiver and some of the radiation is absorbed. The scatterers and absorbers are the atmospheric gaseous molecules, aerosols, and water droplets. Unless the designator and receiver are co-located, then the two paths through the atmosphere are different; and therefore, the energy losses due to the atmospheric attenuation are not the same. Moreover, the nature of the radiation transfer in the two paths is not the same due to the assumption that the target is a Lambertian surface. The two paths will be addressed separately. The two losses will be described mathematically and then related to the maximum lock-on range equation from Chapter II.

In describing the atmospheric energy loss, this report uses the following terminology. Atmospheric attenuation is the process by which energy is scattered and absorbed by the atmospheric constituents. Attenuation coefficients are the constants used to describe the attenuation due to aerosols, molecules, rain and others. Extinction coefficient refers to the sum total of the separate attenuation coefficients. That is, extinction refers to the sum total of all scattering and absorption (Ref 62:5), although this atmospheric process is called attenuation in this report. In much of the literature concerning this subject, attenuation and extinction are used interchangeably.

Atmospheric Effects on Laser Radiation (Laser to Target)

Assuming that there is some constant, σ_t , by which the atmospheric absorption and scattering may be described for given atmospheric conditions, then the intensity of radiation at any point in space is given by the fundamental law of extinction of Beer-Lambert (or Bourguer, in European literature). It states that the extinction process is linearly independent with respect to the intensity of radiation and amount of matter, provided that the physical state (i.e., temperature, pressure, composition) is held constant (Ref 33:23). This law postulates that matter in the optical path is in the same physical state and therefore extinction is dependent only on the amount of matter. Then the monochromatic spectral transmission of radiation in the atmosphere is (Ref 49:10)

$$T = e^{-\int_0^L \sigma_t(l) dl} \quad (9)$$

where σ_t = total atmospheric extinction coefficient per unit path length,

L = total path length,

and dl = incremental path length.

Van de Hulst in Reference 62 states that for diffuse light, Lambert's law is valid for single scattering only for an optical depth of 0.1 or less where one optical depth is defined as the exponent required to reduce the transmission to $1/e$ of its original value. For optical depths of between 0.1 and 0.3, a correction term is necessary to account for double scattering and for optical depths in excess of 0.3

then the full complexities of multiple scattering become a factor (Ref 62:6). Van de Hulst's work, however, refers only to diffuse sources of light and not to the narrow collimated laser light. Zuev, Kalanov, and Savel'ev in Reference 73 have investigated the applicability of the Beer-Lambert law to laser propagation. They experimentally determined the validity of the exponential law for laser radiation up to optical depths of 12 (Ref 73:140). For optical depths greater than 9, however, multiple scattering may be significant for targets that are larger than 9 times the diameter of the laser beam. Optical depths larger than 12 were not experimentally verified by Zuev because of light source and receiver limitations, but this reference predicts validity of the law to optical depths of 30.

In the problem of the laser radiation incident on the target, the loss of energy can be determined then by use of the Beer-Lambert exponential law. The power incident on the surface of the target is then

$$P_t = P_p T_d e^{-\int_0^{R_d} \sigma_t(\ell) d\ell} \quad (10)$$

where $\sigma_t(\ell)$ is the atmospheric extinction coefficient per unit path length as a function of position, $d\ell$ is the incremental path length, and R_d is the distance from designator to target. Thus, the radiant power on the target is a function of the specific atmospheric extinction coefficient, σ_t .

Atmospheric Effects on Reflected Laser Radiation (Target to Receiver). On the surface it would appear that there need be no justification of the use of the exponential law for the reflected laser

radiation. Since our model has assumed a diffuse Lambert reflector, however, justification is essential. Conversely, if our model had assumed specular reflection by the target, then the properties of the laser radiation would have been preserved. Such an assumption is not, however, in agreement with the reflective characteristics of most military targets as we have previously discussed; in addition, such an assumption makes determination of directional reflectance exceedingly complex.

The diffuse reflection of laser from the target requires that for single scattering the Lambert law is limited to optical depths of 0.1 or less as described by Van de Hulst. For larger optical depths, the full multiple scattering problem must be addressed. For extremely narrow receiver fields of view, there is justification for use of the Lambert law (Ref 71:202), but for use in our model it must be acknowledged that the use of the Lambert law for single scattering for the atmospheric attenuation of radiation from target to receiver is a model limitation. Because the multiple scattering problem is not addressed for this portion of the energy transport, then this model may result in underestimation of the maximum lock-on range.

With this caution, when the assumption is made that energy transport from the target to receiver is approximated by the Lambert Law and the maximum laser lock-on range equation becomes

$$R_r^2 = \frac{P_p T_d e^{-\int_0^{R_d} \sigma_t(\ell) d\ell} \rho_t \cos \theta_t A_r T_r}{\pi P_r e^{+\int_0^{R_r} \sigma_t(\ell) d\ell}} \quad (11)$$

where $\sigma_t(\ell)$ is the atmospheric extinction coefficient per unit path length as a function of position, $d\ell$ is the incremental path length, and R_r is the distance from target to receiver. Substituting the design parameters constant (discussed in Chapter 11) into Eq (11) then the laser target designator system maximum lock-on range equation becomes

$$R_r^2 e^{\int_0^{R_r} \sigma_t(\ell) d\ell} = (6.7 \times 10^9 \text{m}^2) e^{-\int_0^{R_d} \sigma_t(\ell) d\ell} \quad (12)$$

which is a transcendental equation that is dependent on the specific atmospheric extinction coefficients.

Atmospheric Extinction Coefficient

The extinction coefficient, as we have discussed, refers to the absorption and scattering of the laser radiation by atmospheric gases and particles. That is, the extinction coefficient is the sum of all absorption and scattering coefficients. It is the sum of the coefficients describing molecular scattering, molecular absorption, aerosol scattering, aerosol absorption, and the scattering and absorption by clouds, rain, ice crystals, fog, snow and others. The total atmospheric attenuation is a complex function of the number of molecules, kinds of molecules, number of aerosols, aerosol composition, aerosol size distributions, number of water, ice, fog, snow, or cloud droplets, droplet composition and droplet size distribution in the volume of air traversed by the radiation. Moreover, these factors are not constant throughout the atmosphere, and therefore atmospheric attenuation becomes a function of the particular radiation path. In

addition, the scattering and absorption is dependent on the particular wavelength of the radiation.

The problem of determination of atmospheric attenuation of 1.06 μ laser radiation may then be reduced to the following subproblems: (1) determination of molecular scattering and absorption, (2) determination of the aerosol scattering and absorption, and (3) determination of the scattering and absorption of other atmospheric particles (such as clouds, rain and fog), and the relationship of these to observables or measurable quantities. These separate forms of scattering and absorption are expressed in terms of separate attenuation coefficients. In general, these separate coefficients are additive yielding the total extinction coefficient.

On a clear day, for example, the atmospheric transmission of laser radiation is a function only of the aerosols and molecules

$$T = e^{-\int_0^L (\sigma_a + \sigma_m) dl} \quad (13)$$

where σ_a is the aerosol attenuation coefficient (per unit length), σ_m is the molecular attenuation coefficient (per unit length) and L is the path length. The aerosol attenuation coefficient is the sum of the scattering and absorption

$$\sigma_a = \alpha_a + \beta_a \quad (14)$$

where α_a is the aerosol absorption coefficient (per unit length), and β_a is the aerosol scattering coefficient (per unit length). Likewise, the molecular attenuation coefficient is the sum of the molecular scattering and absorption

$$\sigma_m = \alpha_m + \beta_m \quad (15)$$

where α_m is the molecular absorption coefficient (per unit length), and β_m is the molecular scattering coefficient (per unit length). The determination of these individual coefficients is the subject matter of the next chapters. We shall successively investigate each of these coefficients by determining in each case the factors that contribute to the radiation attenuation. Next, since the atmosphere is inhomogeneous, the factors must be related to position within the atmosphere. Last, these factors must be related to atmospheric observables or measurables, so that the laser's radiant power at a particular point in the atmosphere is predictable.

IV. Molecular Absorption and Scattering

Radiation is scattered by all of the atmospheric gaseous molecules, but it is selectively absorbed. There are many atmospheric constituents. All are important for the determination of molecular scattering; but only some of the molecules are effective absorbers of radiation and these are effective only at certain wavelengths which depend upon the structure of the molecule.

Molecular (Rayleigh) Scattering

All atmospheric molecules scatter radiation. Their size is on the order of $10^{-6}\mu$ to $10^{-8}\mu$ and therefore the scattering cross-section is quite small. Particles which are small relative to the wavelength of the incident radiation experience the same electric field throughout their entire dimensions, which are *assumed* to be *spherical*. This external electric field establishes a dipole in the small particle which is a function of its polarizability. This dipole then emits radiation in the characteristic dipole pattern which results in the removal of energy from the incident beam (Ref 8:184). This phenomenon is called Rayleigh scattering, and the scattering coefficient can be expressed as

$$\sigma_{\text{RAY}} = \frac{8\pi^3}{3\lambda^4} \frac{(M_g^2 - 1)^2}{N_g} \frac{6 + 3f}{6 - 7f} \quad (16)$$

where λ is the wavelength of incident radiation (cm), M_g is the refractive index of the gas relative to a vacuum, N_g is the number of molecules per cm^3 , and f is the depolarization factor, which for air is 0.042 and is often omitted (Ref 8:189).

It must be emphasized that this equation is valid only for spherical molecules and a correction term must be added for non-spherical molecules. This equation, however, will prove useful in yielding an estimate of the molecular scattering in the atmosphere provided the number of molecules can be determined. According to Avogadro's hypothesis, the number of molecules of any gas per unit volume depends only on temperature and pressure. For the U. S. Standard Atmosphere (15°C and 1013 mb mercury) the number of molecules in one cubic centimeter is approximately 2.547×10^{19} . Then for the U. S. Standard temperature and pressure, the Rayleigh scattering coefficient for 1.064 μ laser radiation is

$$\beta_{\text{RAY}} \approx \frac{8\pi^3 [(1.0002)^2 - 1]^2}{3(1.064 \times 10^{-4} \text{ cm})^4} \frac{2.547 \times 10^{19}}{\text{cm}^3} \approx 8.16 \times 10^{-9} / \text{cm} \quad (17)$$

where $M_g = 1.0002739$ (Ref 27:2).

Expressed in inverse kilometers, the molecular scattering coefficient is

$$\beta_m = \beta_{\text{RAY}} \times (10^5 \text{ cm/km}) \quad (18)$$

The Rayleigh scattering coefficient for 1.064 μ laser radiation at 15°C and 1013 mb mercury is $8.16 \times 10^{-4} (\text{km}^{-1})$. The molecular scattering coefficient for the visible ($\lambda = .55\mu$) at 15°C and 1013 mb is $1.14 \times 10^{-2} (\text{km}^{-1})$.

In addition at higher altitudes (lower temperatures and pressures) this coefficient becomes smaller. For slant path transmissions from altitude, then, the average molecular scattering coefficient would

be even less significant. Increasing the temperature to 35°C and pressure to 1025 mb, conditions not normally encountered, does not significantly affect the scattering. From these calculations, it becomes clear that molecular scattering is not a serious limiting factor for reasonable path lengths of the laser radiation and may be safely ignored for 1.064 μ radiation. Conversely, the Rayleigh scattering in the visible may not always be ignored, but for our purposes now it is rather insignificant.

Molecular Absorption

The molecules are frequently excellent absorbers of radiation. Molecular constituents of the atmosphere that are significant absorbers are: (1) water vapor; (2) carbon dioxides; (3) ozone; (4) nitrous oxide; (5) carbon monoxide; (6) methane; and (7) oxygen. Other trace gases such as sulfur dioxide may also be good absorbers but they do not naturally occur in the atmosphere and significant concentrations are limited to areas with large industrial activity.

The absorption by molecules is due to the changes in molecular states caused by the addition of energy. The molecules absorb the energy by changing vibrational, rotational, or electronic energy levels or a combination of the three. Each single allowed transition gives a particular absorption line. For each allowed vibrational energy level transition there are many rotational energy levels possible thereby creating a band structure or rather a series of closely spaced lines which overlap.

A great amount of work has been done in the field of molecular absorption and molecular spectroscopy. For a detailed account of the

theory of molecular absorption, the reader is referred to References 33, 35 or 36.

From the exhaustive studies on absorption, there have emerged various band models for prediction of average transmission for different spectral regions. Some of the better known broadband models are the Altshuler, Statistical or Mayer-Goody, Elssaser, Random Elssaser, and the Air Force Cambridge Research Laboratories Lowtran II. There are also two approximation schemes used in the band models: the weak-line and the strong-line approximations.

In general, these band models are based on experimental measurements of the solar spectral transmittance or laboratory data. The data is then smoothed to provide continuous curves and average transmittance in the various spectral regions. In addition, these models are statistically extrapolated into spectral regions where data is not available. For purposes of predicting low resolution spectral transmittance, a band model is adequate if it is based on measurements in the spectral region. However, for laser transmittance where high spectral resolution is required, then the band models are woefully inaccurate. Laser wavelengths are assumed to be monochromatic so an average transmittance for a spectral region does not provide laser transmittance. To determine laser transmittance, a line by line calculation is necessary.

Such a compilation of molecular absorption lines has been the ongoing project of the Air Force Cambridge Research Laboratories since 1967. At present, this inclusive work includes the vibration-rotation lines of seven naturally occurring molecules of significance (including their isotopes) in the terrestrial atmosphere.

These seven are the same atmospheric constituents listed earlier in this section. With the exception of oxygen, all of these molecules are minor atmospheric constituents, but they represent most of the absorption lines in the visible and infrared. This work assumes (and investigation seems to support the fact) that all of these gases, with the exception of water vapor and ozone, are uniformly mixed in the atmosphere. Each of the lines in this study (Ref 47) represents either a theoretical calculation based on atomic and molecular theory or actual solar or laboratory data or both.

In order to compute the transmittance of a given spectral line in the atmosphere it is necessary to describe the absorption coefficient as a function of frequency for each line. The four essential parameters for each line are the resonant frequency, ν_0 (cm^{-1}), the intensity per absorbing molecule, S ($\text{cm}^{-1}/\text{molecule cm}^{-2}$), the Lorentz line width parameter, α_0 ($\text{cm}^{-1}/\text{atm}$), and the energy of the lower state, E'' (cm^{-1}). The frequency, ν_0 , is to a close approximation independent of temperature and pressure. The intensity, S , is pressure-independent and its temperature dependence can be calculated from E'' and ν . The line half-width at half maximum, α , is proportional to the pressure and is temperature dependent. The precise line shape is uncertain but theoretical computations usually begin with the Lorentz line shape, which has two limitations: (1) Lorentz lineshape for infrared frequencies requires modification for pressures lower than 100 mb (which is not a factor in our case), and (2) The Lorentz lineshape may be inaccurate in the distant wings of a line ($|\nu - \nu_0| \gg \alpha$) or when collision broadening forces are dipole-quadrupole (Ref 47:2,3).

Reference 47 gives the intensity as a function of a temperature as

$$S(T) = \frac{S(T_s) Q_v(T_s) Q_r(T_s)}{Q_v(T) Q_r(T)} e^{\left[\frac{1.439E''(T-T_s)}{TT_s} \right]} \quad (19)$$

Where E'' is the energy of the lower state of transition (cm^{-1}), Q_v is the vibrational partition function, Q_r is the rotational partition function, T is the temperature ($^{\circ}\text{K}$), and T_s is 296°K . Assuming a Lorentzian line shape, the line half width at half maximum at any temperature, T , and pressure, P , is given by

$$\alpha = \alpha_0 \frac{P}{P_0} \sqrt{\frac{T_0}{T}} \quad (20)$$

where α_0 is the measured or computed line half width at temperature T_0 and pressure P_0 ; P_0 is the pressure at which experimental measurement or theoretical determination of α_0 is made, and T_0 is the temperature of the experimental measurement. The molecular absorption coefficient due to the absorption by one molecule of one molecular species for one absorber line is

$$\alpha_{lm} = \frac{S \alpha}{\pi[(\nu - \nu_0)^2 + \alpha^2]} \quad (21)$$

where S is the line intensity,

α is the line half-width,

ν_0 is the central line frequency,

and ν is the laser frequency, which is assumed to be monochromatic.

Generally, however, a large number of absorption lines belonging to different molecular species contribute to the attenuation at a specific laser frequency; that is, the absorption coefficient per molecule for a laser of frequency, ν , is

$$\alpha_{m/m} = \sum_j \sum_i \frac{S_{ij} \alpha_{ij}}{\pi[(\nu - \nu_{ij})^2 + \alpha_{ij}^2]} \quad (22)$$

where subscript i refers to the different spectral lines of each molecular gas and subscript j refers to the j different molecular gases. Multiplying the absorption coefficient by the total number of molecules along with the path length yields the optical depth. Another more conventional method for our purposes involves defining the total absorber density along the path. Multiplying $\alpha_{m/m}$ by this absorber density gives the molecular absorption coefficient per unit path length, which is the way we have defined all absorption and scattering coefficients. Then

$$\alpha_m = \sum_j \sum_i \frac{S_{ij} \alpha_{ij} m_j}{\pi[(\nu - \nu_{ij})^2 + \alpha_{ij}^2]} \quad (23)$$

where m_j is the number density of each molecular gas, j , per unit path length.

Distribution of Molecular Absorbers. If the density of each molecular absorber were known for all points P in the atmosphere then Eq (23) would yield the molecular absorption coefficient. The molecular concentrations of the atmospheric gases, however, are not uniform. They vary for the different temperatures, pressures,

locations, and air masses. Several approximations will be made.

The first assumption is that the atmosphere is horizontally stratified. All horizontal paths are defined as being through uniform air masses. By this stratification, two categories of atmospheric gases emerge: (1) the uniformly mixed gases, and (2) the unmixed gases. Of the seven molecular absorbers under consideration only two fail to qualify for the first category. These two, ozone and water vapor, are not only a function of atmospheric conditions but they are also a function of geographical location and their evolution properties.

For the uniformly mixed gases, the concentration is generally written as the equivalent length of pure absorber in the path as a function of the pressure and temperature. For the horizontally stratified atmosphere, this concentration, ΔL , is the product of the path length, $R(\text{cm})$, the fractional part of the total atmospheric volume of absorber, f , and the pressure in atmospheres, P . This concentration is most conveniently expressed in units of cm-atm reduced to standard temperature and pressure (STP) (Ref 49:87).

The AFCRL report, *Optical Properties of the Atmosphere*, gives this molecular concentration for a horizontal path at any altitude, z , as

$$\Delta L = fR \left(\frac{P}{P_s} \right) \left(\frac{T_s}{T_z} \right) (\text{cm-atm})_{\text{STP}} \quad (24)$$

where $T_s = 273^\circ\text{K}$ and $P_s = 1 \text{ atm}$. This concept of equivalent absorber path at standard conditions may be extended to vertical paths provided the vertical molecular distribution may be described. For uniformly

mixed gases of fractional concentration by volume, f , the vertical distribution is modeled using the hydrostatic equation which states that the change in pressure along a small vertical path is the product of the molecular density, gravity, and path length. If the hydrostatic equation is integrated from an altitude, z , out to infinity, then the hydrostatic equation may be expressed in terms of the scale height of the atmosphere above altitude, z , $H(z)$

$$P(z) = g\rho(z)H(z) \quad (25)$$

where $P(z)$ = pressure at altitude z ,
 $\rho(z)$ = molecular density at z ,
 g = acceleration due to gravity

For a vertical column of air at STP, $H(0) = 7.99$ Km (Ref 49:88).

The scale height in Km for any altitude z may be determined by

$$H(z) = 10.2 \left(\frac{P(z)}{\rho(z)} \right) \quad (26)$$

After some manipulation then the amount of absorber for a slant path between altitudes z_1 and z_2 becomes

$$\Delta L = f \times 10.2 \left(\frac{P(z_1) - P(z_2)}{\rho_0} \right) \text{Sec } \theta \quad (27)$$

where θ is the angle from the vertical (zenith). Values for the concentration of the uniformly mixed gases along with values in (cm-atm) for vertical paths from sea level are given in Table i. These values for vertical paths when multiplied by the fractional pressure change ^{STP}

and the secant of the zenith angle yield the $(\text{cm-atm})_{\text{STP}}$ of absorber between two pressure levels or rather two altitudes.

Table I
Concentrations of Uniformly Mixed Gases

<u>Constituent</u>	<u>Molecular Weight</u>	<u>PPM by Volume</u>	<u>$(\text{cm-atm})_{\text{STP}}$ in Vertical Path From Sea Level</u>
Air	28.97	10^6	8×10^5
CO ₂	44	330	264
NO ₂	44	0.28	0.22
CO	28	0.075	0.06
CH ₄	16	1.6	1.28
O ₂	32	2.095×10^5	1.68×10^5

This result is useful in that it allows us to determine the number of molecules per unit area in the path. Since there are always Avogadro's number of molecules in 22.4 liters at STP then the following relation for the uniformly mixed gases may be derived

$$1 (\text{cm-atm})_{\text{STP}} = 2.69 \times 10^{19} \text{ molecules/cm}^2 \quad (28)$$

Unfortunately, the gases ozone and water vapor do not behave so simply. These gases are more dependent on their particular production processes and their concentrations in the atmosphere are

subject to wide variation. Ozone production and distribution is important for some absorption problems, but for purposes of this report, its contribution for molecular absorption is negligible for two reasons: (1) ozone concentrations at or below 20,000 feet are quite small, and (2) absorption lines of ozone of sufficient intensity are not within the spectral region of interest. For these reasons, this discussion will be restricted to the atmospheric concentrations of water vapor.

The amount of water vapor in air depends on such diverse atmospheric conditions as the wind speed, atmospheric pressure and temperature and on the history of the air mass and on geographical location. And the concentration of water vapor does not necessarily decrease with altitude or the formation of clouds at an inversion would be a rare phenomena.

The amount of water vapor in a short path is determinable provided the temperature and relative humidity are known. This quantity of water vapor is given in total length of water (liquid) that may be precipitated out of the path per unit area. The precipitable water, W , may be defined as the amount of water contained in a vertical column of air of unit cross section extending between two pressure levels P_1 and P_2 . It is given by

$$W = \frac{1}{g} \int_{P_1}^P w dP \quad (29)$$

where g is the acceleration of gravity and w is the mixing ratio (Ref 61:3-32). If w is assumed constant for the small incremental

change in P and the hydrostatic equation is used then Eq (29) becomes

$$W = \bar{w} \rho_w dz \quad (30)$$

where \bar{w} is the mean mixing ratio in the path dz and where the density of water, ρ_w is constant.

The mixing ratio w is defined as the weight of water vapor contained in mixture with a unit weight of dry air and is related to the relative humidity (RH) by $RH = 100 \times w/w_s$ where w_s is the saturation mixing ratio (Ref 9:155). For water vapor the saturation mixing ratio is given approximately by

$$w_s \approx \frac{\epsilon e_s}{P} \quad (31)$$

where $\epsilon = .622$, a ratio of the molecular weights and e_s is the saturation vapor pressure at a particular temperature (Ref 37:59).

The saturation vapor pressure at a temperature t in $^{\circ}\text{C}$ is given approximately by the empirical relationship of Tetten (1930):

$$e_s \approx 6.11 \times 10^{[7.5t/(237.3 + t)]} \quad (32)$$

where e_s is in millibars and t is the air temperature in $^{\circ}\text{C}$ (Ref 57:9).

Combining Equation (30), (31), and (32) and using the ideal gas law, the following relationship is derived for the precipitable water vapor:

$$W \approx (R.H.) (.458 \times 10^{-6} \text{cm}^{-3}) 10^{[7.5t/(237.3 + t)]} dz \quad (33)$$

Dividing Eq (33) by the path length in cm and converting to km then the precipitable water vapor in grams per cm² per km is

$$W \approx .0458 \left(10^{\frac{[7.5t/(237.3 + t)]}{T}} \right) (RH) \quad (34)$$

If this incremental path is taken as the vertical, then to determine W for slant paths, this value in Eq (34) must be increased by a factor of secant θ where θ is the angle from the vertical (where $\theta < 80^\circ$).

The water vapor concentration per km path length as a function of relative humidity and temperature is shown in Figure 5. Further, the number of gm cm⁻²/km of water vapor is directly convertible into molecules/cm² per km for use in Eq (23) by the relation derived in Reference 49:

$$1 \text{ gm/cm}^2\text{-km} = 3.34 \times 10^{22} \text{ molecules/cm}^2 \quad (35)$$

Distribution Data

At this point, a note of caution is in order. Neither of the expressions derived is exact. They are valid only for small path lengths and are valid only when the pressure, temperature and relative humidity profiles for the paths are known. These profiles fluctuate greatly in just a few hours so an exact determination of molecular absorption is essentially impossible even within the bounds of these simplifications. Very few observations are taken of the vertical profiles and these are usually rawinsonde balloons which are not absolutely accurate.

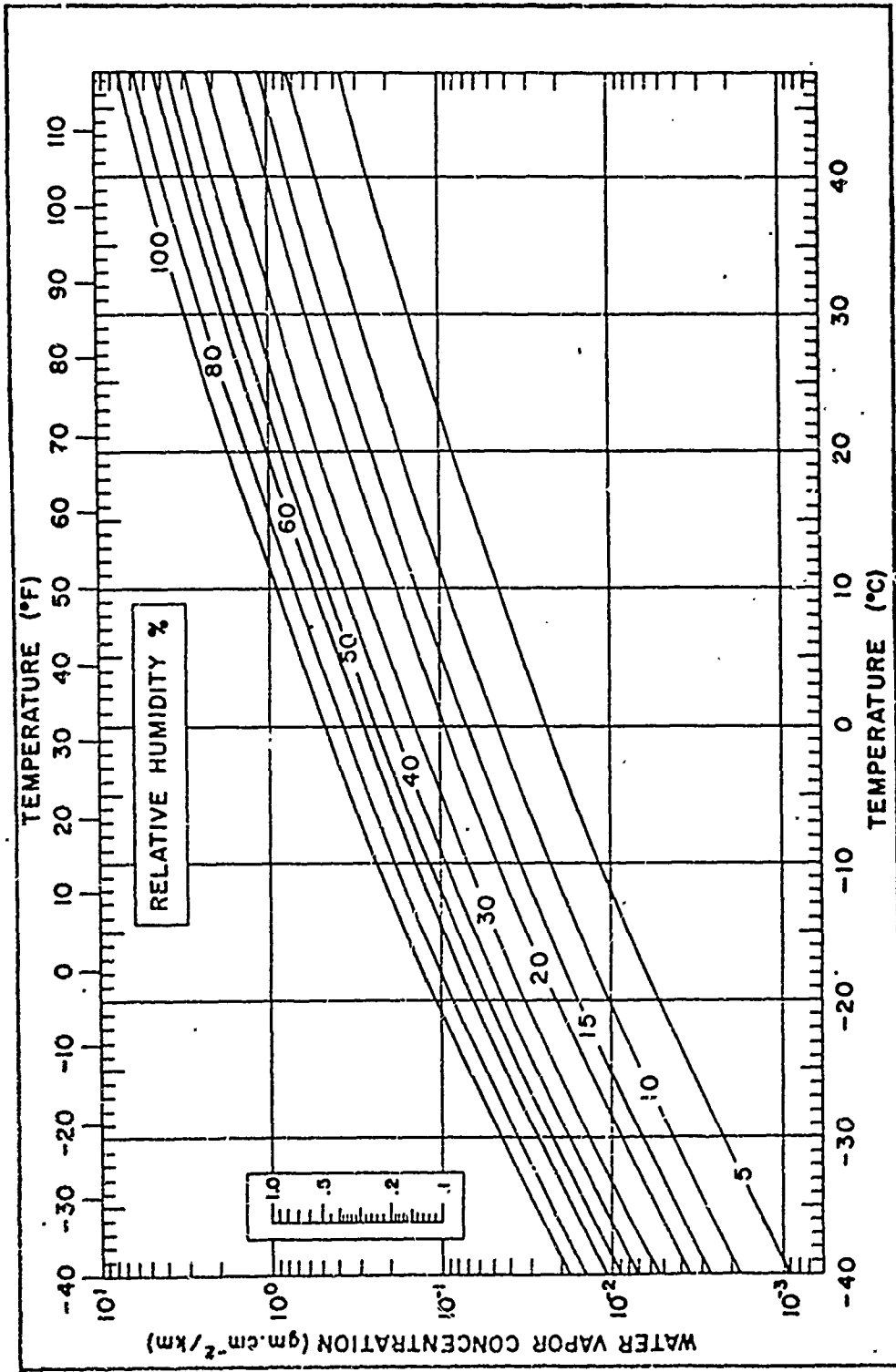


Fig. 5. Water Vapor Concentration per Kilometer Path Length as a Function of Temperature and Relative Humidity (Ref 49:91)

The rawinsonde provides little data on the first 200 feet above ground level because of the lag in lock-on time. Further, the temperature is accurate only within 1°C and the relative humidity within 5 percent (Ref 45).

These balloon observations are relatively sparse. The most that are taken by an individual station is four in a 24 hour period. Most stations take none and a few take one or two. For example, in an area the size of Germany, there was but one station that took 4 observations per day in July, 1970 (Ref 51). Nevertheless, a data base for vertical profiles has been developed and utilized by weather services worldwide in support of aviation. Global Weather Central has the additional capability of prediction of upper level winds, temperatures and pressures for all hours.

Part of this data base has been used by AFCRL in its compilation of model atmospheres. These model atmospheres--Tropical, Midlatitude Summer, Midlatitude Winter, Subarctic Summer, Subarctic Winter, and the U. S. Standard--have been compiled from a large number of observations for the specific regions described. These are average conditions and therefore give only mean conditions. These atmospheres reported in Ref 61 and Ref 49 were used for the theoretical molecular absorption calculations described earlier in this paper.

Comparison of Distributions. The vertical profiles described in the Midlatitude Summer, Midlatitude Winter, and U. S. Standard models are shown in Table II. The profiles are shown from the surface to the 500 mb pressure level which corresponds to an altitude

of approximately 17,000 feet to 19,700 feet depending on atmospheric conditions.

Table II

Vertical Profiles of the Midlatitude Summer, Midlatitude Winter, and 1962 U. S. Standard Atmospheres: Surface to 500 millibars (mb)

<u>Season</u>	<u>Model</u>	<u>Relative Humidity (%) / Temperature (°C)</u>			
		<u>Surface</u>	<u>850 mb</u>	<u>700 mb</u>	<u>500 mb</u>
Winter	Midlatitude Winter	80/-1 (.35) ^a	75/-5 (.22)	60/-11 (.127)	50/-26 (.0315)
Summer	Midlatitude Summer	79/21 (1.4)	60/14 (.70)	50/6 (.33)	32/-11 (.066)
Fall/ Spring	U. S. Standard	60/15 (.772)	67/6 (.43)	70/-6 (.205)	74/-24 (.053)

^aValues in parentheses are the Water Vapor Concentrations in $\text{gm-cm}^{-2}/\text{km}$ determined for the Temperature and Relative Humidity using Figure 5.

The vertical profiles for an area of Germany of longitude 10°E and latitude from 48° to 49°N were provided by USAF ETAC (Environmental Technical Applications Center) that represent means of observations over a six year period. This data, shown in Table iii, was provided by month and then averages for the seasons were computed. The water vapor concentrations for both sets of data were computed using Figure 5. These concentrations are shown in

parentheses in the tables.

Table III
Average Monthly/Seasonal Profiles of Relative Humidity
and Temperature for Germany (49° N 10° E)
Surface to 500mb*

Season	Month	Relative Humidity(%) /		Temperature (°C)	
		Surface	850mb	700mb	500mb
Winter	Dec	93/0	69/-1	51/-8	39/-24
	Jan	80/2	54/-2	44/-9	42/-26
	Feb	80/2	63/-2	52/-10	47/-26
	Avg	84/1 (.42) ^a	62/-2 (.28)	49/-9 (.12)	43/-25 (.020)
Spring	Mar	65/6	69/0	53/-8	46/-25
	Apr	61/10	69/2	57/-7	44/-23
	May	67/14	65/6	49/-4	37/-19
	Avg	64/10 (.58)	68/3 (.40)	53/-6 (.17)	42/-22 (.038)
Summer	Jun	77/16	66/10	59/-1	50/-17
	Jul	77/19	66/12	59/1	35/-14
	Aug	77/20	57/12	65/2	42/-14
	Avg	77/18 (1.2)	63/11 (.63)	61/1 (.31)	42/-15 (.065)
Fall	Sep	77/15	61/10	51/1	46/-15
	Oct	87/9	61/6	46/-2	34/-18
	Nov	75/4	69/1	53/-6	48/-22
	Avg	80/9 (.66)	64/6 (.45)	50/-2 (.20)	43/-18 (.053)

*Data provided by USAF Environmental Technical Applications Center

^aValues in parentheses are the Water Vapor Concentrations in gm-cm⁻²/km determined for the Relative Humidity and Temperature using Figure 5.

Comparisons of the concentrations show that the Midlatitude Summer reasonably approximates the mean summer concentrations in Germany. Likewise, the Midlatitude Winter model approximates the winter profiles for Germany. A correlation was also found between the U. S. Standard model and Fall and Spring conditions reported for Germany, although the correlation was not nearly as good for the latter. For the Spring Season, the model tends to be overly pessimistic for mean atmosphere conditions for this area of Germany. Nevertheless, the correlation of the three models with the four seasons in this area was sufficiently good that the models should provide an approximation of the atmospheric molecular absorption for mean conditions.

Wavelength Dependence of Absorption. As we discussed previously, for monochromatic transmission, which is the approximate case for lasers, a line by line calculation of absorption is necessary. For each laser frequency the transmission is dependent on the particular absorption lines around the laser frequency, their strengths, and their number. Because the molecular absorption is so sensitive to the exact laser frequency, then the exact laser frequency must be specified.

Unless the temperature of a laser can be continuously monitored, little can be said about the exact laser frequency. The frequency range can and must be determined for the temperature range expected for laser operation. Since the frequency is so important in determination of the molecular absorption, a frequency must be specified. Calculation based on the center frequency of the expected operating range is not correct and may be entirely misleading. On the

other hand, a line by line calculation of absorption over a specific range and then taking an average is also incorrect and can lead to errors much larger than those induced by deviations from the mean atmospheric conditions as shown in the tables in Appendix A. Assuming that the laser is not equipped with a temperature or frequency monitoring device, then the exact laser frequency is unknown. In order to calculate the molecular absorption, a worst case frequency must be assumed.

For the purpose of this thesis a range of wavelengths for the laser was selected extending from 1.063μ (9407.3377cm^{-1}) to 1.065μ (9389.6714cm^{-1}) in an attempt to make this thesis applicable to as many users as possible. Within this specified range, there are two molecular absorbers with line intensities of 1.0×10^{-27} ($\text{cm}^{-1}/\text{molecule} \cdot \text{cm}^{-2}$) or more (Ref 50). A graph of these intensities may be found in Appendix A. Some mention, at this point, must also be made about the determination of these intensities.

In general, line intensities of the individual molecules are very difficult to determine especially in the atmospheric environment where the bands overlap. Where the data has been supplied by laboratory measurement under vacuum conditions, then the intensity determination is much more reliable. For a spectral region of few lines (the lines overlap only slightly), then the intensities may be expected to be quite reliable even for atmospheric studies. There is every indication that the intensities within this region of our study are accurate; however, for other regions the intensities may be less accurate.

Absorption at 1.063 μ . Calculations using the atmospheric models were made for frequencies throughout the interval 1.063 μ to 1.065 μ . Within this region, the molecular absorption at 1.0636 μ (9401.760 cm^{-1}) was the greatest; that is, transmission at this wavelength was the worst case. Calculations for the absorption coefficient for five wavelengths in the interval and two just outside the given spectral region are shown in Appendix A.

General results of the molecular absorption calculations include the following points. The absorption increases as the temperature and relative humidity increase. Laser frequencies that fall precisely on absorber lines will be affected most by absorption in this region; and those that do not fall on lines are less sensitive to atmospheric conditions. Frequencies that fall precisely on water lines are especially sensitive to temperature and humidity variations. The absorption coefficients within the region vary over three orders of magnitude for the different frequencies, but for any given frequency the variation due to the mean temperature, pressure, and relative humidity models is on the order of a factor of eight or less for each altitude considered. The extreme sensitivity of absorption to the laser frequency is shown most graphically by comparison of the two frequencies, corresponding to the wavenumbers 9388.98 cm^{-1} and 9407.07 cm^{-1} , with the worst of the frequencies within the region, corresponding to the wavenumber 9401.760 cm^{-1} .

Calculation of the Absorption Coefficient

As an approximation for laser molecular absorption coefficients for Germany, the model atmospheres were used as a basis for the

calculations. The coefficients were determined using the AFCRL program for the worst case wavelength (1.0636μ) for the mean atmospheric conditions (model) at each altitude in km. The absorption coefficients are then averaged for the mean absorption coefficient per layer (1 km thick). Next, the coefficients (in km^{-1}) are summed up to the altitude of interest, multiplied by the altitude (in km) of the designator or aircraft, and then multiplied by the secant θ to yield the entire optical depth.

These calculations are designed to yield the approximate molecular absorption for atmospheric conditions normally encountered in Germany. In order to use the approximation scheme, no particular meteorological parameters are required for table entry. For this atmospheric approximation, the molecular absorption is found to vary only with the season. In reality, however, large deviations from mean conditions may be encountered. Caution should be exercised when using this scheme for concurrent high temperatures and high humidities. Calculations show that for extreme conditions in summer, transmission may be reduced by more than fifty percent.

In addition, this approximation scheme should not be arbitrarily extrapolated to fit other similar mean meteorological profiles unless an analysis similar to the one here has been conducted. Large errors would be induced by extrapolating this absorption data to more tropical climates. Also, in no circumstance should this data be used for laser frequencies outside of this spectral region.

V. Atmospheric Aerosol

In addition to the gaseous molecules, the atmosphere contains many suspended aerosols. Aerosols are defined as dispersed solid or liquid matter in a gaseous medium, in this case, air. If we neglect cloud, rain, and fog droplets, and consider only the aerosols found in dry air, the aerosols range in size from clusters of several molecules to particles of radius of 20μ as shown in Figure 6 (Ref 44:111). In spite of the fact that aerosol concentrations are orders of magnitude less than molecular concentrations, the aerosols are very important in atmospheric transmittance of radiation. These particles scatter and absorb radiation, and in addition they affect the processes of atmospheric condensation resulting in the formation of clouds, snow, rain, and fog.

This chapter will discuss atmospheric aerosol processes in general and how these affect the scattering and absorption of radiation. This discussion is necessarily limited to those processes that limit atmospheric transmission. Its purpose is to provide a minimum background from which later conclusions may be drawn about atmospheric aerosols. For a detailed aerosol discussion, the reader is referred to References 41 and 44.

Aerosol Attenuation. The use of Mie Theory for calculations of aerosol absorption and scattering requires that the shape of the aerosol be a sphere and that certain other aerosol properties be known.

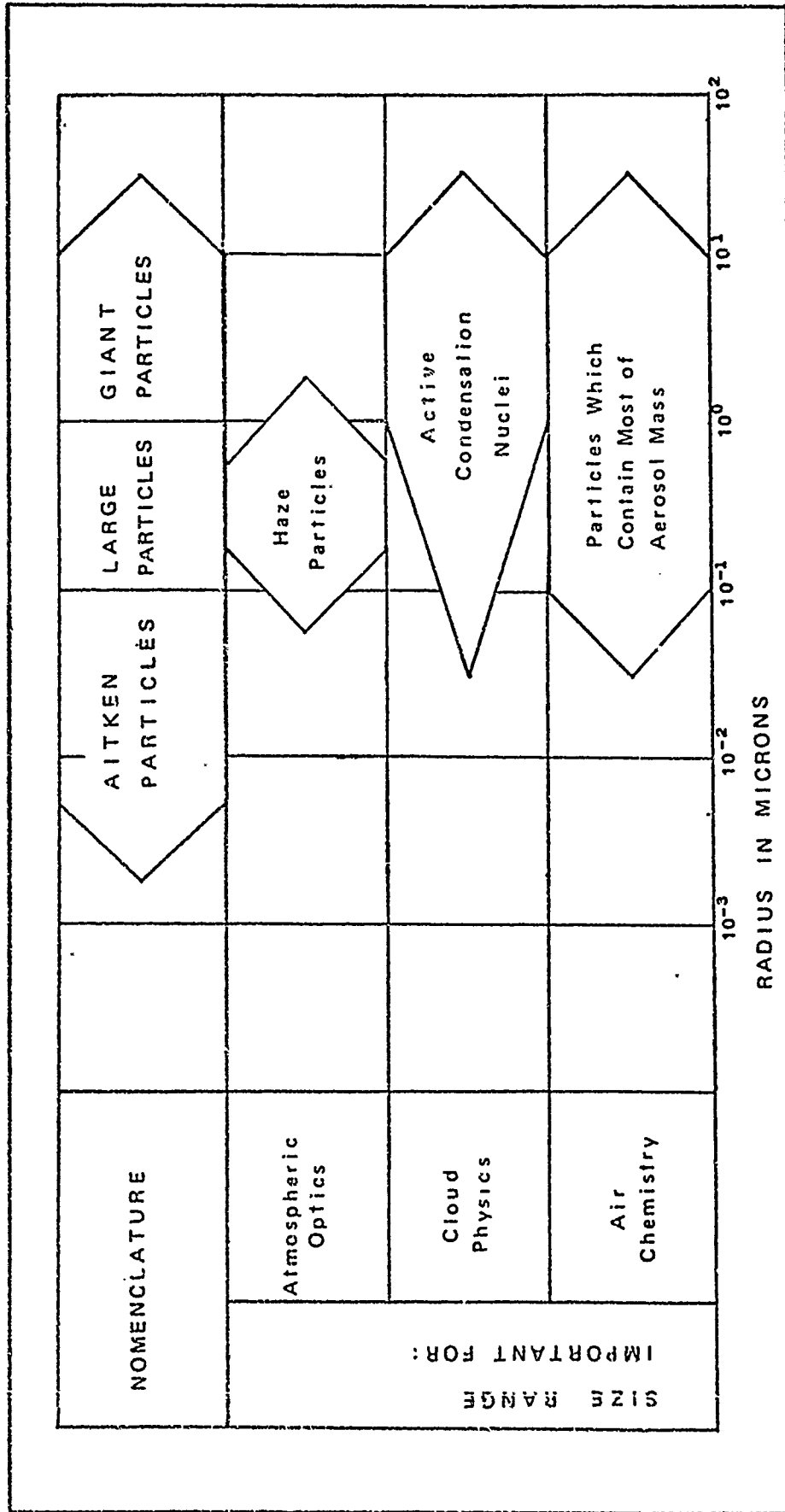


Fig. 6. Size Ranges of Aerosols (after Ref 41:112)

Mie theory is the exact determination of the intensity of radiation in the far field based on the aerosol properties and incident radiation (see Appendix B). Parameters required for this computation are the size and complex index of refraction of the particle, and the wavelength of the incident radiation. When extending this computation to a population of polydisperse particles, the size distribution is required as well as the particle number density. If all particles are not of the same composition, then the composition of particles must be associated with several particle distributions which are additive.

There are, however, three important limitations to the use of this theory. The first is that the assumption is made that all scattered radiation has the same wavelength as the incident radiation. All quantum transitions are prohibited. The second limitation is that only independent scattering is considered. Scattering by a diffuse medium is not included. In order to qualify as an independent scattering medium, the particles must be arranged in such a random or inhomogeneous fashion that the scattering of the medium is not the cooperative effect of all the particles. In addition, the particles must be separated by some minimum distance. In practical meteorological problems, this limitation is not restrictive as even in the most dense fogs the distance between particles is twenty times the radius; estimates have shown that separation distances of three times the particle radius are sufficient (Ref 62:5). The third restriction is that the effects of multiple scattering are neglected. This requires that the energy removed from the original beam be equal to sums of that removed by each individual particle;

or in other words, each individual particle is subject to the radiation of the original beam.

Formation and Removal of Particles in the Atmosphere. Particles found in the atmosphere are formed by a variety of processes. Some of these processes are man's activities, but others are strictly natural phenomena. Among the important formation processes are: (1) grinding or impaction such as produced by industrial activities; (2) breakup of liquids such as the mist caused by sea spray or a tire on wet pavement; and (3) condensation of particles in flames. Other processes serve as apparent aerosol sources but in fact are part of the aerosol evolutionary cycle: (1) coagulation of smaller particles; (2) nucleation, which is important in cloud formation; (3) reactions on the surfaces of particles resulting in particle growth; (4) breakup of large particles that occur mechanically or due to phase change; and (5) gaseous interaction with water droplets (Ref 8:160). Such a variety of formation processes produces a wide range of particle sizes and physical composition.

Other processes remove particles from the atmosphere. The larger particles are affected by gravity and settle to the earth's surface if they are not transported by advective and convective currents. Particles of all sizes are removed by impaction on plants and other objects. In addition, particles are removed by washout and rainout. Rainout refers to the loss of particulate matter by condensation and formation of precipitation. Washout refers to the interaction between precipitation droplet and aerosol particle.

Particle Size and Size Distribution (General). Such a variety of production and removal mechanisms leads to a range of possible sizes and number densities. The size distributions and densities are controlled by the production and removal mechanisms. Early measurements of aerosol led to the conclusion that aerosol distributions could be approximated by an equilibrium distribution (Ref 59:22). The distribution is the result of continual production and evolution of particles and removal of particles by the mechanisms previously discussed.

Unfortunately the measurement of aerosol sizes and number densities is extremely difficult due to the range of particle size. Until recently, measurement of the entire distribution required that several different measurement techniques be utilized simultaneously. This led to incomplete measurements and the mistaken impression that atmospheric aerosols were composed of several distinct and separate sizes of particles: Aitken particles ($r < 0.1\mu$), large particles ($0.1\mu < r < 1.0\mu$) and giant particles ($r > 1.0\mu$). In addition, many of these measurement techniques employed impactor plates (often mounted on aircraft) and then subsequent analysis in the laboratory. These techniques often led to inaccuracies because they required that the aerosol particle be removed from its natural habitat, the air. The method of collection often caused physical alteration of particle shape and the method of analysis, the electron microscope in the laboratory, often caused chemical alteration. Recently, however, improved instrumentation described in Reference 69 has given more accurate measurements of aerosol size distributions.

From the various aerosol measurements came attempts to represent the aerosol distribution as an analytical function. There are three such general distribution forms in common use: the power law, the log-normal, and the modified gamma distributions. Junge (Ref 41), Bullrich (Ref 7), Whitby (Ref 68), and others have demonstrated that the power law distribution of the form

$$\frac{dN}{d(\log r)} = Cr^{-\beta} \quad (36)$$

is a good approximation of aerosol distribution in the atmosphere (Ref 8:174). The constant C is a function of particle concentration and the power β describes the relative amounts of large and small particles; N is the total concentration of aerosol particles of radius smaller than r. Because of the wide range of particle sizes and concentrations, it is more convenient to use logarithmic scales. Hence, the log radius-number distribution is defined by (Ref 41:115):

$$n(r) = \frac{dN}{d(\log r)} \text{ cm}^{-3} \quad (37)$$

Using this notation, then the power law is most commonly expressed by

$$\frac{dn(r)}{dr} = Cr^{-v} \quad (38)$$

where $v = \beta + 1$ and β has values ranging from 2.5 to 4.0 to fit experimental data. On the average, $\beta = 3$ usually gives the best results for a range between 0.04μ and 10μ (Ref 44:108). When this distribution is used to determine scattering and the upper aerosol radius limit is ignored ($r_2 \rightarrow \infty$) then this compares quite favorably with Angstroms well-known empirical formula for the wavelength

dependence of total scattering (Ref 41:142). In addition, this power law is most useful from the standpoint that it describes the size distribution by a simple mathematical expression. One disadvantage to the power law distribution is that the boundaries must be specified and have a strong influence on the integrations and scattering calculation.

A more complex distribution is the log-normal distribution; it requires a third parameter, standard deviation, in addition to the two required by the power law distribution. This distribution, however, has the advantages that it can handle large ranges of particle sizes and it represents the extreme radii values more accurately in the integration process. This distribution also represents the particle sizes produced by several comminution processes in nature. The normalized log-normal function is usually written

$$\frac{dn(r)}{d(\log r)} = \left(\frac{1}{(2\pi)^{\frac{1}{2}} \log \sigma_g} \right) e^{-\left[\frac{(\log r - \log r_g)^2}{2 \log^2 \sigma_g} \right]} \quad (39)$$

where σ_g and r_g are the geometric standard deviation and mean radius respectively and $dn(r)$ is the normalized number of particles between radii r and $r + dr$ (Ref 8:169).

The modified gamma distribution has also been used to describe wet and dry aerosol size distributions (Ref 17 and 18). The wet aerosols include rain, hail and clouds and the dry aerosols are haze. In general, the modified gamma is mathematically as advantageous as the log-normal distribution, but the modified gamma has not been

linked to any specific natural processes. In addition, it has more parameters which are not relatable to any aerosol property. The modified gamma distribution, however, offers the advantage that the one generalized distribution describes the various meteorological phenomena. This family of distributions is described by

$$n(r) = ar^{\alpha} \exp(-br^{\sigma})$$

or

$$\frac{dn(r)}{dr} = ar^{(\alpha-1)} (\alpha-\sigma br^{\sigma}) \exp(-br^{\sigma}) \quad (40)$$

where a , b , and σ are positive real constants and α is a positive integer (Ref 17:15,76).

Although there are other distributions used to describe aerosol measurements, these three are the most common and most widely accepted in describing aerosol distributions. The distributions will now be discussed in terms of applicability to measured results and physical considerations.

Particle Size and Size Distribution (Specific). The particle size distribution and number density is controlled by the particular production and removal mechanisms. This statement necessarily implies that if there are different production mechanisms associated with various geographical locations, then it can be expected that there would not be one worldwide aerosol distribution function. In fact, the distribution function at one geographical location would be to some degree a function of the local aerosol production mechanisms.

If it were not for the constant mixing of the atmosphere, then one or more generalized mathematical functions would not be descriptive

of the atmospheric aerosol. In fact, description of atmospheric aerosol would be a point by point computation. Fortunately, there is continual smoothing of the aerosol distribution function due to the transport of aerosols and continual atmospheric modification processes. Nevertheless, local aerosol sources are important but not for large scale distributions.

There is, for example, a difference in the general aerosol distribution and number density found over a large land mass and that found over the oceans. Because of advective and convective currents, there is no sharp division between the maritime distribution and continental distributions. In fact, aerosols of maritime origin have been detected thousand of miles inland; likewise, continental particles are measured in the center of the oceans (Ref 41:176). In like manner, an area with a large amount of industrial activity would have a different aerosol size distribution and number density than a region that was free of such activity. On the smaller scale, the area around a large industrial city may be expected to have a slightly different distribution than a rural area located some distance away, though mixing will provide continual smoothing of the different distributions and particle number densities.

There are two distributions that have been used extensively to describe global dry aerosol distributions. They are the Deirmendjian Continental and Maritime Haze Distributions and variations of these original models. The Continental Haze model uses the power law with exponent of four. The number of large particles compared to the small particles is described by the exponential power. The Maritime model is a modified gamma distribution. It describes the

aerosol distribution of extremely maritime air and its use over land areas is limited to coastal regions. In general, the differences in the air masses are as follows: (1) the number of particles in the maritime air is less (usually substantially less) than the continental air; (2) continental air has more Aitken particles by orders of magnitude; and (3) a greater portion of the maritime particles than continental particles are in the large particle range. The existence of two generalized distributions, maritime and continental, as well as these general distribution characteristics, is well accepted. Such model distributions are useful quantitatively, but it is important to realize that these are characteristic distributions and that in specific instances, conditions may deviate considerably from these mean distributions.

There are two important conclusions that may be drawn from this discussion. One is that aerosol distributions in the atmosphere are affected by local aerosol sources. The other is that aerosol distributions tend to smooth out yielding generalized aerosol distributions for larger geographical regions provided the air mass circulates. Point sources of aerosols are still important, but if there is sufficient circulation a smoothing or quasi-steady state distribution is approached. Regardless, it becomes apparent that geographical location and air mass circulation are extremely important in determining aerosol size distribution and number of particles.

Particle Composition. Aerosol chemical composition is important in determining the complex refractive index for Mie Theory calculations. The chemical composition of the aerosol is determined by the source and

evolutionary process of the aerosol. Several extensive investigations have been made of the effect of both of these processes on the aerosol composition. These investigations, like the size measurements, have been hampered by the difficult nature of the task of measuring composition.

One of the difficulties of determining composition is the inability to measure composition of the smaller (Aitken) particles. In general, the composition of large and giant particles is measured and the composition of the smaller particles is assumed to be similar. Several workers have measured the distillate from rainwater or other forms of precipitation and assumed this measurement was representative of the dry aerosol. This method also fails to measure the small particle composition, because condensation nuclei are limited in large to the giant and large particles although there may be some small particle contribution due to washout. Despite these limitations, a remarkable feature of these investigations is that their findings are surprisingly similar. In addition, it is the large and giant particles that affect the transmission of radiation in the visible and infrared regions.

Aerosol is composed of particles from a variety of sources. Average global aerosol is composed of the following general classes of compounds: Sulfur, Nitrogen, Chlorine, soils, and combustion products (Ref 59:12). Table IV shows estimates of the magnitude of particle formation ($r < 20\mu$) for the surface layer of the atmosphere. The percentage composition of these compounds in various aerosol measurements is found to differ from location to location. Aerosol composition over ocean areas is found to have a large chloride component.

Table IV

Estimates of Particle Formation in Millions of Metric
Tons Per Year for Particles < 20 μ Radius
(Ref 40:189)

<u>Natural</u>	
Soil and rock debris ^a	100-500
Forest fires and slash-burning debris ^a	3-150
Sea salt	(300)
Volcanic debris	25-150
Particles formed from gaseous emissions:	
Sulfate from H ₂ S	130-200
Ammonium salts from NH ₃	80-270
Nitrate from NO _x	60-430
Hydrocarbons from plant exudations	75-200
Subtotal	773-2200
<u>Man-Made</u>	
Particles (direct emissions)	10-90
Particles formed from gaseous emissions:	
Sulfate from SO ₂	130-200
Nitrate from NO _x	30-35
Hydrocarbons	15-90
Subtotal	185-415
Total	958-2615

^a Includes man-made contributions

The existence of chlorides is not limited to maritime areas, however, nor does it suggest a particle of maritime origin since industrial activities have been linked to chloride aerosol production (Ref 41: 170).

The physical constitution of aerosol particles in the atmosphere varies between the extremes of a dry insoluble dust particle and a droplet of completely soluble material. In general, though, particles consist of mixtures of many materials, both soluble and insoluble. Throughout the particle lifetime, it is subject to the influence of other particles through the processes of coalescence and coagulation. It is also subject to many atmospheric gases, some of them trace gases, which are known to play an important role in aerosol evolution. In fact, it is now believed that perhaps the majority of particles in suspension in the atmosphere are secondary products formed from material which entered the atmosphere as a gas (Ref 40:192). Some idea of the complexity of the problem may be illustrated by Table V.

Since the particle is changing in time and can be affected by any of a number of processes, and generally its definite origin is unknown, the concept of a mixed particle evolved. This is the most general concept for an atmospheric aerosol particle. This concept attaches an average composition or average index of refraction to the entire distribution of particles. The value of this concept is the limitation it places on determining a distinct aerosol distribution for each chemical composition.

Table V

Possible Atmospheric Gases From Which Particles May Be
Formed Through Secondary Reactions
(from Ref 8:4,5)

<u>Symbol</u>	<u>Name</u>
N ₂	Nitrogen
O ₂	Oxygen
⁴⁰ Ar	Argon
CO ₂	Carbon dioxide
Ne	Neon
He	Helium
CH ₄	Methane
Kr	Krypton
H ₂	Hydrogen
Xe	Xenon
CO	Carbon monoxide
N ₂ O	Nitrous oxide
SO ₂	Sulfur dioxide
NO	Nitric oxide
NO ₂	Nitrogen dioxide
HCHO	Formaldehyde
NH ₃	Ammonia
O ₃	Ozone

Complex Index of Refraction. Since particles are being formed by $g \rightarrow s$ conversion and are evolving through gas absorption, condensation and coagulation, only a relatively few measurements have been made from which the index of refraction can be inferred (Ref 59:15). Bullrich (Ref 41:114) calculated a real index of refraction of 1.54 based on assumed atmospheric constituents. Volz (Ref 65:822) computed a real refractive index of 1.53 based on distillation residues from rain water. Recent measurements shown in Table VI seem to indicate that these earlier determinations of the real refractive index were in fact accurate. The wavelength dependence of the refractive index (real and imaginary part) is illustrated in Table VI.

The determination of the imaginary (absorptive) part of the refractive index is less well established. Values for the absorptive part at 1.0μ range from .072 (Fisher 1971) to approximately .015 (Ref 66) as shown by comparing the figures in Table VI. The determination of the complex index is extremely difficult and errors of from 10% to an order of magnitude can be expected in these values (Ref 59:15).

Particle Growth. Some of the difficulty in determining aerosol index of refraction and size distribution is attributable to the growth of atmospheric aerosol with increase in relative humidity. The water vapor affects the dry particle in two ways. One, it condenses on the particles thus causing the individual particles to increase in size. This growth of the particles affects the entire size distribution. Second, the water vapor condensing on the particle causes a change in the complex index of refraction.

Table VI

Refractive Indices (Real and Imaginary Parts)

		Wavelength (Microns)			Source
		$\frac{.40}{.70}$	$\frac{.55}{1.61}$	$\frac{1.00}{1.61}$	
Model 1 Mainz, Germany Summer, 1966	Real	1.64	1.62	1.61*	Hanel
	Imag.	.044	.051	.072	Fischer
Model 5 Mainz, Germany Jan 1970	Real	1.57	1.55	1.53	Hanel
	Imag.	.042	.048	.068	Fischer
Model 6 Hohenpeissenberg Germany Summer 1970	Real	1.53	1.51	1.49*	Hanel
	Imag.	.013	.015	.020	Fischer
Global** Water Soluble	Real	1.53	1.53	1.52	Volz
	Imag.	.005	.006	.016	

* Data of Hanel and Fischer extend only to 1.00μ . Values for 1.06μ have been linearly extended.

** Values published by Volz are not at .40, .55, .70, 1.00. Interpolation was necessary to obtain these values.

Present studies indicate that particle growth is determined by a number of factors. One of the most important factors is the original particle composition--soluble or insoluble material or mixture. Another is the particle shape, although the shape of the atmospheric aerosol is usually *assumed* to be spherical. Another factor affecting particle growth is the relative humidity change and starting point (size).

Particle growth raises a number of questions in terms of Mie theory calculations. Three questions that must be considered are:

- (1) How does the index of refraction change with relative humidity?
- (2) How is the particle size distribution affected by particle growth?
- and (3) How is original composition important to particle growth?

The first and third questions may be answered together because the particle composition is directly related to the index of refraction. There is a range of particle compositions between totally water soluble material and insoluble material. Consider the case of the water soluble material first. As water condenses on the outer surface of the particle, a shell of water is formed on the sphere. As the relative humidity increases, a point is reached at which the vapor pressure of the aqueous solution at the surface is less than the vapor pressure of water in the ambient air. At this point, water vapor from the air is collected until the substance is dissolved and in equilibrium with the air (Ref 8:222). During this period the aerosol experiences a tremendous growth. This description is valid for a pure soluble material such as sodium chloride. This process is called deliquescence. If aerosols were all pure soluble materials, this particle growth would be a very complex phenomena. In fact, the

measurement of growth rates that are less rapid than pure soluble materials supports the concept of the mixed particle.

On the other hand, the dry aerosol particle may be insoluble and grow very little. In any case, the question of how to deal with the particle as water is condensed about it remains. There are two distinct possibilities. One involves working the problem of a sphere covered with a spherical water shell. In other words, a two step problem with separate indices of refraction. The second involves working the one sphere problem but changing the overall refractive index as the sphere grows in size.

This second method is more acceptable to the mixed particle concept (not to mention the increased difficulty in problem solution if the first method is utilized). It is, however, important to realize the two important conditions that must be fulfilled in order to ignore shell structure for haze calculations: (1) the mixing ratios of the components must differ only slightly; and (2) the radius of the particle must approximate the wavelength of the incident radiation (Ref 44:115). That is, if these two conditions are met, we assume the refractive index can be determined from the mixing ratio of its components.

The second major question is just as complex. Since the particle sizes are different they grow at different rates because of the difference in curvature at their surfaces. If their compositions were different then the problem would be compounded. Assuming that the particles are mixed in composition allows an approximation to the increase in the size distribution. If no particles are being added

or removed from the distribution, then for relative humidities up to 95% the growth rate by particle size is rather uniform. This is borne out by experimental measurement as shown in Table VII. Beyond 95% relative humidity (R.H.) the larger particles grow more rapidly, and hence the large and giant particles become the fog and cloud droplets.

Table VII

Particle Growth With Relative Humidity (RH):
 Ratio r/r_0 of Radii of Wet (r) and Dry (r_0) Aerosol Particles
 Radii (r_0) Given in Microns (Ref 7:547)

r_0 (μm)	0.04	0.1	1	10
RH	r/r_0			
0	1	1	1	1
0.3	1.038	1.040	1.042	1.042
0.6	1.153	1.159	1.165	1.165
0.8	1.400	1.414	1.426	1.426
0.9	1.656	1.695	1.720	1.720
0.95	1.93	2.01	2.05	2.06
0.975	2.29	2.48	2.58	2.59
0.99	2.79	3.19	3.45	3.48
0.995	3.13	3.83	4.30	4.36
0.998	3.48	4.69	5.81	5.91

Yet another particle growth mechanism is coagulation. This process effectively forms the lower limit of particle sizes. In a stagnant or equilibrium case where the production of small (Aitken) particles has ceased, the particle size distribution is shifted to the larger particle sizes as shown in Figure 7. This growth mechanism was convincingly demonstrated in the comprehensive 1969 Los Angeles Smog Experiment (Ref 68:186-196). This growth mechanism is not as important as it might seem because it affects largely the inefficient scatterers for our purposes.

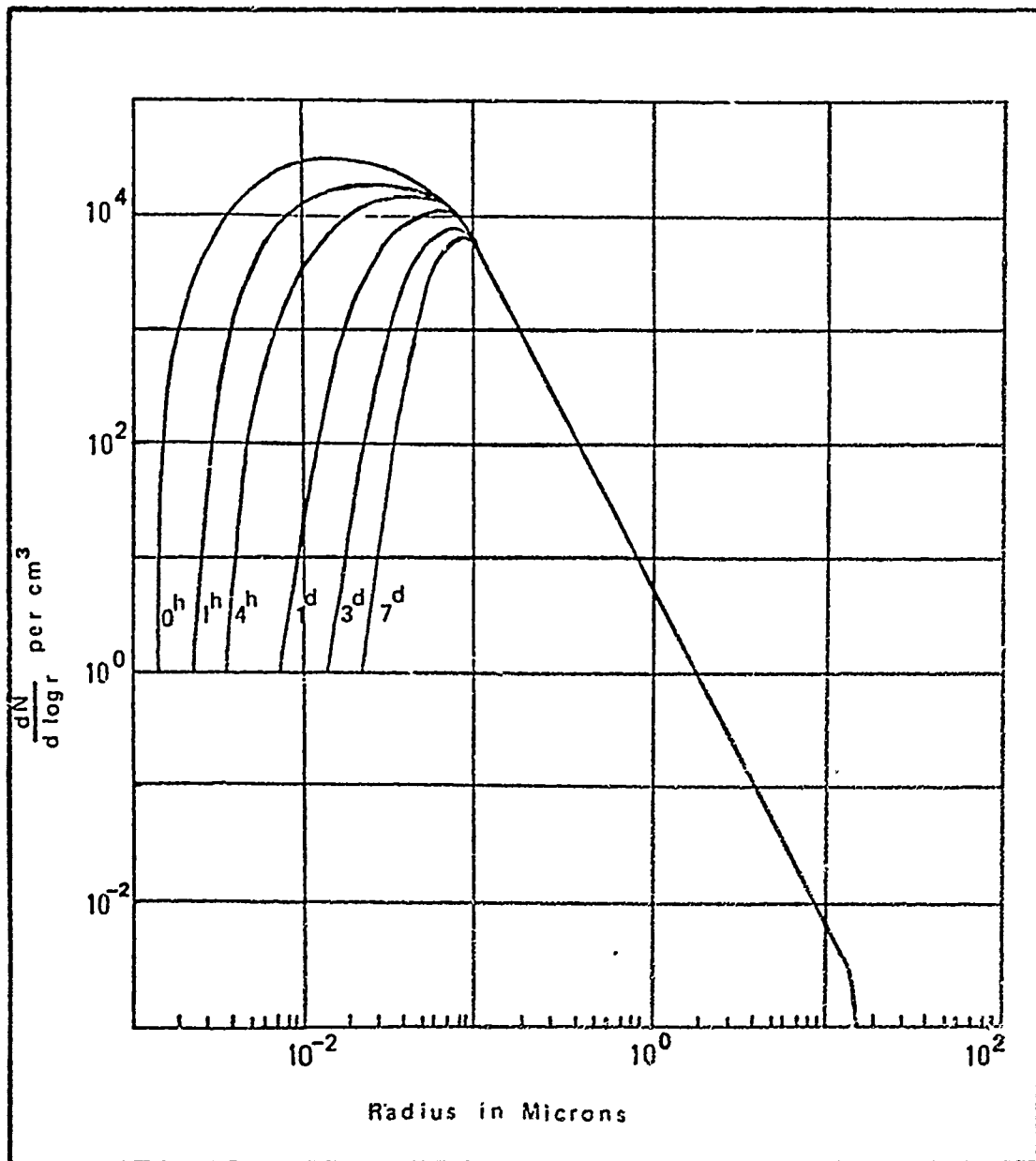


Fig. 7. Particle Size Distribution Shift Due to Coagulation. Superscript h refers to hours, d to days (after Ref 41:130)

Vertical Distribution. The particle size distributions tend to remain constant with increase in altitude except for particles with radii larger than 1μ . A decrease in percentage concentration of these larger particles is noticeable in the absence of convective mixing currents that would force them aloft (Ref 41:127). In general, there is a decrease in particle concentration with increase in altitude, and this is rather uniform for all particle sizes (Ref 41:128).

The vertical aerosol distribution, however, is affected by a number of factors. One of the most important is the aerosol size distribution at the surface and the particular production mechanisms. Another is the origin and history of the air mass. Others are the vertical temperature and pressure profiles and the strength of the vertical mixing.

Since most particle sources are on land masses then the lower layers of the continents are the most polluted (naturally and artificially) in terms of aerosol concentrations. The vertical extent of this layer over the continental areas varies by season and geographical region. The height or extent of the mixing layer depends on existing and past meteorological conditions. It has been well documented how sensitive particle distributions reflect the vertical temperature distribution. Haze layers beneath temperature inversions are a frequent, and quite striking, phenomena (Ref 41:183).

Over ocean areas and above the continental mixing layer the aerosol concentrations are noticeably smaller than in the mixing layer. In fact, the distribution above the mixing layer is fairly constant and differs only from the maritime distribution in numbers of large particles (Ref 40:202). This background distribution is representative

of the troposphere above the mixing layer (over ocean and continent) and is considered a typical very clean air distribution. The vertical distribution of aerosols, however, is the subject of a more lengthy discussion later in this paper.

VI. Aerosol Attenuation for Horizontal Path at Ground Level

The previous chapter discussed the physical aerosol mechanisms and their relationship to aerosol attenuation. The purpose of this chapter is to discuss aerosol attenuation models for application to a specific geographical region. Existing models are evaluated on the basis of their suitability for use in describing aerosol attenuation over continental Germany. Aerosol attenuation, as predicted by the model, is then linked to meteorological observables.

Particle Size Distribution

Several different particle size distributions have been used successfully by various authors to explain measured attenuation values. In general, all distributions are the result of aerosol attenuation measurements. Particle size distributions are chosen on the basis of the best analytical fit to data. Other quantities such as the number of particles and the refractive index of the particles have been difficult to obtain for reasons discussed in Chapter V. In addition, these quantities are not always measured concurrently with the attenuation, and therefore determination of a *unique* size distribution has been quite complicated.

An example of this difficulty is the set of attenuation coefficients described in Reference 14. This Naval Research Laboratory (NRL) project involved attenuation measurements taken over two over-water paths in the Chesapeake Bay area from April, 1959, to January, 1960, for various meteorological conditions. Figure 8 shows typical reported experimental scattering curves from this report.

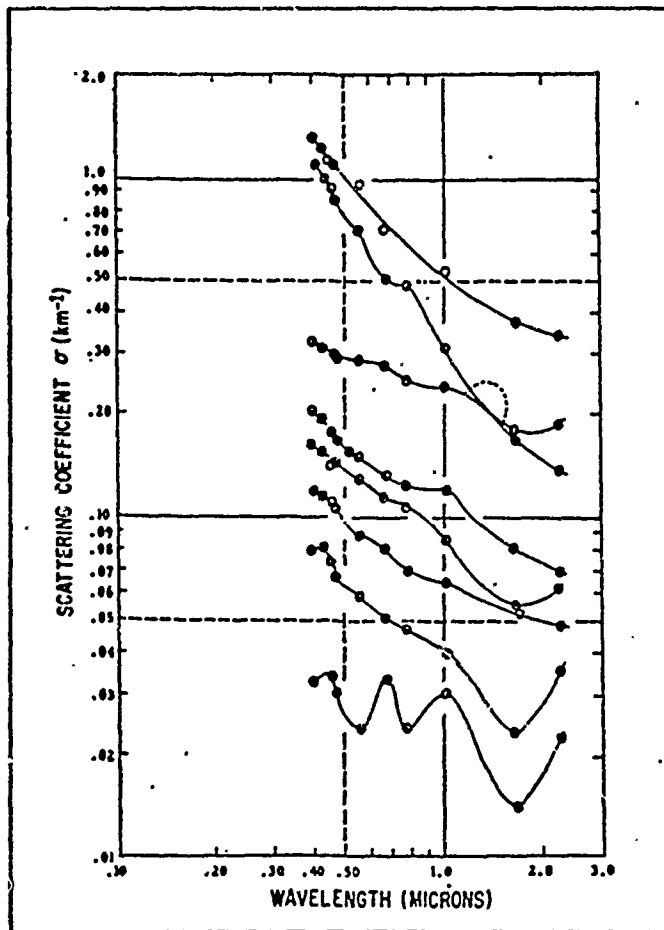


Fig. 8. Typical Experimental Aerosol Scattering Coefficient Curves for Meteorological Ranges of 4 to 160 km (Ref 14:12)

The difficulty in describing analytically this set of measurements by one aerosol size distribution is apparent from the figure. Reference 72 analyzes the thirty-six reported observations from this project and classifies the resultant size distributions in no less than five categories.

To some degree, this difficulty has been exaggerated, for the NRL project was accomplished over a large body of water and hence in an area where a mixing of two general distributions, maritime and continental, is common. In fact, one of the findings of the report was that the aerosol size distribution above or near water can generally be considered as having a Junge-type distribution plus a small component of larger particles (Ref 15:551).

For most of Germany, however, the assumptions of a generalized continental particle size distribution is realistic (Ref 30). Areas of Germany that border large bodies of water such as the Baltic Coastline are likely to have distributions that are similar to the composite distributions measured at Chesapeake Bay. For the remainder of Germany, the aerosol size distribution may be described approximately using a form of power law described in Chapter V. This generalized distribution, of course, is modified where local aerosol sources abound (large cities or industrial complexes).

A study of general air mass movement and source regions for Europe supports the theory of a continental aerosol distribution. A study of European air masses and their source regions with particular emphasis on Germany was conducted by the German meteorologist Schinze and described in Reference 9. Even the maritime-polar air (mp) which is a predominant air mass in central and western Europe is extensively

modified by transport across land areas (Ref 9:282).

Additional evidence which supports the use of a continental distribution is the set of attenuation models and measurements reported by Reference 7 and Reference 34 for locations in Germany. These measurements were modeled using a straight power law and a Deirmendjian type continental haze model. The use of both will be discussed in the next section.

Analysis of Size Distributions

If a relationship is desired between a meteorological observation recorded in the visible and attenuation at another wavelength, then using Mie theory and an assumed aerosol size distribution the relationship is approximately determined. The use of the word approximately is important here, for the index of refraction as we shall later see does have some effect on this relationship.

Additionally, as long as the number of particles is unknown, then a theoretical determination of aerosol attenuation using Mie theory yields only a relative scattering coefficient. Since the total particle density is essentially unobtainable even with today's improved equipment, then each size distribution is normalized such that the attenuation is the attenuation given per particle per unit volume. This concept is used throughout this analysis of the different particle size distributions. For the present, the total particle density is unimportant. The important factors to be analyzed are the size distribution (with respect to the wavelengths of interest) and the particle index of refraction.

Using exact Mie theory calculations as described in Appendix B, the aerosol attenuation coefficients per particle per cm^3 per km

path length were computed for wavelengths from $.40\mu$ to 1.0636μ . Assumed indices of refraction for the different wavelengths are given in Table VIII.

Table VIII

Assumed Indices of Refraction Values Obtained
by Taking Mathematical Average of Models 5 and 6 in Table VI

	Wavelengths in Microns				
	<u>.40</u>	<u>.55</u>	<u>.70</u>	<u>1.00</u>	<u>1.0636</u>
R	1.55	1.53	1.52	1.51	1.51
I	.022	.031	.035	.044	.046

R = Real Part
I = Imaginary Part

Using these indices, aerosol attenuation coefficients were compared for the different distributions. The different size distributions investigated were: (1) Deirmendjian Maritime Haze; (2) Deirmendjian Haze C; (3) A combination distribution using varying contributions of the two components--Maritime Haze and Haze C; (4) The modified Deirmendjian Haze C used by AFCRL; (5) Deirmendjian Haze L; and (6) a straight power law. The exact distributions used are given in Table IX.

Table IX
Aerosol Size Distributions
Radius, r, in Microns

<u>Model</u>	<u>Distribution</u>	
Deirmendjian Maritime	$5.333 \times 10^6 \times r \times e$	$(-8.9443 \times \sqrt{r})$
Deirmendjian Continental .02 μ \rightarrow 20 μ	0 9.677419×10^4 $9.677419 \times r^{-4}$	$r < .02\mu$ $.02\mu \leq r \leq .1\mu$ $.1\mu < r \leq 20\mu$
Maritime	$5.333 \times 10^6 \times r \times e$	$(-8.9443 \times \sqrt{r})$ $r < .02\mu$
+	$5.333 \times 10^6 \times r \times e$	$(-8.9443 \times \sqrt{r})$
Continental	$5.333 \times 10^6 \times r \times e$	$(-8.9443 \times \sqrt{r})$ $.02\mu \leq r \leq .1\mu$ $+9.677419 \times r^{-4}$ $.1\mu < r < 20\mu$
AFCL Continental	$8.823532 \times r^{-4}$ 8.823532×10^4	$.1\mu \leq r \leq 10\mu$ $r < .1\mu$
Deirmendjian Haze L	$4.9757 \times 10^8 \times r^{+2} \times e$	$(-15.1186 \sqrt{r})$
Power Law	$8.1 \times 10^{-1} \times r^{-4}$	$.03\mu \leq r \leq 20\mu$

The upper and lower bounds of integration were chosen as 20μ and $.003\mu$ respectively except in the case of the power law where $.03$ was used as the lower limit. The published Deirmendjian Haze C distribution was used except the upper bound was extended to 20μ .

Comparison of the distributions yields the following general characteristics as shown in Figure 9. A 100% Maritime distribution gives the highest per particle attenuation; this attenuation increases as the wavelength is increased from the visible to near IR then begins to drop off around 1μ such that the aerosol attenuation at 1.0636μ is approximately equal to the attenuation at $.55\mu$. As the percentage of maritime contribution is reduced and the continental increased then the attenuation at 1.0636μ becomes less than that at $.55\mu$, although this decrease is not significant until the percentage maritime is less than 10%. This suggests that for regions such as coastal regions and ocean areas the aerosol attenuation at 1.0636μ may not be significantly less than that in the visible spectrum.

The attenuation per particle increases by approximately one order of magnitude from a distribution containing 10% maritime and 90% continental to a distribution of 100% maritime. Haze L was found to approximate a distribution of about 40% maritime and 60% continental with the exception that there was a noticeable slope to the curve. That is, attenuation was less at 1.0636μ than at $.55\mu$.

A straight power law was used from $.03\mu$ to 20μ to compare the attenuation coefficients against those computed using Deirmendjian Haze C. The resulting attenuation coefficients were approximately one order of magnitude less than those computed for Haze C but the slope of the resulting curve was essentially identical to the Haze C slope.

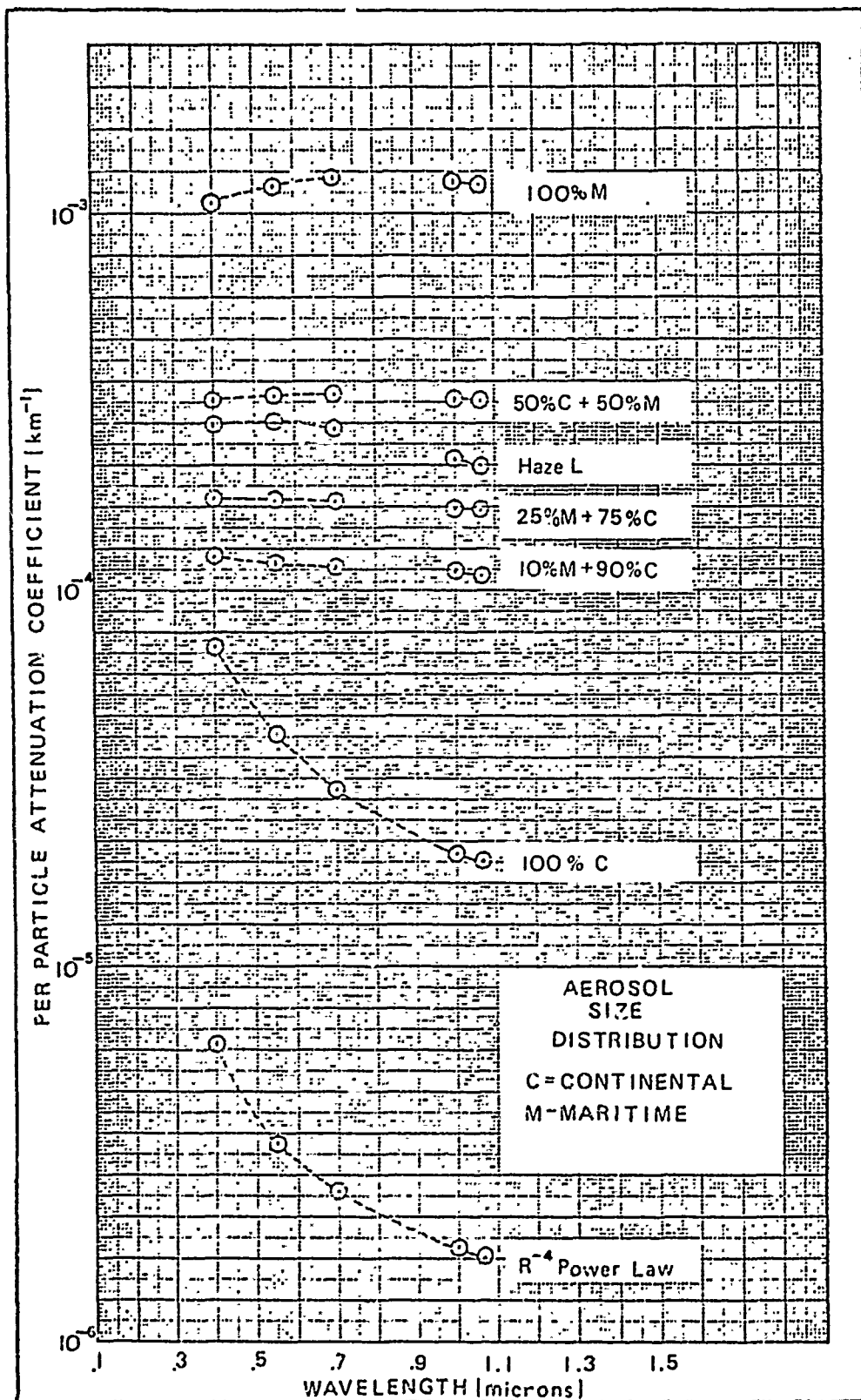


Fig. 9. Aerosol Attenuation Coefficient Curves for Different Aerosol Size Distributions

Other powers were not investigated by this author, but such an investigation has been made in Reference 14 and results are shown in Figure 10. The power $r = -3$ in this figure corresponds to the integrated power law (R^{-4}); that is, the distributions are identical with the exception of the lower limit of $.01\mu$ used in the NRL investigation. There is the additional difference of the index of refraction which for the curves in Figure 10 is assumed to be 1.33 with no imaginary part. Although the curves from Figure 10 do not yield attenuation coefficients that are exactly comparable with those computed here, their importance is that they display the relative change with respect to wavelength of the attenuation coefficient as the power is changed on the size distribution.

An additional analysis involved the change of the lower limit of the Haze C distribution to $.02\mu$. The result was a subsequent reduction in the attenuation coefficients which is expected since the distribution is normalized. There was, however, no significant change in the slope of the attenuation coefficient curve as shown in Figure 9.

Two distributions were used to check the effect of changing the upper limit of the Haze C type distribution: A Haze C model with a lower limit of $.02\mu$ (such as the one used by AFCRL) and a Haze C with lower limit $.03\mu$, the lower limit used by Deirmendjian (Ref 16: 406). The assumed indices of refraction are those of water and are given in Table X with the computed attenuation coefficients. This computation allowed a check with published values for the Deirmendjian Haze C ($.03\mu-5\mu$) (Ref 18:189).

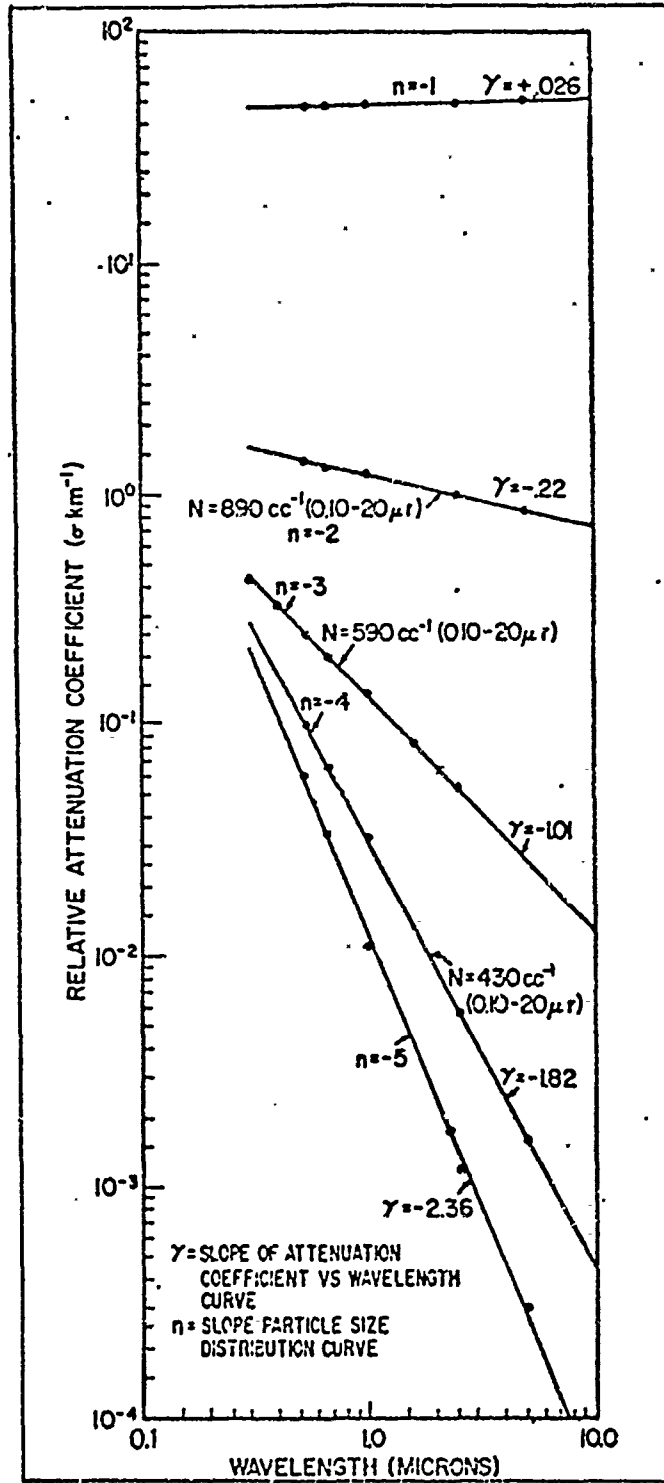


Fig. 10. Effect of Changing Power Law on Slopes of Attenuation Curves (Ref 14:12)

Table X

Sensitivity Analyses on Effect
of Changing Limits of Integration*

Wavelength in Microns	Index of Refraction		Attenuation Coefficient of Distribution	
	Real	Imag	.02 → 5 μ	.03 → 5 μ
.45	1.34	0	.478E-04	.524E-04
.55	1.34	0	.396E-04	.434E-04
.70	1.33	0	.304E-04	.333E-04
1.0636	1.33	0	.197E-04	.217E-04
1.61	1.315	0	.121E-04	.132E-04
			.02 → 10 μ	.03 → 10 μ
.45	1.34	0	.484E-04	.531E-04
.55	1.34	0	.402E-04	.441E-04
.70	1.33	0	.310E-04	.340E-04
1.0636	1.33	0	.203E-04	.223E-04
1.61	1.315	0	.127E-04	.139E-04
			.02 → 20 μ	.03 → 20 μ
.45	1.34	0	.487E-04	.534E-04
.55	1.34	0	.404E-04	.444E-04
.70	1.33	0	.312E-04	.343E-04
1.0636	1.33	0	.206E-04	.226E-04
1.61	1.315	0	.130E-04	.142E-04

*Values determined for Continental Haze Model

As the upper limit is increased the ratio of the attenuation coefficient at .55 μ to the one at 1.0636 μ decreases. The addition of larger particles to the distribution increases the attenuation more at the longer wavelength.

Analysis of Refractive Index

The two distributions, $.03\mu$ to 20μ and $.02\mu$ to 20μ , computed with the refractive index of water, yield a comparison with the same distributions computed with a different refractive index assumed in the previous section. A comparison of the resulting attenuation coefficients demonstrates the fact that for an assumed size distribution an increase in the refractive index results in a decrease in the ratio of the coefficient at $.55\mu$ to the one at 1.0636μ , a fact explainable by Mie Theory.

Additional sensitivity studies were conducted on the imaginary part of the refractive index holding the real part constant. Results are shown in Table XI.

Table XI
Effect of Changing Imaginary Part of the
Refractive Index Holding Real Part Constant

<u>Wavelength</u>	<u>Index of Refraction</u> <u>Real</u>	<u>Imag</u>	<u>Total Attenuation</u> <u>Coefficient</u>	<u>Absorption</u> <u>Coefficient</u>
.55	1.54	.005	.657E-04	.034E-04
.55	1.54	.011	.658E-04	.063E-04
.55	1.54	.035	.664E-04	.141E-04
.55	1.54	.048	.667E-04	.173E-04
1.0636	1.54	.017	.356E-04	.049E-04
1.0636	1.54	.022	.358E-04	.059E-04
1.0636	1.54	.033	.362E-04	.079E-04
1.0636	1.54	.045	.367E-04	.098E-04
1.0636	1.54	.068	.377E-04	.128E-04

The values selected for the imaginary part were those reported in references 66 and 34, the later of which were taken from measurements from two locations in Germany. In addition, calculations were made for mean imaginary indices of refraction. The results show that the various reported values for the imaginary part do not significantly

affect the overall computed attenuation. It must also be noted that the reported values for this wavelength region are not wildly varying so a comparison of lowest reported values at one wavelength (.55 μ) to the highest reported values at another (1.0636 μ) is not valid.

A more important analysis was that conducted using the refractive indices reported by Hanel in Reference 34 for measured German aerosol and values provided by Volz for water soluble aerosol. The modified Deirmendjian Haze C size distribution was used (.03 μ to 20 μ). Results of the computation show that later reported values (Model 5, Model 6, Volz) are rather consistent. The computed ratios of the coefficient at .55 μ to the coefficient at 1.0636 μ showed a trend. The values computed from the indices reported at Mainz, Germany showed close correlation as shown in Table XII. The computed values for indices provided by Volz and those from Hanel's Model 6 showed some similarity. These later values are probably from a more natural aerosol since the Model 6 site was elevated and away from urban influence, and the values provided by Volz are from a variety of sources (Ref 64).

The difference in refractive indices reported by Volz, Hanel, and Fischer (Ref 31:95) may well be due to the fact that European aerosols are modified by carbons (soot) and fossil fuel wastes (Ref 60). An investigation of the aerosol absorption coefficient in New York City reported values similar to those reported in Germany (Ref 12).

Based on the analysis of the refractive indices previously described and comparison of various reported values, this author elected to use an average of the indices reported for Models 5 and 6 (Ref 34:379) as the aerosol index for continental Germany.

Table XII

Per Particle Aerosol Attenuation Coefficients
for Continental Haze Model (.03 μ to 20 μ)
for Reported Indices of Refraction

Model	Wavelength in Microns	Index of Refraction*		Attenuation Coefficient
		Real	Imag.	
Model 1 (Mainz)	.40	1.64	.044	.952E-04
	.55	1.62	.051	.737E-04
	.70	1.61	.058	.595E-04
	1.00	1.61	.072	.436E-04
	1.0636	1.61	.077	.414E-04
Model 5 (Mainz)	.40	1.57	.042	.883E-04
	.55	1.55	.048	.676E-04
	.70	1.54	.055	.544E-04
	1.00	1.53	.068	.394E-04
	1.0636	1.53	.072	.374E-04
Model 6 (1000m above sea level Germany)	.40	1.53	.013	.842E-04
	.55	1.51	.015	.630E-04
	.70	1.50	.016	.499E-04
	1.00	1.49	.020	.351E-04
	1.0636	1.49	.021	.331E-04
Volz (Water Soluble)	.40	1.53	.005	.843E-04
	.55	1.53	.006	.647E-04
	.70	1.53	.007	.519E-04
	1.00	1.52	.016	.366E-04
	1.0636	1.52	.017	.345E-04
Average of Models 5 and 6	.40	1.55	.022	.864E-04
	.55	1.53	.031	.654E-04
	.70	1.52	.035	.522E-04
	1.00	1.51	.044	.373E-04
	1.0636	1.51	.046	.353E-04

*Values of refractive indices are those used in Table VI.

These reported values were extrapolated to 1.0636μ by this author. When these average values are used in the modified Haze C distribution, the resulting attenuation coefficients closely approximate those computed using the Volz indices:

Aerosol Model

This computation model assumes a size distribution of the form of the Deirmendjian Haze C with the exception of the upper limit which is extended to 20μ . The index of refraction varies with wavelength but is an average of the values reported by Hanel. Resulting Mie Theory computations shows the aerosol attenuation coefficient at 1.0636μ to be related to the aerosol attenuation coefficient at $.55\mu$ by

$$\sigma_a(1.0636\mu) = .5394 \sigma_a(.55\mu) \quad (41)$$

where the constant $.5394$ is determined uniquely by Mie Theory for an assumed distribution and the average indices of refraction shown in Table XII. Constants for other distributions are given in Table XIII.

Effect of Relative Humidity on Model

The effect of increasing relative humidity on aerosol size distributions and index of refraction was discussed in Chapter 5. This effect of particle growth (and shift in size distribution) and change in index of refraction has been investigated by several workers. These investigations may be classified as either computer simulation programs or as experimental determinations.

Notable among the former investigations are the works of Barnhardt and Stræete (Ref 2) and John A. Hodges (Ref 38).

Table XIII

Ratios of 1.0636 μ Attenuation Coefficient to .55 μ Attenuation Coefficient for Several Aerosol Distributions with Same Assumed Refractive Indices*

Aerosol Distribution	$\frac{\sigma(1.0636\mu)}{\sigma(.55\mu)}$
Haze L	.796
Power Law $R^{-4}(.1\mu \rightarrow 20\mu)$.538
Maritime (.003 $\mu \rightarrow 20\mu$)	1.004
25% Maritime + 75% Continental	.932
50% Maritime + 50% Continental	.977

*Refractive Indices used are the Average Model Indices from Table XII.

Both provide a growth factor computation based on the fractional growth of a particle developed by Wright in 1939. Using the growth factor, a new distribution is computed based on the relative humidity and assumptions of the physical rate of growth. Computations of one growth factor for the entire distribution also assumes that all particles grow at the same rate. In addition, these programs compute a real index of refraction, which is an analytical fit to the data of Bulirich (Ref 2: 1339).

This method was rejected for use in this report for three reasons: (1) the technique involved assumptions that were not necessarily applicable to Germany (indices of refraction); (2) the results of the technique have not yet been compared to measured data; and (3) the technique involved lengthy computer programming. Instead, the results of aerosol measurements were investigated.

Only one of the reports investigated offered the relationship of particle growth at various wavelengths. This information is imperative for use in the aerosol model since the model relates attenuation at 1.0636μ to that at $.55\mu$. This investigation (Ref 7) reported several significant results. First, it was found that the growth rate of all particle sizes was approximately the same up to a Relative Humidity of 95%. Beyond 95% the large particles grow at a faster rate skewing the distribution. In addition, the aerosol attenuation coefficient was measured for various relative humidities as shown in Figure 11. The wavelength dependence of extinction is shown at the left in Figure 11 for different relative humidities. The findings of this report are largely substantiated by similar measurements by Winkler and Junge (Ref 70).

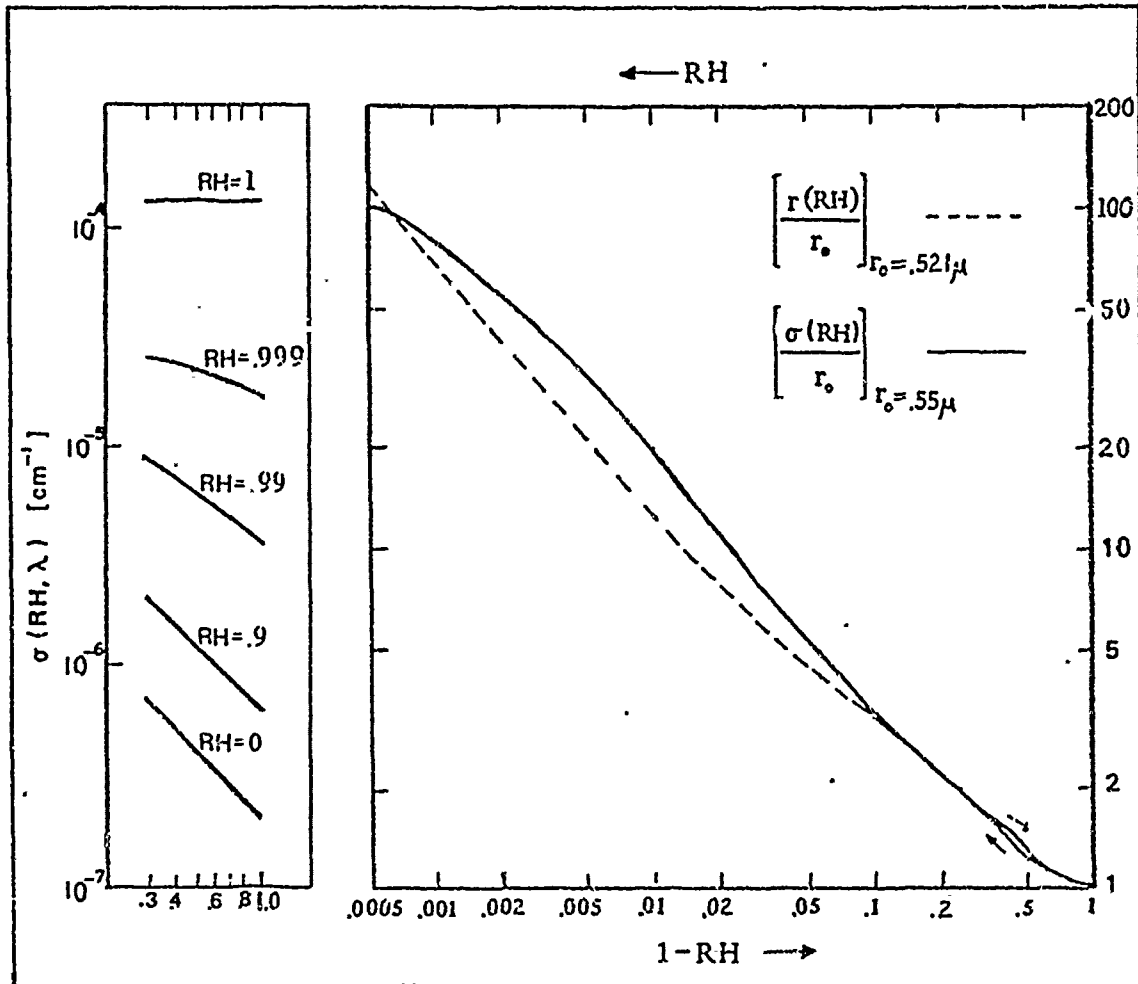


Fig. 11. Particle Growth with Change in Relative Humidity (RH) for Power Law Particle Size Distribution. Two Solid Curves are for Increasing and Decreasing Relative Humidities. At left, Wavelength Dependence with Change in Relative Humidity (Ref 7:549)

The effect on the aerosol model, then, is negligible up to a relative humidity of 95% (Ref 30). Beyond this value, however, the size distribution is altered and therefore determination of a new size distribution necessary. Aerosol processes with a relative humidity of 95% or more are exceedingly complex and therefore no solution will be attempted here. The aerosol model is, then limited for use at or below 95% relative humidity.

The increase in relative humidity does have some effect, however, on attenuation as shown in the figure. The ratio of these coefficients is given as a function of the relative humidity. Then as the relative humidity increases there will be an increase in the attenuation coefficient which is equal for wavelengths $.55\mu$ and 1.0636μ . *The important concept at this point is that the ratio between coefficients at the two wavelengths stays the same.*

Aerosol Attenuation from Meteorological Observables

Sophisticated equipment for measuring the attenuation of radiation due to aerosols is not widely available nor practical. Because of this fact, it becomes necessary to relate some atmospheric quantity to the aerosol attenuation. Such a relationship for daylight was first expressed by Koschmieder (Ref 43) and later repeated more elaborately by Middleton (Ref 53). Koschmieder's law is expressed by

$$M.R. = \frac{3.912}{\sigma_a} \quad (42)$$

where M.R. = Meteorological Range (Km) and σ_a = aerosol attenuation coefficient (Km^{-1}).

Meteorological range in white light is the maximum distance at which an observer can barely detect a large dark object against a white background. It is the distance at which the object to background contrast (inherent contrast) is reduced to .02 of its original value at the eye of the observer (apparent contrast). In addition, the large dark object must subtend so large an angle at the eye of the observer that if the subtended angle were greater, the reported value of

meteorological range would not be changed (Ref 23:186).

It must be emphasized that meteorological range is not visibility as reported by the meteorologist. The meteorologist reports prevailing visibility, which is the greatest horizontal visibility prevailing throughout at least half of the horizon circle which may not necessarily be continuous (Ref 29:A-6-3). In addition, distant dark objects of sufficient angular size are rarely available to the meteorologist (Ref 23:186). These objects when available are usually limited in number and not randomly distributed so as to reduce the statistical probability of selecting the exact meteorological range (Ref 52:40). Because of these factors the reported prevailing visibility (v) is usually less than the actual meteorological range (MR).

A comparison of reported prevailing visibilities with measured meteorological ranges by the Tiffany Foundation and the National Bureau of Standards concludes that, on the average, the reported prevailing visibility was 75% of the true meteorological range (Ref 23:186).

Equation (42) now becomes

$$v = \frac{2.934}{\sigma_a} \quad (43)$$

where V = Reported visibility, prevailing visibility, or "visibility."
For determination of the aerosol attenuation this relationship is assumed to be valid at the discrete wavelength $.55\mu$ which is the approximate center of eye sensitivity for photopic vision (ordinary color vision in daylight).

Visibility at night is a more complex phenomena. In the absence of a lighted object, the eye detects contrast of the object but the wavelength sensitive region of the eye has shifted to approximately $.53\mu$ (scotopic or rod vision). The threshold detectable contrast at the eye for night vision is complicated by a chemical process commonly called dark adaptation which is the process by which the eye adjusts to lower levels of illumination. Dark adaptation for the normal eye (scotopic region) takes approximately 30 minutes, although dark adaptation time for the photopic region generally occurs in approximately 8 minutes (Ref 54:39).

Because of dark adaptation, meteorologists generally use light sources as meteorological range markers. The meteorological range at night as determined by observing a point source of light is given by

$$\text{NMR} = \frac{1}{\sigma_a} \left[\ln\left(\frac{I}{E_t}\right) - 2 \ln(\text{NMR}) \right] \quad (44)$$

where NMR = Night Meteorological Range,

E_t = Threshold flux density of the eye,

and I = Intensity of light source

This transcendental equation known as Allard's Law is best solved graphically. The proper value of E_t depends on the luminance of the background and on the probability of detection (Ref 53:138). A graphical solution to this equation is presented in Figure 12. This solution is based on a 95% detection probability and assumes no other light within the field of view.

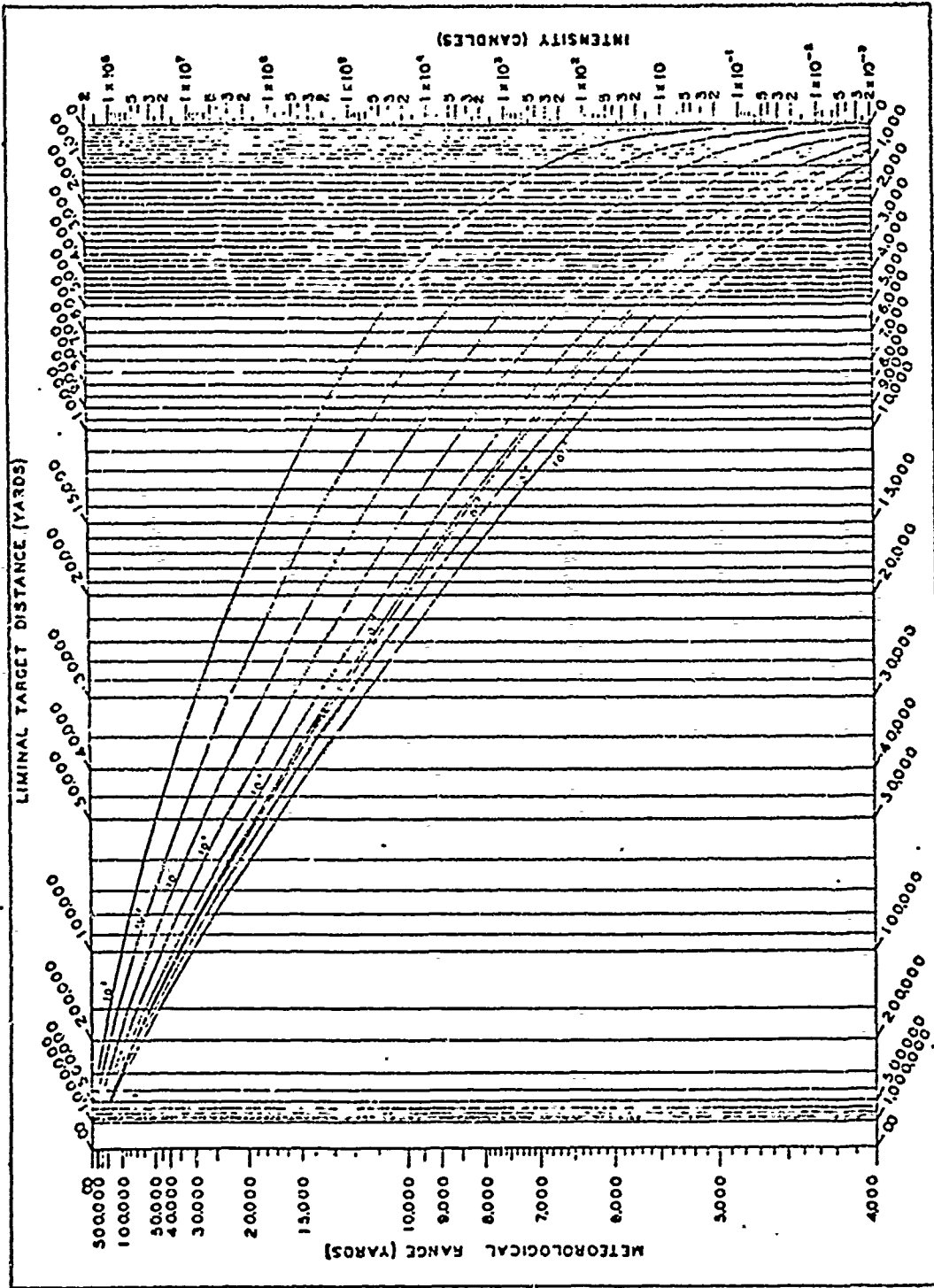


Fig. 12. Graphical Solution of Willard's Law. Nine curves represent various background illuminance values. To use the chart, join the meteorological range on left with light intensity on right. Where straight line intersects background illuminance, read target distance (Ref 53:139).

As is evident from Figure 12, the changes in threshold with variations in surrounding brightness are much more pronounced at night than daytime (using $1 \cdot 10^3$ footlamberts for daytime). As we have also seen, the state of dark adaptation of the observer's eye is an important factor. For this reason, the adoption of a standard threshold of flux density at night has little practical value (Ref 54:56). In addition, meteorological observers are rarely, if ever, dark adapted for night visibility observations so that these observations must be considered quite unreliable and useless for comparative studies of visibility (Ref 54:40).

Because night visibilities as reported are considered less reliable than day visibilities and because there are additional complicating factors in measuring visibility at night, night observations were not used in determining the aerosol attenuation coefficient. The computations within this report are limited, therefore, to daylight hours.

Use of the Model

As we have discussed previously, the total particle density is essentially unmeasurable. For this reason, we have limited our discussion to the per particle attenuation. The per particle attenuation is useless unless there is a method of measuring the number of particles. This number is determined by the visibility.

In the last section we discussed a method (based on visual observations) to determine the attenuation coefficient at $.55\mu$. Given the reported visibility, Eq (43) determines the coefficient at $.55\mu$. If one divides this attenuation coefficient by the one determined by

Mie calculations at $.55\mu$ then the number of particles may be determined. This exercise is not necessary, however, since the relationship between attenuation coefficients at the two wavelengths ($.55\mu$ and 1.0636μ) has been established by Eq (41). Given the reported visibility then one may determine directly the attenuation coefficient at 1.0636μ by combining Eqs (41) and (43)

$$\sigma_a(1.0636\mu) = \frac{1.5825}{V} \quad (45)$$

where $\sigma_a(1.0636\mu)$ = aerosol attenuation coefficient in Km^{-1} for a horizontal path.

Other Models

During the course of this study several models for determination of aerosol attenuation coefficients were investigated. These included: (1) the AFCRL Report *Optical Properties of the Atmosphere* (Ref 49); (2) 1964 AFCRL Report by Elterman (Ref 26); (3) *Handbook of Geophysics and Space Environments* (Ref 61); (4) *Electro Optics Handbook* (Ref 24); (5) 1968 AFCRL Report by Elterman (Ref 27); and (6) 1970 AFCRL Report by Elterman (Ref 28). Briefly, this investigation focused on differences in reported attenuation coefficients, in basic model assumptions, and on differences with the model derived in this report.

The 1964 and 1968 AFCRL reports by Elterman, the *Electro-Optics Handbook*, and the *Handbook of Geophysics and Space Environments*, are all based on measurements made by Curcio (Ref 14) in the NRL project discussed earlier. The attenuation coefficients given in these reports are based on the measurements reported by Curcio for visibility of 25

km (although the *Electro-Optics Handbook* reports this visibility as 23.5 km). The *Electro-Optics Handbook* then apparently extrapolates these values to other meteorological ranges using Eq (42) as shown in Figure 13. Curves of the original values are shown in Figure 8 and again grouped in Figure 14 (Ref 14:12). The curvature of the lines of equal visual range in the NRL reports is not the same; in fact, an analysis of the data shows only Meteorological Ranges between 6 and 12 miles and approximately 25 miles give identical slopes. In addition, it is recalled that these data were taken in an area where the aerosol attenuation is influenced to some degree by a maritime distribution component. In fact, the data indicates a general correlation between meteorological range and slope of the particle size distribution curve such that a change from high to low meteorological range generally indicates a steeper slope to the particle size distribution curve (Ref 14:12). Because of these factors, these reports may not offer a method for determination of the aerosol attenuation coefficient for continental geographical locations.

The 1970 AFCRL Report by Elterman provides a method for determining aerosol attenuation coefficients for eight surface meteorological ranges from 2 to 13 km. This report has utilized the measurements taken by Curcio for 4 km and extrapolated from 2 to 13 km by using this relation from Reference 28:

$$\sigma_a(V_\eta, \lambda) = \sigma_a(V_4, \lambda) \cdot \left[\frac{3.91}{V_\eta} - \beta_r(\lambda_{.55}) \right] / \left[\frac{3.91}{V_4} - \beta_r(\lambda_{.55}) \right] \quad (46)$$

where $\sigma_a(V_\eta, \lambda)$ = aerosol attenuation coefficient at the visual range, η , and the wavelength, λ

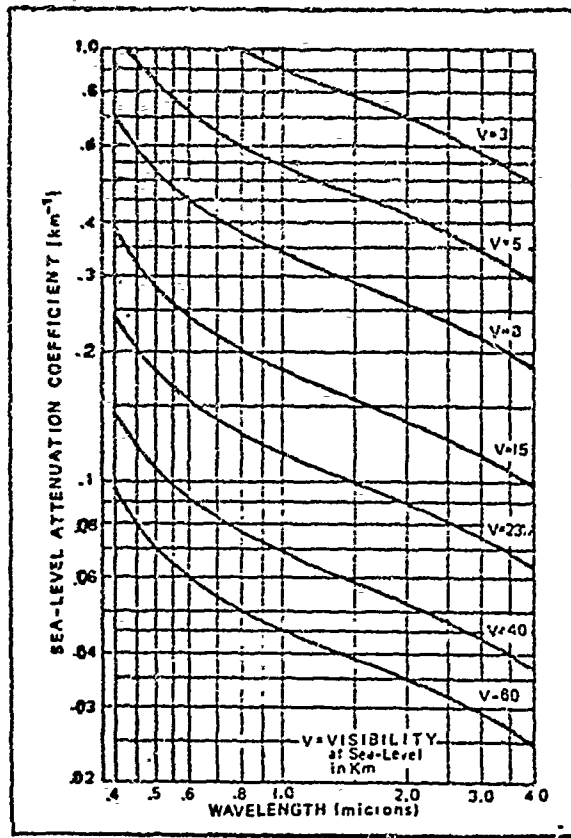


Fig. 13. Attenuation Coefficient Curves for Various Meteorological Ranges (Ref 52:39)

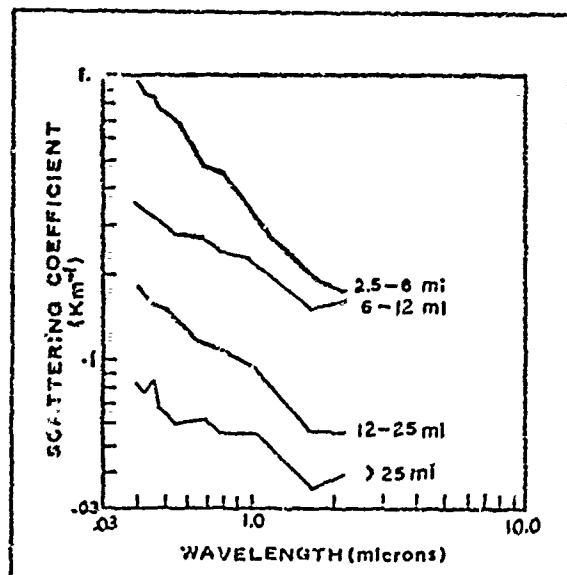


Fig.14. Experimental Scattering Coefficient Curves for Various Meteorological Ranges (Ref 14:12)

$\sigma_a(V_4, \lambda)$ = the measured aerosol attenuation coefficient at visual range of 4 km and wavelength, λ , and

$\beta_r(\lambda_{.55})$ = Rayleigh (molecular) scattering coefficient. The use of this relation assumes a constant particle size distribution for this meteorological range which apparently is not supported by Curcio's measurements (Ref 14:11,12). Elterman's report also has the same disadvantage for use at continental geographical locations as discussed previously.

The 1972 AFCRL Report titled *Optical Properties of the Atmosphere* uses a Continental Haze model after the one originally used by Deirmendjian (Ref 49:8). The distribution used in this CRL report differs from the one developed here in upper and lower limits of integration; the CRL distribution is defined from .02 μ to 10 μ (Ref 49:8). In addition, the index of refraction used is 1.50 for $\lambda = .55\mu$ and 1.50 - .033 for $\lambda = 1.0636\mu$. These differences cause a reduction in the ratio of the attenuation coefficients at 1.0636 μ to .55 μ . In other words, this AFCRL report tends to be slightly more optimistic than the model developed here. This AFCRL model was discussed previously in the size distribution and index of refraction analysis section.

Model Limitations/Assumptions

The model developed in this report for determination of the aerosol attenuation coefficient for a horizontal path at ground (observation) level is restricted for use in areas where the particle size distribution is described approximately by the assumed continental haze model. It is also restricted for use in areas where the index of refraction is approximately the one used here, although index of

refraction is not as sensitive a factor in establishing the relationship between wavelengths as the size distribution.

This model also assumes that the reported visibilities are 75% of the true meteorological range. The concept of meteorological range further assumes that Rayleigh scattering and molecular absorption are negligible. This assumption is valid for meteorological ranges on the order of those used in this analysis for tactical application. The model is further limited to relative humidities at or below 95%.

VII. Aerosol Attenuation for a Slant Path

Chapter VI determined the aerosol attenuation coefficient at ground level based on surface observations. This chapter discusses the distribution of aerosols with respect to altitude and relates this distribution to atmospheric phenomena. It then discusses the feasibility of determining aerosol attenuation coefficients from ground-based observations.

Particle-Size Distribution (Function of Altitude)

We have discussed briefly the particle size distribution as a function of altitude in Chapter V. The particle size distribution is found to remain relatively constant with altitude, with the exception of the giant particles which are more affected by sedimentation (Ref 41:182). There is a decrease in the percentage concentration of giant particles with increasing altitude in the absence of convective currents that force them aloft. These larger particles settle into more dense air where the increased Brownian motion will keep the particles airborne.

There is evidence to support the existence of a world-wide background aerosol distribution. This aerosol distribution is the aerosol distribution for the troposphere outside the contamination layers. These contamination layers are the layers closest to the earth's surface, and therefore they are affected by the local production mechanisms. This background aerosol distribution is represented as a modified continental aerosol distribution (Ref 41:189). That is, the distribution differs significantly from the continental distribution only in the relative concentration of larger particles.

There is some disagreement, also, as to the exact lower particle limit just as in the case of the continental distribution. Some contend that the lower limit should be somewhat higher, and the concentration of the smaller particles (radius $< .1\mu$) be less than the continental distribution (Ref 40:201). Recent laboratory studies, however, have established that small particles may be produced in the atmosphere by sunlight ionization of trace gases (Ref 40:202). The lower limit is not important, however, as long as this limit is less than $.1\mu$ since particles smaller than this limit are ineffective scatterers of visible and infrared radiation.

The background aerosol distribution, then, differs from the continental aerosol distribution in the concentration of giant particles, particles whose radii are larger than 1μ (Ref 41:127). Because the measurement of aerosols at altitude presents formidable problems and because of the expense of such measurements, the change in the relative concentration of these larger particles with altitude is not well documented.

Total Particle Concentration (Function of Altitude)

In contrast, the decrease in the concentration of measureable aerosols is well documented. The results of early investigations show that the *average* decrease in particle number concentration is approximately exponential with altitude (Ref 41:184). Some of these investigations show an exponential decrease to a certain altitude; above this altitude, the number concentration decreases less rapidly or is constant as shown in Figure 15.

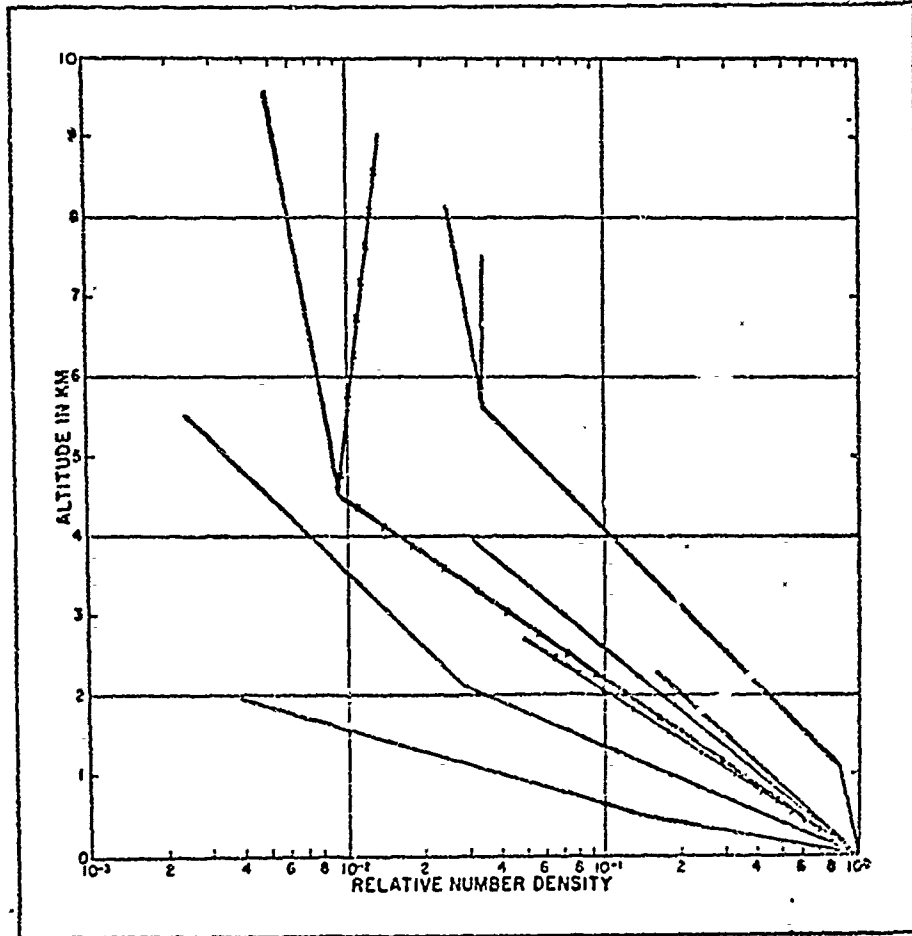


Fig. 15. Average Vertical Aerosol Concentrations from various sources. All data refer to Central Europe (Ref 41:184)

In 1964, Dr. Louis Elterman used these early measurements to develop a vertical aerosol model distribution (Ref 26). This model is an *average* of the results of the measurements, which in large part were taken over Central Europe. The result was an average vertical aerosol distribution which represented a wide range of meteorological conditions at several locations. This vertical aerosol model was subsequently revised in 1968 to include the results of a rather

extensive vertical aerosol study conducted by AFCRL in 1966 (Ref 25). This 1966 study included a total of 119 profiles of the troposphere (and stratosphere). These profiles taken over New Mexico were comprised of absolute values of aerosol attenuation coefficients. A comparison of the two resulting models (Elterman, 1964, and Elterman, 1968) is shown in Figure 16.

Mixing Depth Concept

Individual attenuation measurements and average profiles have led to the mixing layer concept in an attempt to physically explain the vertical aerosol distribution. As we discussed earlier in this chapter, the average aerosol concentration above a certain altitude is either constant or gradually decreasing. Below this altitude, the time-average aerosol concentration profile shows a rather steep exponential decrease. This lower layer described by the steep exponential profile is called the mixing layer (although this is *not* the strict meaning of the term).

Basically, the mixing layer is the vertical expanse above the surface that is affected by the aerosols being produced at the surface. This boundary layer as it is also called is the layer in which vigorous vertical and horizontal mixing of the air takes place (Ref 55:1). Thus, the boundary or mixing layer is largely affected by the aerosol production mechanisms. Above this layer, the aerosol concentration is related to the air mass itself.

The depth of the mixing layer (or the maximum altitude of the boundary layer) has been the subject of several investigations.

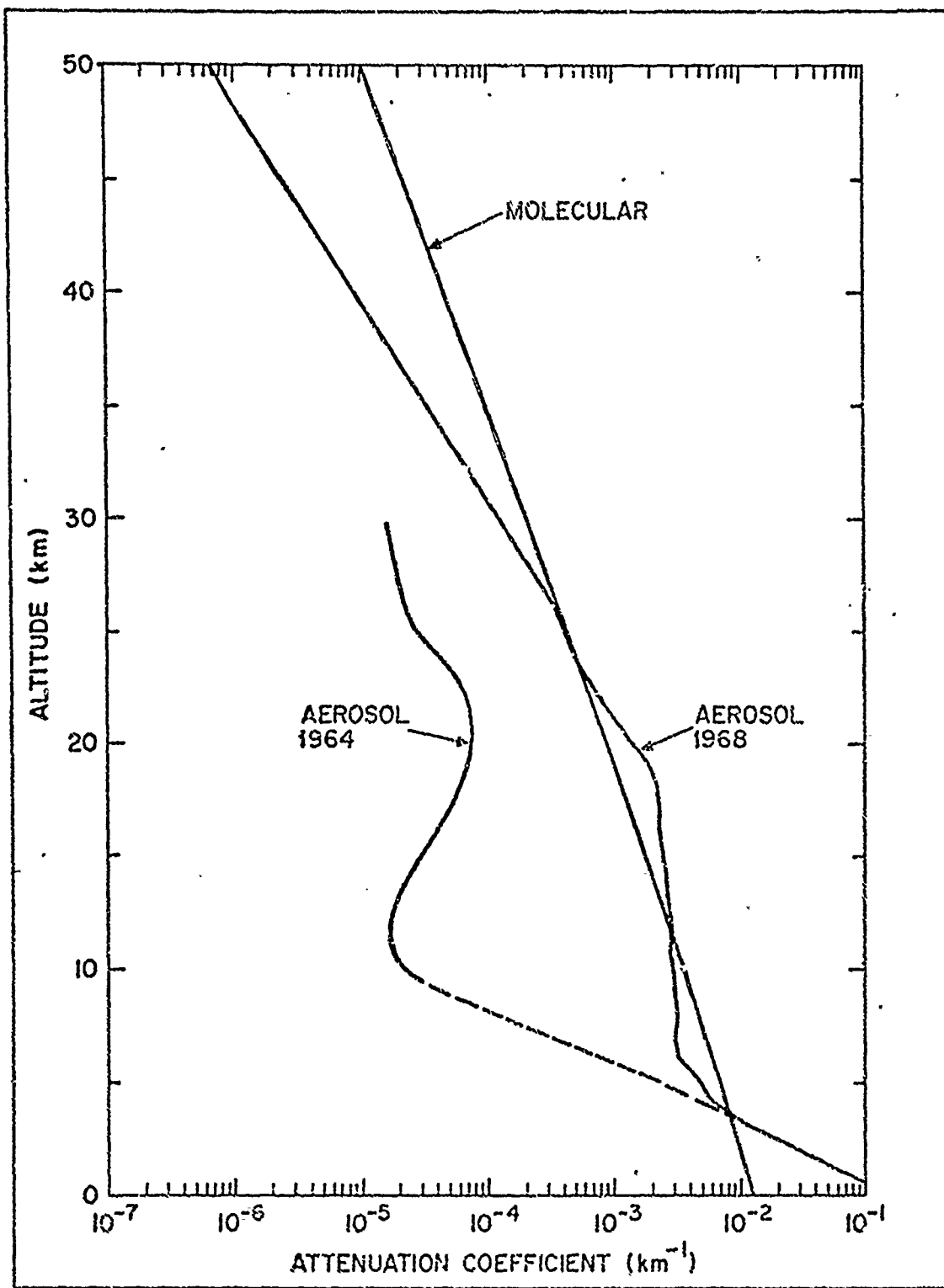


Fig. 16. Comparison of Vertical Aerosol Distribution Models by Elterman (Ref 27:17)

The studies of Siedentopf (1944), Penndorf (1954), Faraponova (1965), Rosen (1967), and others reported in Reference 58, show that the average boundary layer depth is approximately 5 km, although the reported average height varies from 3 km to 6.5 km (Ref 28:7,8). Such large values of the mixing depth do not agree with meteorological computations of the mixing depth based on convective and advective currents some of which are discussed briefly later.

AFCRL Vertical Aerosol Model

Based on the evidence available at the time, Dr. Elterman devised an extensive vertical aerosol model. This 1970 AFCRL model (Ref 28) assumes the mixing depth to be 5 km. The aerosol attenuation coefficients above 5 km are those reported in the 1968 vertical aerosol model revision (Ref 27). Below 5 km the aerosol attenuation coefficient exponentially decreases with altitude up to 5 km. Eight surface meteorological ranges are used and these surface meteorological ranges are based on the aerosol attenuation coefficients and ranges reported by Curcio (Ref 14) as we discussed earlier in Chapter VI. Each of these eight surface attenuation coefficients is exponentially decreased to agree with the same reported 5 km value. Hence, different exponential scaling factors are used as shown in Figure 17.

The most recent AFCRL model of the aerosol attenuation coefficient (Ref 49) also uses the exponential scaling factor concept. This model, however, uses different attenuation coefficients at ground level--these based on computations using a Deirmendjian Haze C model as we discussed earlier. The aerosol attenuation coefficients above 5 km are the same as those in the 1968 AFCRL Elterman Report (Ref 27).

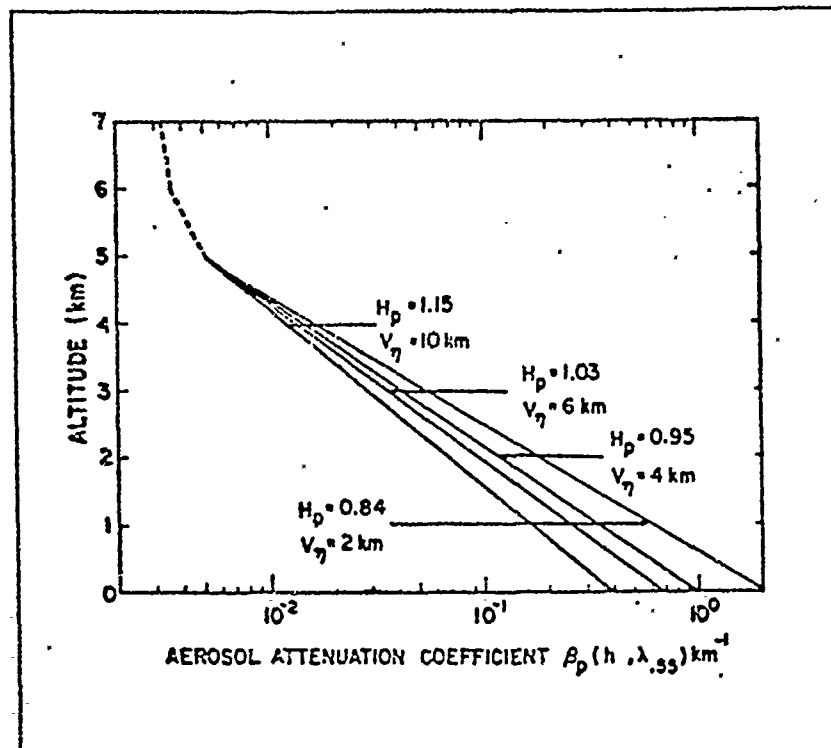


Fig. 17. Family of Scaling Factors Used by Elterman to Relate Different Ground Level Attenuation Coefficients to 5 km Attenuation Coefficient. The Scale Heights, H_p , are Computed at Reference Frequency $.55\mu$ (Ref 28:9).

Latest Attenuation Measurements

Recent aircraft aerosol attenuation measurements made for AFCRL (Ref 20 and 21) do not support the model developed by Elterman (Ref 30 and Ref 67). These extensive total volume scattering measurements were made in New Mexico under project name Atom and in Southern Germany under project name Haven View. These measurements show that the mixing layer is somewhat less than the 5 km computed from averages of many measurements. In fact, the measurements show that the mixing layer extends from ground level to altitudes from

approximately five hundred meters up to around 2.5 km with levels of 1.5 km predominating (Ref 30).

These measurements also show that in the mixing layer the attenuation coefficient shows a very slow exponential decrease (on the order of 7.99 scale height used with the standard atmosphere for molecular computations) or it is approximately constant. At the mixing layer boundary, the aerosol attenuation coefficient shows a sharp decrease to a clean air mass attenuation value or a gradual transition to such a clean air mass value through a 200 meter layer. Above the boundary layer, the attenuation coefficient again shows a gradual exponential decrease but this decrease is frequently less than the density lapse rate (i.e., 7-8 km scale height) (Ref 22:7-17).

These whole-volume attenuation measurements described in References 20, 21 and 22 are well documented, and extensive sets of meteorological data were recorded in the course of these studies. Consequently, various attenuation coefficients are related to specific meteorological processes. Measurements of high values for aerosol attenuation in the mixing layer are associated with temperature inversions or layers of high stability. The aerosol attenuation coefficient is relatively constant throughout the mixing layer, then at the mixing height there is a sharp (step function) decrease to the air mass attenuation coefficient above the layer as shown in Figure 18.

When the mixing layer attenuation coefficient is low (that is, the visibility is good indicating very clean air) then measurements show that there is a slow exponential decrease in the attenuation coefficient with increasing altitude.

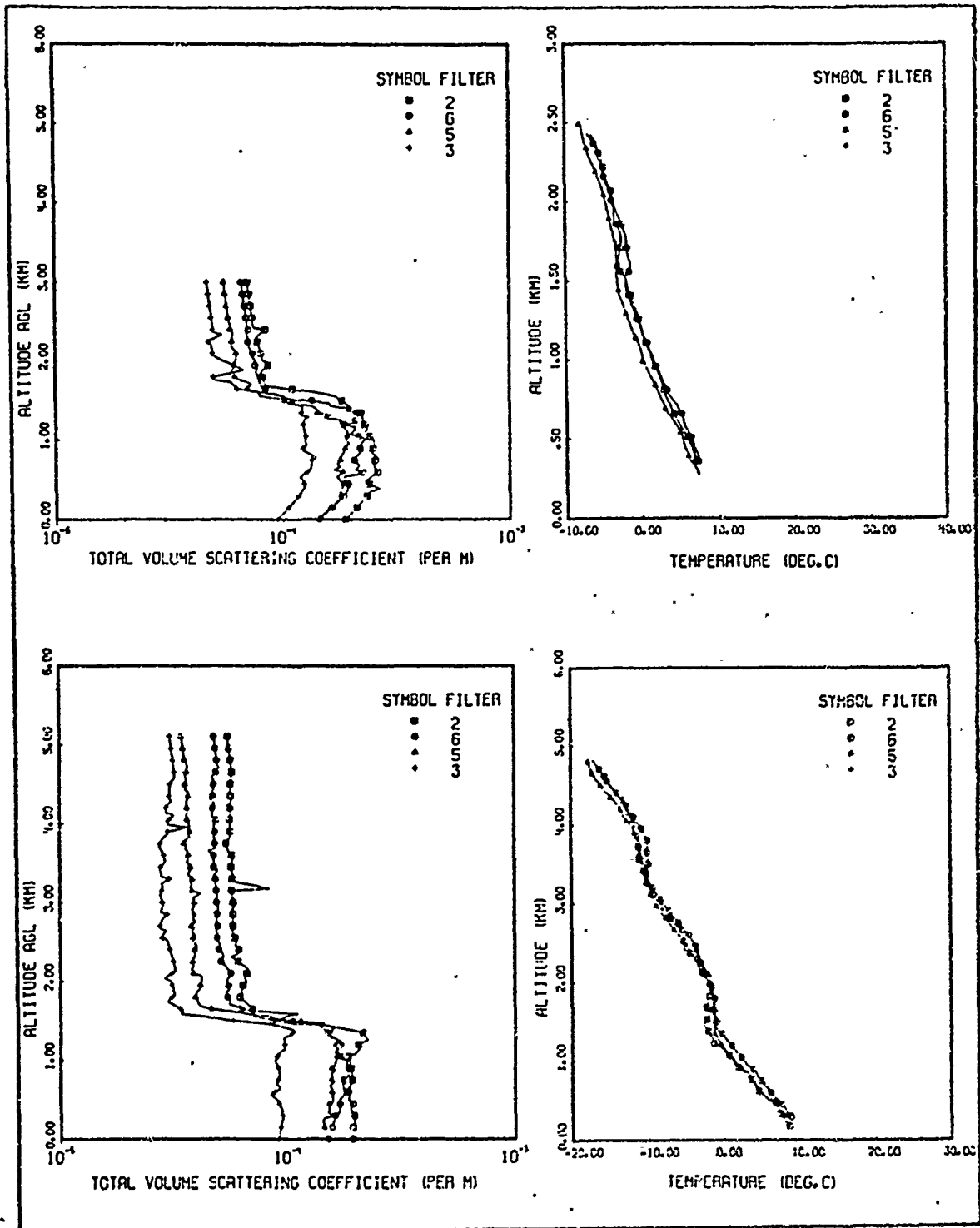


Fig. 18. Vertical Temperature and Whole Volume Scattering Coefficient Distributions Measured by AFCRL Over Germany. The top set is from Flight C-137 and the lower set is from Flight C-139. Filter Number 5 approximates the photopic ($.557\mu$).

This slow exponential decrease is evident even in cases where a strong inversion exists. The inversion then has relatively little effect on clean air.

In addition, there is some variance in the value of the aerosol attenuation coefficient reported for the air mass above the mixing layer as shown in Figure 18. This indicates that the air mass above the mixing layer may be affected to some degree by the aerosol concentration of the boundary layer. Some mechanical or convective transport must occur (Ref 30). However, generally the air mass above the mixing layer approximates a clear day or better.

Average Aerosol Profiles

Individual vertical aerosol profiles as discussed in the previous section show certain characteristics which are lost when average values are taken. The fact that these *average* profiles tend to show some exponential decrease is probably due to a correlation between a changing height of the mixing layer and the concentration of the particles within the layer (Ref 41:183,184). In addition, the fact that earlier measurements of the vertical aerosol distribution yielded higher mixing height values is possibly due to the fact that aircraft flights, and particularly those of several years ago, usually occur in good weather flying conditions. This higher average mixing layer height may also be due to the changing individual mixing layer height.

The difficulty in using such average vertical profiles may best be illustrated by the following *reductio ad absurdum*. Suppose that in the course of one year, a station recorded 6 months of fairly good weather. That is, the visibility is excellent and the aerosol

attenuation coefficients are low values. Further, suppose that during the other 6 months the visibilities are extremely low (on the order of 2 km) and aerosol attenuation coefficients are high. If the missile system being evaluated is effective only in clear air, then an average profile might unjustifiably lead to the conclusion that this missile would be ineffective at this location when in fact it might be quite effective 50% of the time.

Vertical Aerosol Model

For reasons we have discussed in the previous section, it was decided that a more representative vertical aerosol model would be a model that accurately represented individual characteristic aerosol profiles. These profiles are based on the published results of Project Haven View and Project Atom (Ref 20, 21, and 22) and discussions with the project manager Dr. Robert Fenn (Ref 30).

These measurements demonstrated that there is probably a mixing or boundary layer in which the particles are fairly uniformly mixed and that above the layer the air is clear. In fact, measurements of the aerosol attenuation coefficient in the air mass above the boundary layer showed the coefficient to be characteristic of air in which the meteorological range is 45 km or more. The individual measurements gave ranges from approximately 45 km to approximately 100 km (Ref 20 and 21), although there may be some error in the exact value due to difficulty in calibrating equipment in very clear air. That is, the Rayleigh scattering component is no longer negligible in the visible region at such meteorological ranges. In fact, the Rayleigh scattering component at a meteorological range of 40 km is 12% and it increases

as the meteorological range increases. These measurements were taken with a filter centered at $.557\mu$ (an approximation of photopic vision).

A clear air model is thus representative of the air mass above the mixing or boundary layer. An air mass whose meteorological range is approximately equal to 40 km (prevailing visibility of 30 km) was chosen for the air mass model because this value represented a worst case among the reported measurements.

The mixing or boundary layer is assumed to be uniformly mixed vertically and horizontally. Its depth is dependent on a number of factors. These factors are the thermal and mechanical forces of the atmosphere. The measurements conducted by AFCRL in Southern Germany indicate the mixing depth extends to 1.5 km during late May and early June when the measurements were taken. A recent study by USAF ETAC (Ref 55) based on theoretical meteorological processes (thermal and mechanical) for one location in Germany indicates that during this period (May to June) the mixing depth varies from 150-1175 km. The wide range of reported values is due to the fact that the ETAC study covered the 24 hour period while aircraft measurements were made during daylight hours. However, the maximum theoretical computations do not predict the mixing height measured by AFCRL.

This same USAF ETAC study for Stuttgart, Germany, indicates that the mixing depth extends to lower altitudes in winter than during other times of the year (see Figure 19). This corresponds to what others have observed to be true: Winter is the low-level haze season in Germany (Ref 30). There have been too few aircraft measurements; however, to substantiate this seasonal variation.

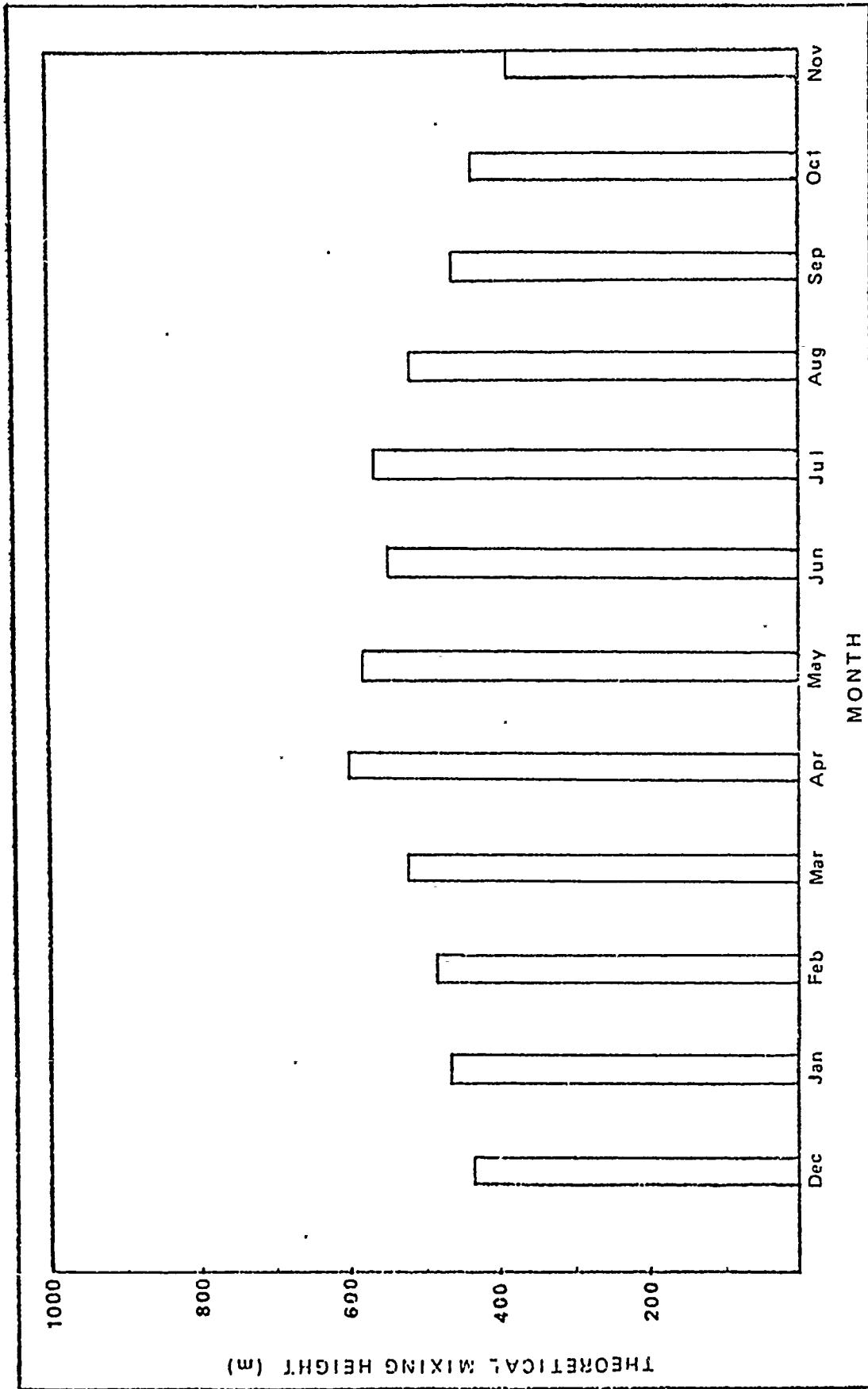


Fig. 19. Mean Monthly Theoretical Mixing Heights for Stuttgart, Germany. Values from Theoretical Model by USAF ETAC (Ref 55)

Moreover, the theoretical model does not show significant variation in the mean seasonal mixing depths (Fig 19).

Boundary (Mixing) Layer Depth

There are many methods for calculation of the mixing depth. Some are based on aircraft/balloon measurements; others are theoretical in nature. Still others combine both. The measurements of Elterman and AFCRL have been discussed; the measurements of others (Siedentopf, etc.) have also been mentioned. This section discusses two theoretical models and discusses the meteorological processes involved.

One of the theoretical methods of determining mixing depth height is the method of Miller and Holzworth (Ref 39). This method is currently being used by the Environmental Protection Agency (EPA) and the National Weather Service (NWS) together with radiosonde data to predict the thickness of the mixing layer. This method is based on the maximum and minimum surface temperatures and the radiosonde data. The maximum mixing depth height is the height to which a parcel of ground air (at maximum temperature) will ascend if lifted dry adiabatically until its temperature is in equilibrium with the environment (Ref 5:3). This method, however, fails to account for moisture in the air and it is restricted to occasions when there is no precipitation and no air mass change. It is also restricted for use to locations where radiosonde balloon observations are made.

The method proposed by USAF ETAC (Ref 55) uses weighted contributions of thermal and mechanical parts. The weighting factors are Pasquill stability factors which are based on meteorological conditions as shown in Figure 20.

PASQUILL STABILITY CATEGORIES

SURFACE WIND SPEED (at 10 m) m/sec	<u>INSOLATION</u>		NIGHT THINLY OVERCAST OR >4/8 LOW CLOUD	<3/8 CLOUD
	STRONG	MODERATE	SLIGHT	
< 2	A	A-B	B	F
2-3	A-B	B	C	F
3-5	B	B-C	C	E
5-6	C	C-D	D	D
> 6	C	D	D	D

THE NEUTRAL CATEGORY, D, SHOULD BE ASSUMED FOR OVERCAST
CONDITIONS DURING DAY OR NIGHT

- A -- EXTREMELY UNSTABLE
- B -- MODERATELY UNSTABLE
- C -- SLIGHTLY UNSTABLE
- D -- NEUTRAL
- E -- SLIGHTLY STABLE
- F -- MODERATELY STABLE

Fig. 20. Pasquill Stability Factors as a Function of Weather Conditions. The categories are used to weight the thermal and convective parts of theoretical mixing height. Category A contributes all its weight to the thermal part and so on.

The mixing height is then calculated based on ground observations and estimates of upper level winds.

Observations using these and other methods show that there is great variability of the mixing depth during the day and also from day to day. On the other hand, aircraft measurements do not show such wide variations in the mixing height on an hour to hour basis. This may best be explained by considering the history of the air mass. If the mixing occurs in the lower levels of a clean air mass, then the aerosols are distributed to the maximum mixing layer height. Later in the day (evening and night) when the convective mixing processes diminish, the aerosols remain aloft if there are no convective currents forcing them downward. The particles are influenced by gravity but the settling rate is slow. Thus, on subsequent days, the aerosols remain mixed to nearly the height of the previous day. Subsequent mixing height measurements yield a vertical particle distribution that is an indicator of the previous mixing height maximum and not necessarily the mixing height at the time of measurement (Ref 46:1183).

Other processes are often involved, however. During the night a surface inversion frequently develops. These inversions are formed largely by turbulent transfer of heat down toward the ground (Ref 55:13). Thus, in many cases the aerosol layer would follow the theoretical pattern of a decreasing mixing layer depth. Because of the paucity of aircraft measurements in varying meteorological conditions and because of the complex atmospheric processes involved, this author feels that a real time determination of mixing layer height is impossible unless there is detailed knowledge of the history of the air mass and probably upper air soundings.

Mixing layer depth may be determined for such a study as this, however, based on a knowledge of the meteorological processes for this geographical location, Germany. One would certainly expect that this mixing layer would not apply to other locations such as Southeast Asia where the thermal and mechanical atmospheric processes differ in magnitude. *This model also fails to predict the hour by hour and day to day variations of the mixing layer depth, but it is representative of the real vertical aerosol profile based on mean meteorological conditions.*

Aerosol Model and Use

The model consists of two parts: the mixing layer aerosol attenuation coefficient and the aerosol attenuation coefficient of the clear air mass above. Key to the use of the model is ground-level (horizontal) prevailing visibility. If the prevailing visibility is 30 km or more (meteorological range 40 km or more) then the vertical attenuation coefficient decreases as the density. The aerosol attenuation coefficient at any altitude, H (in km), is given by

$$\sigma_a(H) = \sigma_a(o) e^{-\left[\frac{H}{7.99 \text{ km}}\right]} \quad (47)$$

where $\sigma_a(o)$ is the ground level attenuation coefficient. There is a slight difference in the determination of the ground level attenuation coefficient for use in this vertical model. Since there is an indication the upper particle size limit decreases with altitude then the continental distribution used thus far was modified to extend to the upper particle limit of 10μ (Ref 41:118). The relationship between

the aerosol attenuation coefficient at 1.0636μ and $.55\mu$ is modified only slightly

$$\sigma_a(1.0636\mu) = .535 \sigma_a(.55\mu) \quad (48)$$

where the particle composition (index of refraction) is assumed to be the same. Combining Equations (43) and (48), the ground level attenuation coefficient at 1.0636μ is

$$\sigma_a(o) = \frac{1.57}{V} \quad (49)$$

where V is the prevailing visibility. The aerosol attenuation coefficient at any altitude, H , then becomes

$$\sigma_a(H) = \frac{1.57}{V} e^{(-H/7.99)} \quad (50)$$

Using Eq (50) then the attenuation coefficients are determined for the different altitudes. This model follows the technique used by others (Ref 49) in averaging the two computed values to determine an average attenuation coefficient for a 1 km layer. These average values are then added and multiplied by $\sec \theta$ for use in slant path problems. The angle θ is the angle between the vertical to the ground and the angle to the transmitter/receiver. Use of this model is explained in Appendix C.

If the prevailing visibility is less than 30 km then the upper air mass is the clear air model for a visibility of 30 km, but the

ground layer attenuation coefficient is determined by the horizontal prevailing visibility. This layer is assumed to be uniformly mixed. Thus, the attenuation coefficient for the layer is determined by Eq (45). The depth of the layer varies, but useful computations may be made by using a mean mixing depth of 1500 m (Ref 30). These are characteristics daytime values which are probably very realistic for midmorning to late afternoon cases. For early morning and late evening calculations where a low inversion is known to exist, a mixing depth of 300 m offers a good approximation, although this may be high for some nocturnal inversions (Ref 60).

VIII. Other Atmospheric Attenuating Mechanisms:

Clouds, Fog and Precipitation

This chapter discusses briefly the effects of other atmospheric phenomena on laser radiation at 1.0636μ . This discussion is limited to the attenuating effects of clouds, fog and rain. Other phenomena are mentioned but are not covered in any detail. In addition, the sensitivity analyses accompanying previous discussions in this report are not included in this chapter. The purpose of this chapter is, then, to provide a useful method for estimating the attenuation at 1.0636μ due to clouds, rain, and fog. Further, it is desirable that the attenuation be related to some meteorological observable.

Attenuation by Rain

Attenuation, as we have discussed, is dependent on droplet size and droplet size distribution. For rain both size and size distribution are highly variable. In fact, different rain droplet distributions occur within the same rain shower. Since these droplet size distributions are also virtually unmeasurable, exact Mie calculations have very little meaning.

For distributions where the droplet radius is large compared to the wavelength of radiation, the geometrical approximation to Mie theory may be used. For rain drops, whose radius is approximately 1 mm or larger (Ref 13:727), the extinction cross section asymptotically approaches two. In addition, the imaginary index of refraction of water is on the order of 10^{-6} for wavelengths in the visible and 1.0636μ ; hence, the absorption is negligible.

Because size distributions were not definable and the geometrical approximation is valid for rain, Chu and Hogg (Ref 13) found instructive the calculation of attenuation coefficients for rain droplet distributions having a single radius. For this ideal case, the attenuation coefficient becomes

$$\sigma_R = 3.25 \frac{Q_{\text{ext}} W}{r} \quad (51)$$

where σ_R = total attenuation in dB/km,

r = drop size radius in microns,

Q_{ext} = scattering cross section efficiency,

and W = liquid water content in mg/m³.

Using the asymptotic value of two for Q_{ext} and the conversion factor for dB/km, then Eq (51) becomes

$$\sigma_R = \frac{28.21}{r} W \text{ (km}^{-1}\text{)} \quad (52)$$

which is in terms agreeable with those for other attenuation coefficients in this report.

The energy intercepted by precipitation particles is, however, partially scattered forward (toward the receiver) and this reduces the attenuation coefficient determined by Eq (52). When scattering is a maximum then so is the forward scatter component. The larger the scattering, then the more that Eq (52) is in error. This problem is more pronounced in cases of heavy rain (Ref 13:739). A forward scattering correction factor has been derived in Reference 13 assuming

a gaussian beam profile with an effective aperture equal to the geometrical cross section of the water sphere. This correction factor is

$$\bar{\beta} = \frac{1}{L} \cdot \frac{Q_{sca}}{Q_{ext}} \int_0^L \frac{\omega_t^2}{\omega_s^2 + \omega^2 \left(\frac{L}{z}\right)^2} dz \quad (53)$$

where L = path length,

z = distance to the scattering particles from the source,

ω = half-width of the transmitted beam pattern (in cm),

ω_s = radius of the water droplet (in cm),

and ω_t = half-width of the beam pattern at the receiver (in cm)

if no attenuation is assumed. For visible and near infrared, there is no absorption so that Q_{sca}/Q_{ext} becomes one. Chu and Hogg in Reference 13 have made calculations of the correction factor assuming the minimum beam radius at the uniphase aperture to be .25 cm (Ref 13:738). An additional assumption of this forward scattered correction factor is that this scattered energy rejoins the original beam (Ref 13:736). Integrating over different rain drop sizes then one obtains the attenuation curves depicted in Figure 21. The correction factor at 1.0636μ will be the same as that calculated at $.63\mu$ by Chu and Hogg since there is no absorption in either case.

The exact correction factor for the laser designator problem is incalculable because of the complex geometry in each case. If one assumes a similar correction factor applies in this problem, then a crude multiple scattering attenuation coefficient may be calculated for rain.

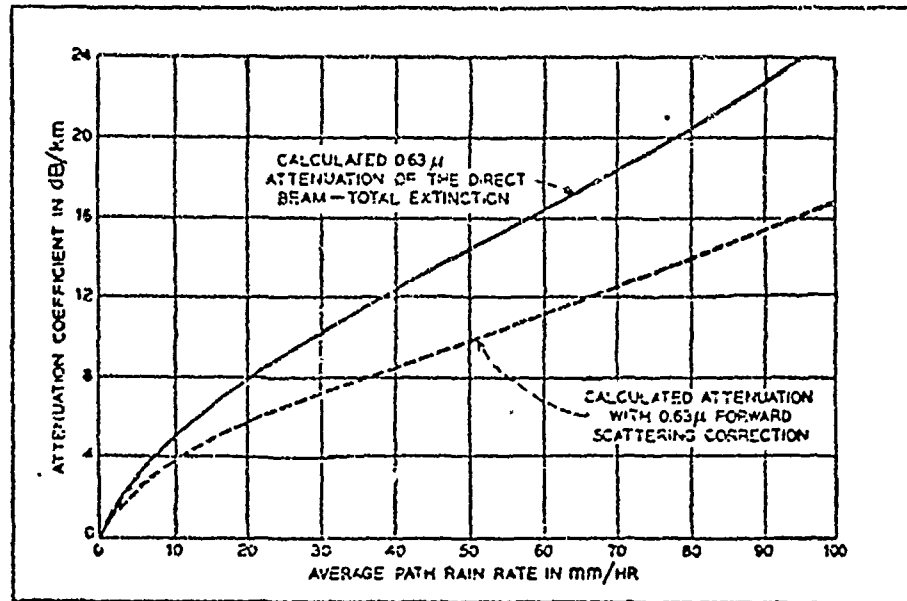


Fig. 21. Rain Attenuation Coefficient Curves for Different Rain Rates, Curves Calculated from Measurements Made over 2.6 Km Path (Ref 13:734).

Note: $[dB/Km \div (4.34) = \sigma(km^{-1})]$

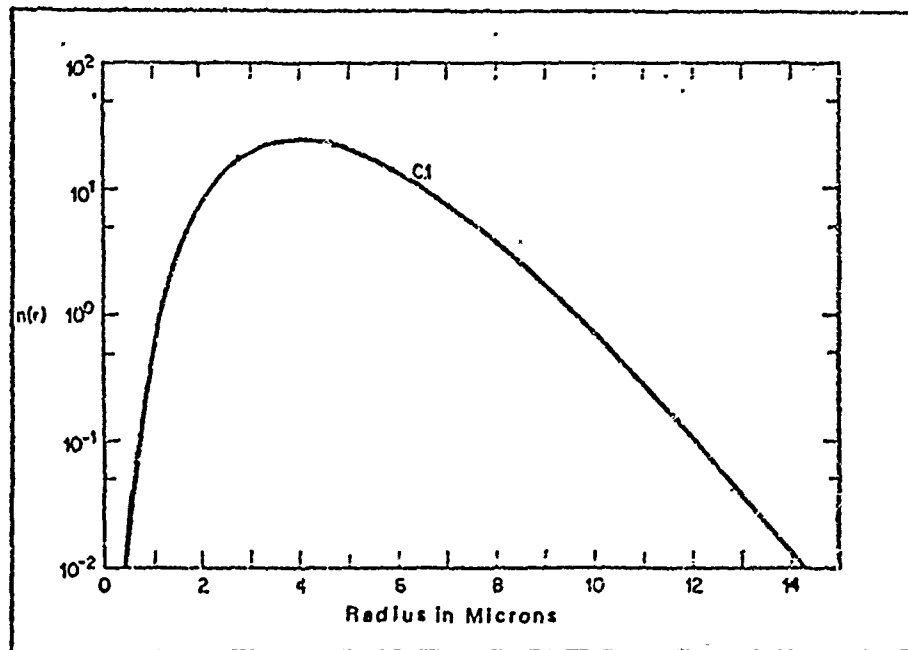


Fig. 22. Deirmendjian Cloud Size Distribution, C1 (Ref 17:80)

Meteorological Parameters for Rain Attenuation

To calculate the attenuation in rain, a knowledge of both rain drop size and liquid water content (mg/m^3) is needed. As we discussed previously, precise droplet size is unknown, but a median droplet size may be related to the source mechanism. The source mechanisms, convective showers or stratus drizzle or rain, can exist separately or in combination.

It is an accepted atmospheric phenomena that the droplet size and size distribution is modified as the droplet falls from cloud to ground. The large droplets (2500μ or more) break up and become smaller droplets; the very small droplets evaporate shifting the droplet size distribution measured at the ground level to larger median values. For the purpose of making an approximation, however, the droplet size will be assumed to be constant from cloud to ground. Typical median droplet sizes as a function of source mechanism are given in Table XIV.

Table XIV

Typical Median Rain Droplet Sizes
as a Function of Source Mechanism

<u>Cloud Condition</u>	<u>Drop Size (μ)</u>
Low Stratus (\approx 2000 ft AGL)	500*
Middle Stratus (\approx 12000 ft AGL)	800
Convection	1500

*These droplet sizes are valid for vicinity of Cloud Base, but for this model these sizes are assumed uniform to ground level.

These values from Reference 10 are the result of a comprehensive literature search by Captain Caratula. The median stratus values were obtained from Reference 1 (Page 14) and Reference 11; the convective values were obtained from Reference 44 (Page 357). It must be emphasized that these values are necessarily somewhat arbitrary, but nevertheless representative of these source mechanisms.

The water content is determined by the reported rain rate and cloud type (Source Mechanism). The water content, $W(\text{mg}/\text{m}^3)$, for stratiform rainfall is (Ref 44:369)

$$W = 72(R)^{0.88} \quad (54)$$

where R = Rainfall rate in mm/hr. A similar relationship for convective rain is (Ref 44:369)

$$W = 52(R)^{0.97} \quad (55)$$

where R = Rainfall rate in mm/hr. Rainfall reported by the meteorologist is categorized as light, moderate, or heavy. These categories are given in Table XV where the metric equivalent values are noted. Since the rainfall categories encompass a range of rain rates, a mean attenuation coefficient for each category is meaningless. Calculations were made using the best and worst cases in the particular categories; the results of those calculations are shown in Table XVI. These values are uncorrected for the forward scattered component since the correction factor depends on the exact rain rate. For the light rain category the correction factor varies from 0 to approximately 10% (Figure 21);

for the moderate rain category it varies from 10 to about 20% (Figure 21). In extremely heavy rain, the correction might reduce the attenuation by almost 50%.

Table XV
Reported Rainfall Categories

<u>Classification</u>	<u>Rainfall Rate</u>	<u>Metric Eq</u>
Light	$R < .1 \text{ in/hr}$	$R < 2.54 \frac{\text{mm}}{\text{hr}}$
Moderate	$.1 \frac{\text{in}}{\text{hr}} \leq R < .3 \text{ in/hr}$	$2.54 \frac{\text{mm}}{\text{hr}} \leq R < 7.62 \frac{\text{mm}}{\text{hr}}$
Heavy	$R > .3 \text{ in/hr}$	$R > 7.62 \frac{\text{mm}}{\text{hr}}$

Table XVI
Attenuation Coefficients for Rain (Km^{-1})
By Source Mechanism and Reported Rainfall Category

<u>Classification</u>	<u>Low Stratus</u>	<u>Middle Stratus</u>	<u>Convection</u>
Light	0-9.226	0-5.766	0-2.415
Moderate	9.226-24.26	5.766-15.162	2.415-7.011
Heavy	> 24.26	> 15.162	> 7.011

Values calculated from values in Tables XIV and XV using Eqs (52), (54), and (55).

Attenuation by Fog

Fog is by international agreement a water droplet aerosol that reduces visibility below 1 km (Ref 8:223). The fog-haze boundary, however, has been identified by Foitzik (1938), and later confirmed by

Neiburger and Chien (1960), Bullrich (1963) and Eldridge (1969), as being at a meteorological range of about 1.2 km (Ref 28:3). For this report, a fog is identified as a water aerosol reported by the meteorologist regardless of the visual range.

Fogs in general are quite inhomogeneous which is due in large part to their formation mechanism. In addition, the vertical extent of fog may vary from a few feet to hundreds of meters. Also the vertical extent of fog is rarely reported by the meteorologist except as a general classification of fog (i.e., shallow fog). For these reasons, fog as reported by the meteorologist is of little practical value to this operational problem especially if the sky is totally obscured.

Some calculations were accomplished, however, for the purpose of establishing representative attenuation values that could be compared to other attenuation coefficients previously calculated. This model of the attenuation coefficient assumes that fog is homogeneous in both the horizontal and vertical directions. It also assumes that the visibility recorded in fogs is the true visibility or meteorological range.

In addition, the attenuation coefficient in fog is assumed to be independent of wavelength for the visible and near infrared. This is an assumption that was found to be reasonably accurate by Reference 4. This author theoretically verified this fact using several fog models used by others (Ref 4:47). For the four models investigated, the attenuation at 1.0636μ was larger than at $.55\mu$, but by only about 3%. The attenuation coefficient for fog, σ_F , may be determined by

$$\sigma_F = \frac{3.912}{V} \quad (56)$$

where V is the visibility. It has been determined experimentally that this relationship is valid only for visibilities of more than 200 m (Ref 4:65). For visibilities less than this, multiple scattering becomes extremely important.

Attenuation by Clouds

Clouds like fog are the greatest attenuators of later radiation. Like rain and fog, the cloud droplet size distribution is quite difficult to describe. The water content and other properties of clouds vary with cloud type and formation mechanism. There are, however, several cloud models available and one, in particular, in wide general use. This model cloud is the Deirmendjian Cloud C1, which represents a cumulus cloud of moderate thickness.

This cloud model size distribution is shown in Figure 22. The liquid water content of this cloud model is 0.063 gm^{-3} (Ref 17:79). It would have been desirable to investigate other cloud distributions. Time constraints on this project, however, limited this investigation to the one cloud size distribution described by

$$n(r) = 2.373 r^6 \left[\exp(-1.5r) \right] \quad (57)$$

where r is the droplet radius in microns and the particle density is assumed to be 100 cm^{-3} . Mie calculations using this droplet size distribution and refractive indices of water gave approximately the same attenuation coefficient as was calculated for visibility of 250 m in fog (see Table XVII).

Table XVII
 Cloud and Fog Attenuation
 Coefficients (Km^{-1})

Cloud	
<u>Wavelength (μ)</u>	<u>Attenuation Coefficient</u>
.45	16.34
.55	16.57
.70	16.82
1.0636	17.34

Fog	
<u>Visibility</u>	<u>Attenuation Coefficient</u>
2000m	1.956
1500m	2.608
1000m	3.912
900m	4.347
800m	4.890
700m	5.589
600m	6.520
500m	7.824
400m	9.780
300m	13.040
200m	19.560

Cloud Attenuation Coefficients were calculated using Mie calculations and the Deirmendjian Cl distribution. Fog attenuation coefficients were calculated using Eq (56).

This cloud model indicates that clouds may in general be strong attenuators of radiation. In any case, transmission paths of several hundred meters through such a cloud would greatly reduce the amount of radiation. For example, a path length of 100m through this cloud reduces the energy to about 18% of the original. Such attenuation is an important factor in determining the maximum acquisition and tracking range of the laser-guided weapon system.

Other Attenuating Mechanisms

Several other attenuators are worthy of mention at this point. Some such as snow are highly relevant to this discussion because of their occurrence, but others such as hail were not mentioned because of their rarity.

Snow, freezing rain, and sleet are of the most important of these other attenuating mechanisms. They are important because of their occurrence in this geographical region. Unfortunately, the assumption we have made for our solution using Mie Theory--that is, that the particle is spherical--is not valid for snow. In addition, there are the other complicating factors (such as snow rate) like those encountered for rain. Other phenomena such as blowing dust, hail, and others were not discussed because of their rarity in Germany.

Backscatter

This chapter would be quite incomplete without the mention of backscatter. This term is generally used to describe the problem of that component of the scattered radiation that is scattered directly backward. Backscatter becomes a serious problem when the laser designator (transmitter) and receiver are in close proximity. The problem is perhaps best illustrated by the following example.

Backscatter is a common problem while motoring in heavy fogs at night. If the driver actuates his high beams then he is able to see considerably less than when he was using his low beams. The reason for this is backscattering; that is, more light is being backscattered into the driver's eyes reducing his overall sensitivity. Backscattering is improved by separating the viewing angle and the illumination plane (lights). Separation of the receiver and transmitter is the precise

reason for fog lights on motor vehicles.

This same problem exists in the event the receiver and transmitter for the laser target designator system are in close proximity. This problem increases in magnitude as the amount of scattering increases; the larger the scattered radiation the larger the backscattering. Backscattered radiation is detected by the receiver and therefore becomes an undesirable background signal. Unfortunately backscattering is largest when detector sensitivity must be an optimum. When the scattering is large as in fogs and clouds, the magnitude of the received radiation (reflected from the target) is quite small. The receiver then is not likely to sense the target signal at all.

The magnitude of the backscatter component is dependent on the angle subtended at the receiver by the scatterer (droplet). Since the geometry of each backscatter problem is extremely complex, then the backscatter is generally given in terms of a coefficient expressed in $\text{km}^{-1}/\text{steradian}$. Representative values of the backscatter coefficient are given in Table XVIII.

Use of Attenuation Coefficients in Model

In this chapter, we have derived attenuation coefficients that estimate the attenuation of laser radiation in clouds, rain and fog. All of these coefficients are not additive to yield the extinction coefficient. Clouds and fog are formed on condensation nuclei, for example, and therefore reduce the number of aerosols. In fact, as a good approximation, the attenuation of aerosols is neglected in calculating the atmospheric attenuation in fogs and clouds. The atmospheric extinction coefficient in clouds and fog, then, is the sum

Table XVIII

Representative Per Particle Backscattering Coefficients
for Various Models at .55 μ and 1.063 μ

Model	Refractive Index		Wavelength in Microns	Backscattering Coefficient in (Km ⁻¹ /ster.)
	R	I.		
Continental	1.55	.048	.55	.0159
Haze	1.53	.072	1.0636	.0146
(.03 μ →20 μ)	1.53	.031	.55	.0194
	1.51	.046	1.0636	.0167
Maritime	1.53	.031	.55	.0300
Haze	1.51	.046	1.0636	.0141
Haze	1.53	.031	.55	.0262
L	1.51	.046	1.0636	.0116
Cloud	1.334	.0	.55	.0505
Cl	1.325	.00001	1.0636	.0625

of the molecular attenuation coefficient and the fog or cloud attenuation coefficient discussed in this chapter. Since the former is generally quite small compared to the latter, a reasonable approximation of the atmospheric attenuation coefficient in clouds and fogs is given by the value from Table XVII and Eq (56) respectively.

Unlike the cloud and fog attenuation coefficients, the attenuation coefficient for rain is additive. Although there is evidence that rain does remove atmospheric particulate matter by the processes of rainout and washout discussed earlier, the efficiency of these removal processes is relatively low (Ref 32:161). One of the findings of a six year study in the United States of atmospheric attenuation coefficients is: precipitation in itself does not appear to have a noticeable effect in cleaning the air. Such noticeable atmospheric clearings are associated with frontal passage occurring simultaneously with the rain (Ref 39:961,962). Calculation of atmospheric attenuation in rain, then is the result of the attenuation by the molecules, aerosols, and raindrops.

IX. Summary, Conclusions, and Recommendations

Summary and Model Use

In summary, this report develops a model for prediction of maximum laser target designator system range or stand-off distance where atmospheric attenuation of 1.0636μ laser radiation is the limiting system factor. This report develops an optimum lock-on range equation in which atmospheric conditions and system geometry are the only variables. Major assumptions made in the development of this equation are: (1) the laser designator and receiver have specific electrical and optical design characteristics, (2) the laser beam is reflected only from the target, (3) the target is a diffuse Lambertian surface with ten percent reflectivity, (4) the receiver is designed to electrically discriminate against continuous background signals, and (5) the target is within the field of view of the receiver. In addition, it is assumed that the Beer-Lambert Law describes the atmospheric transmittance of laser radiation.

Maximum lock-on range or standoff distance is reduced to a determination of atmospheric attenuation due to each of the atmospheric attenuating mechanisms: aerosol scattering and absorption, molecular absorption, molecular (Rayleigh) scattering, and scattering of clouds, rain, and fog. Theoretical calculations of the coefficients which describe these attenuating mechanisms are dependent upon four important assumptions: (1) the laser radiation is monochromatic, (2) the atmosphere is characteristic of Central European atmospheric conditions, (3) the atmosphere is horizontally stratified above a flat

earth, and (4) the one kilometer thick vertical layers are assumed to be homogeneous. In addition, calculation of attenuation due to scattering is limited to single scattering theory.

Theoretical calculations show that the greatest attenuators of 1.0636 μ laser radiation are clouds, rain and fog. For dry atmospheric conditions, the aerosol is the largest attenuator, followed by (usually by an order of magnitude or more) molecular absorption and by molecular (Rayleigh) scattering which is negligible. Each of these coefficients is related to the physically measureable or observable ground level meteorological quantities listed below:

σ_m (Molecular attenuation coefficient)	Relative Humidity Temperature Pressure
σ_a (Aerosol attenuation coefficient)	Prevailing visibility
σ_F (Fog attenuation coefficient)	Prevailing visibility
σ_R (Rain attenuation coefficient)	Rain Rate cloud type
σ_c (Cloud attenuation coefficient)	None (For this model- the attenuation coefficient is constant for all clouds.)

Vertical distributions of the molecular and aerosol coefficients are calculated based on mean vertical distributions (for Germany) of the meteorological quantities listed above.

Use of this atmospheric model requires knowledge of the following parameters which are listed together with the attenuation coefficient they determine:

<u>Attenuation Coefficient</u>	<u>Parameter</u>
Molecular	Season of year
Aerosol	Prevailing visibility (Real Time Mixing Height Desired)
Fog	Prevailing visibility
Rain	Rain Rate (cloud type desired)
Cloud	None

The molecular attenuation coefficients are determined using Table XXIV, Page 152. The boundary (mixed) layer aerosol attenuation coefficients are determined using Equation (45) and the aerosol attenuation coefficients for the air mass above are determined using Table XXVIII, Page 164. The cloud attenuation coefficient is obtained from Table XVII, Page 129. Fog attenuation coefficients are obtained from either Table XVII, Page 129, or Equation 56, Page 128. Rain attenuation coefficients are obtained from Table XVI, Page 126.

Each individual attenuation coefficient is summed over the vertical path. The total individual sums (which are now individual vertical optical paths and no longer coefficients) are now added to yield a total attenuation vertical optical path, σH_T , as shown below:

$$\begin{aligned} \sigma H_T &= \sigma H \text{ molecular} + \sigma H \text{ aerosol} \\ \text{For Clouds: } \sigma H_T &= \sigma H \text{ molecular} + \sigma H \text{ cloud} \\ \text{For Fog: } \sigma H_T &= \sigma H \text{ molecular} + \sigma H \text{ fog} \\ \text{For Rain: } \sigma H_T &= \sigma H \text{ molecular} + \sigma H \text{ aerosol} + \sigma H \text{ Rain} \end{aligned}$$

where σH is the attenuation coefficient summed vertically to the required vertical height, H .

To calculate the slant path attenuation, then multiply the resulting σH_T by secant θ , where θ is the angle between the vertical and the line connecting the target and designator or receiver. For cases in which the receiver and designator are not co-located then each optical path must be calculated separately. The total optical depth for the receiver σ_{tr} (where $\sigma_{tr} = \sigma H_T \times \text{secant } \theta$) and total optical depth for the designator σ_{td} (where $\sigma_{td} = \sigma H_T \times \text{secant } \theta$) are then substituted into Equation (67), the laser lock-on range equation.

Use of the model is demonstrated in Appendix C.

Conclusions

Several conclusions may be drawn from the results of this investigation:

1. Current models for the radiative transfer of laser radiation through the atmosphere are limited in their predictions to single scattering solutions with crude multiple scattering correction factors in some cases. The model developed in this report is limited to single scattering theory and hence may underestimate the maximum laser lock-on range.

2. The study of attenuation of laser radiation in the atmosphere due to atmospheric molecular gases is quite far advanced compared to the study of aerosol attenuation. Molecular scattering may be ignored for 1.0636μ radiation. Molecular absorption in this small spectral region ($1.063-1.065\mu$) is not extensively complicated by overlapping molecular absorption lines, but is a function of water vapor absorption lines. Hence, molecular absorption is dependent upon atmospheric water vapor concentration.

3. Aerosol attenuation of 1.0636μ radiation is by comparison to molecular attenuation a more important factor in limiting maximum laser lock-on range. Precise knowledge, however, concerning aerosol particle size distributions, number densities, and vertical distributions is lacking because of the difficulty in measuring such quantities. Of particular consequence for this tactical problem is the vertical aerosol distribution. The model developed in this report employs the boundary layer concept which is suggested by recent extensive aircraft measurements. The boundary layer is an aerosol particle dense layer where the particles are approximately uniformly mixed. Above the boundary (mixed) layer the air mass is relatively clear and the particle concentration markedly less. The height of such a layer is variable and difficult to measure from ground based observations. In fact, hourly predictions of aerosol attenuation coefficients are impossible without a detailed history of air mass and current surface and upper level meteorological conditions.

4. The aerosol attenuation of 1.0636μ radiation is quite sensitive to the particle size distribution used, for particle size distribution establishes the primary relationship among aerosol attenuation coefficients at various wavelengths. Particle composition (index of refraction) and upper and lower particle size limits are less important factors.

5. The total aerosol attenuation coefficient at 1.0636μ is related to atmospheric particle concentration which is determined by measuring prevailing visibility. Prevailing visibility, however, is a rather inexact meteorological observable; it depends on many scientifically unmeasurable factors including the local terrain, visual objects available, and visual acuity of the observer. Such visual observations would not be highly reliable for real-time operational calculation of attenuation. In fact, such observations most probably would not be available for hostile areas.

6. Calculation of attenuation due to the scattering by clouds, rain, and fog are based on assumptions of homogeneity of the scattering media and other assumptions concerning particle size distribution. Such calculations then are necessarily crude, but can be relied upon to yield relative attenuation magnitudes and estimates of maximum lock-on range.

Recommendations

The following are problem areas and should be investigated to improve knowledge in this area and increase the reliability of estimating laser lock-on ranges:

1. The model developed in this report is limited because of the assumptions made in its development. These assumptions may only be checked and the model validated through extensive meteorological measurements made during the course of flight tests. Weapon systems may be properly designed and evaluated only with a complete knowledge of the environment in which they operate. The lack of proper and reliable meteorological data for flight weapons tests to date is quite evident.

2. Since clouds are a common atmospheric phenomena and they are also a chief attenuation mechanism then atmospheric data records of cloud cover and height should be correlated with current cloud-free line-of-sight methodology to contribute to determination of lock-on range.

3. The effectiveness of any weapon system in any geographical region may be evaluated as a function of atmospheric conditions only in light of the relative occurrence of the different conditions. Such information with cloud data included was requested by this author, but due to technical delays was not available for inclusion in this report.

4. This model like other laser attenuation models is limited to the assumption of single scattering. This assumption may limit the effectiveness of these models to predict laser lock-on ranges when a *diffuse* Lambertian target is assumed. If typical military targets are diffuse reflectors (as current literature suggests), then the applicability of the Beer-Lambert law to such reflected radiation must be investigated.

Bibliography

1. *Air Force Surveys in Geophysics, No. 212.* AFCRL-69-0487. AFCRL-69-0487. Revision of Chapter 5 in *Handbook of Geophysics and Space Environments*. L. G. Hanscom Field, Bedford, Massachusetts: Air Force Cambridge Research Laboratory, November 1969.
2. Barnhardt, E. A. and J. L. Streete. "A Method for Predicting Atmospheric Aerosol Scattering Coefficients in the Infrared." *Applied Optics*, 9:1337-1344 (June 1970).
3. Bell, Ely E., *et al.* "Spectral Radiance of Sky and Terrain at Wavelengths Between 1 and 20 Microns. II. Sky Measurements." *Journal of Optical Society of America*, 50:1313-1320 (December 1960).
4. Blattner, W. and Michael B. Wells. *Monte Carlo Studies of Light Transport Through Natural Atmospheres*. RRA-T7304. Radiation Research Associates, Fort Worth, Texas. Prepared for Air Force Cambridge Research Laboratories, Bedford, Massachusetts, January 1973.
5. Breitling, Lt. Col. P.J. Personal Communication. Headquarters Air Weather Service, Scott Air Force Base, Illinois.
6. Buck, A. L. "Effects of Atmosphere on Laser Beam Propagation." *Applied Optics*, 6:703-708 (April 1967).
7. Bullrich, K. *et al.* "New Aspects of Scattering and Absorbing Properties of Atmospheric Aerosol Particles," *Journal of Colloid and Interface Science*, 39:546-550 (June 1972).
8. Butcher, Samuel S. and Robert J. Charlson. *An Introduction to Air Chemistry*. New York: Academic Press, 1972.
9. Byers, Horace R. *General Meteorology*. New York: McGraw-Hill Book Company, Inc., 1944.
10. Caratula, Captain Carl. *Precipitation Attenuation of 10.6 Micron Radiation*. Unpublished Report. Air Force Weapons Laboratory, Kirtland Air Force Base, New Mexico, 1972.
11. Caton, P. G. F. "Raindrop Size Distribution in the Free Atmosphere." *Quarterly Journal of the Royal Meteorological Society*, 92:15 (January 1966).
12. Chin-I Lin, Baker, M. and R. J. Charlson. "Absorption Coefficient of Atmospheric Aerosol: A Method for Measurement." *Applied Optics*, 12:1356-1363 (June 1973).

13. Chu, T. S. and D. C. Hogg. "Effects of Precipitation on Propagation at 0.63, 3.5 and 10.6 Microns." *Bell System Technical Journal*, 48:723-759 (May-June 1968).
14. Curcio, J. A. *et al.* *Atmospheric Scattering in the Visible and Infrared*. NRL Report 5567. Radiometry Branch, Optics Division, U.S. Naval Research Laboratory, January 1961.
15. Curcio, Joseph A. "Evaluation of Atmospheric Aerosol Particle Size Distribution from Scattering Measurements in the Visible and Infrared." *Journal of the Optical Society of America*, 51:548-551 (May 1961).
16. Deirmendjian, D. "Atmospheric Attenuation of Infrared Radiation." *Quarterly Journal of the Royal Meteorological Society*, 85:404-411 (October 1959).
17. Deirmendjian, D. *Electronic Scattering on Spherical Polydispers ms.* New York: American Elsevier Publishing Company, 1969. Also Rara Corporation Report Number R-456-PR.
18. Deirmendjian, D. "Scattering and Polarization Properties of Water Clouds and Hazes in the Visible and Infrared." *Applied Optics*, 3:187-196 (February 1964).
19. Duff, Edward A. *Atmospheric Contrast Transmission: Application to the Visual Detection and Electro-Optical Lock-on Problems*. Masters Thesis. Wright-Patterson AFB, Ohio: Air Force Institute of Technology, June 1972. AD743560.
20. Duntley, Seibert Q. *et al.* *Airborne and Ground-based Measurements of Optical Atmospheric Properties in Central New Mexico*. AFCRL-72-0461 and SIO Ref 72-71. University of California, San Diego, Scripps Institution of Oceanography, Visibility Laboratory, September 1972.
21. Duntley, Seibert Q. *et al.* *Airborne Measurements of Optical Atmospheric Properties in Southern Germany*. AFCRL-72-0225 and SIO Ref 72-64. University of California, San Diego, Scripps Institution of Oceanography, Visibility Laboratory, July 1972.
22. Duntley, Seibert Q. *et al.* *Airborne Measurements of Optical Atmospheric Properties, Summary and Review, Final Report*. AFCRL-72-0593 and SIO Ref 72-82. University of California, San Diego, Scripps Institution of Oceanography, Visibility Laboratory, November 1972.
23. Duntley, Seibert Q. "The Reduction of Apparent Contrast by the Atmosphere." *Journal of the Optical Society of America*, 38:179-191 (February 1948).

24. *Electro-Optics Handbook*, RCA Defense Electronic Products, P.O. Box 538, Burlington, Mass., October 1968.
25. Elterman, L. *An Atlas of Aerosol Attenuation and Extinction Profiles for the Troposphere and Stratosphere*. AFCRL-66-828. L.G. Hanscom Field, Bedford, Massachusetts: Air Force Cambridge Research Laboratory, 1966.
26. Elterman, L. *Atmospheric Attenuation Model, 1964, in the Ultraviolet, Visible, and Infrared Regions for Altitudes to 50 Km*. AFCRL-64-740, L. G. Hanscom Field, Bedford, Massachusetts: Air Force Cambridge Research Laboratory, 1964.
27. Elterman, L. *UV, Visible, and IR Attenuation for Altitudes to 50 Km, 1968*. AFCRL-68-0153. L. G. Hanscom Field, Bedford, Massachusetts: Air Force Cambridge Research Laboratory, April 1968.
28. Elterman, L. *Vertical-Attenuation Model with Eight Surface Meteorological Ranges 2 to 13 Kilometers*. AFCRL-70-0200. L. G. Hanscom Field, Bedford, Massachusetts: Air Force Cambridge Research Laboratory, March 1970.
29. *Federal Meteorological Handbook, Number One. Surface Observations*. U. S. Department of Transportation, U. S. Government Printing Office, Washington, D. C., January 1970.
30. Fenn, Robert W. Personal Communication. Optical Physics Laboratory, Air Force Cambridge Research Laboratories, Bedford, Massachusetts.
31. Fischer, K. "Massenabsorptionskoeffizient naturliches Aerosolteilchen im Wellenlängenbereich Zwischen 0.4 and 2.4 μm ." *Beiträge zur Physik der Atmosphäre*, 46:89-100 (1973).
32. Flowers, E. C. *et al.* "Atmospheric Turbidity over the United States. 1961-1966." *Journal of Applied Meteorology*, 8:955-962 (December 1969).
33. Goody, R. M. *Atmospheric Radiation, I. Theoretical Basis*. Oxford: Oxford University Press, 1964.
34. Hanel, Gottfried. "Computation of the Extinction of Visible Radiation by Atmospheric Aerosol Particles as a Function of the Relative Humidity, Based on Measured Properties." *Aerosol Science*, 3:377-386 (1972).
35. Herzberg, G. *Molecular Spectra and Molecular Structure. I. Spectra of Diatomic Molecules*. New York: Van Nostrand, 1950.
36. Herzberg, G. *Molecular Spectra and Molecular Structure. II. Infrared and Raman Spectra of Polyatomic Molecules*. New York: Van Nostrand, 1945.

37. Hess, S. L. *Introduction to Theoretical Meteorology*. New York: Harcourt, Brace and World, Inc., 1959.
38. Hodges, John A. "Aerosol Extinction Contribution to Atmospheric Attenuation in Infrared Wavelengths." *Applied Optics*, 11:2304-2310 (October 1972).
39. Holzworth, George C. *Mixing Heights, Wind Speeds, and Potential for Urban Air Pollution Throughout the Contiguous United States*. AP-101, U. S. Environmental Protection Agency, Research Triangle Park, N.C., 1972.
40. *Inadvertent Climate Modification*. Report on the Study of Man's Impact on Climate Hosted by the Royal Swedish Academy of Sciences and Royal Swedish Academy of Engineering Sciences. Cambridge: The MIT Press, 1971.
41. Junge, Christian E. *Air Chemistry and Radioactivity*. New York: Academic Press, 1963.
42. Jungling, Maj. K. C. Personal communication. Air Force Institute of Technology, Air University, Wright-Patterson AFB, Ohio.
43. Koschmieder, H. "Theorie der horizontalen Sichtweite." *Beitr. Physikfreier Atm.* 12:33-53, and 171-181, 1924.
44. Landsberg, H. E. and J. V. Miegheem. (Editors). *Advances in Geophysics, Volume 10*. New York: Academic Press, 1964.
45. Lydon, Major David S. Personal communication. USAF Environmental Technical Applications Center, Navy Yard Annex, Washington, D.C.
46. McCaldin, Ray O. and R. S. Sholtes. "Mixing Height Determination by Means of an Instrumented Aircraft." *Paper No. ME398*. Second International Clean Air Congress, Washington, D.C., December 6-11, 1970.
47. McClatchey, R. A. *et al.* *AFCRL Atmospheric Absorption Line Parameters Compilation*. AFCRL-TR-73-0096. L. G. Hanscom Field, Bedford, Massachusetts: Air Force Cambridge Research Laboratories, 26 January 1973.
48. McClatchey, R. A. and J. E. A. Selby. *Atmospheric Transmittance From 0.25 to 28.5 Microns: Computer Code Lowtran 2*. AFCRL-72-0745. L. G. Hanscom Field, Bedford, Massachusetts: Air Force Cambridge Research Laboratory, 29 December 1972.
49. McClatchey, R. A. *et al.* *Optical Properties of the Atmosphere*. AFCRL-72-0497. L. G. Hanscom Field, Bedford, Massachusetts: Air Force Cambridge Research Laboratory, 24 August 1972.

50. McClatchey, R. A. Tables of Values Used for the Absorption Lines Parameters. L. G. Hanscom Field, Bedford, Massachusetts: Air Force Cambridge Research Laboratory.
51. McQuage, Captain Neil D. Personal communication. Air Force Avionics Laboratory, Wright-Patterson Air Force Base, Ohio.
52. Mardis, James V. *Lock-on Ranges of Laser-Guided Systems*. Masters Thesis. Wright-Patterson AFB, Ohio: Air Force Institute of Technology, June 1972. AD744814.
53. Middleton, W. E. K. *Vision Through the Atmosphere*. Toronto: University of Toronto Press, 1952.
54. Neuberger, Hans. *Introduction to Physical Meteorology*. University Park, Pennsylvania: Pennsylvania State University, 1966.
55. Nazaki, Kenneth Y. *Mixing Depth Model Using Hourly Surface Observations*. Report 7053. Building 159, Navy Yard Annex, Washington, D.C.: USAF Environmental Technical Applications Center, November 1973.
56. Ross, M., A. R. Kraemer, and D. J. Freeman. *Space Data Relay Subsystem Laser Communications Preliminary Subsystem Design*. Final Report. AF Unit Post Office, Los Angeles, California: Headquarters Space and Missile Systems Organization, Air Force Systems Command, November 1970. SAMSO Technical Report TR71-251.
57. Saucier, Walter J. *Principles of Meteorological Analysis*. Chicago: University of Chicago Press, 1955.
58. Thekaekara, M. P. "Proposed Standard Values of the Solar Constant and the Solar Spectrum." *Journal of Environmental Sciences*, pp 6-9 (September/October 1970).
59. Try, Major Paul D. *An Investigation of the Influence of Aerosols on the Solar Radiation Field and the Heating of a Multiple Scattering Polluted Urban Atmosphere*. Unpublished Dissertation. University of Washington, Seattle, Washington, November 1972.
60. Try, Major Paul D. Personal communication. Headquarters Air Weather Service, Scott Air Force Base, Illinois.
61. Valley, Shea L. (Editor). *Handbook of Geophysics and Space Environments*. New York: McGraw-Hill Book Company, Inc., 1965.
62. Van de Hulst, H. C. *Light Scattering by Small Particles*. New York: John Wiley and Sons, Inc., 1957.
63. Vatsia, Mishri, L. *Atmospheric Optical Environment*. Research and Development Technical Report ECOM-7023. United States Army

Electronics Command, Fort Monmouth, N.J., September 1972.

64. Volz, Frederic E. "Infrared Absorption by Atmospheric Aerosol Substances." *Journal of Geophysical Research*, 77:1017-1013 (February 1972).

65. Volz, Frederic E. "Optik der Tropfen." *Handbook der Geophysik*, Volume VIII, 1956.

66. Volz, Frederic E. Tables of Values for the Refractive Index (to be published). L. G. Hanscom Field, Bedford, Massachusetts: Air Force Cambridge Research Laboratory.

67. Waggoner, Alan. Personal Communication. Department of Atmospheric Chemistry, University of Washington, Seattle, Washington.

68. Whitby, K. T. *et al.* "The Aerosol Size Distribution of Los Angeles Smog." *Journal of Colloid Science and Interface Science*, 39:177-204 (April 1972).

69. Whitby, K. T. *et al.* "The Minnesota Aerosol-Analyzing System Used in the Los Angeles Smog Project." *Journal of Colloid and Interface Science*, 39:136-164 (April 1972).

70. Winkler, Peter and Christian Junge. "The Growth of Atmospheric Aerosol Particles as a Function of the Relative Humidity. Part I: Method and Measurements at Different Locations." *Journal De Recherches Atmospheriques*, 617-637 (1972).

71. Wolfe, W. F. (Ed). *Handbook of Military Infrared Technology*, Office of Naval Research, Department of the Navy, Washington, D.C., 1965.

72. Yamamoto, G. and Masayuki Tanaka. "Determination of Aerosol Size Distribution from Spectral Attenuation Measurements." *Applied Optics*, 8:447-453 (February 1969).

73. Zuev, V. E. *et al.* "Propagation of Laser Beams in Scattering Media." *Applied Optics*, 8:137-141 (January 1969).

APPENDIX A

Molecular Absorption Calculations and Tables

For absorption coefficient calculations in the 1.0636μ case, Eq (23) reduces to

$$\alpha_{in} = \sum_i \frac{S_{i_o}(296) \cdot \frac{Q_{v_o}(296)}{Q_{v_o}(T)} \cdot \left(\frac{T}{296}\right) \cdot e^{\left[\frac{1.439E''(T-296)}{296T}\right]} \cdot \alpha_{i_o} \left(\frac{P}{1013}\right) \sqrt{\frac{296}{T}} \cdot m_o}{\pi \left[(v-v_{i_o})^2 + \left(\alpha_{i_o} \left(\frac{P}{1013}\right) \sqrt{\frac{296}{T}} \right)^2 \right]} + \sum_k \frac{S_{k_w}(296) \frac{Q_{v_w}(296)}{Q_{v_w}(T)} \cdot \left(\frac{T}{296}\right) \cdot e^{\left[\frac{1.439E''(T-296)}{296T}\right]} \cdot \alpha_{k_w} \left(\frac{P}{1013}\right) \sqrt{\frac{296}{T}} \cdot m_w}{\pi \left[(v-v_{k_w})^2 + \left(\alpha_{k_w} \cdot \frac{P}{1013} \sqrt{\frac{296}{T}} \right)^2 \right]} \quad (58)$$

where the i subscript indicates the i lines of oxygen and k the k lines of water vapor. The w and o indicate water vapor and oxygen respectively.

The rotational partition function is proportional to $(T/296)$ in the case of oxygen and $(T/296)^{1.5}$ in the case of water vapor. This has been included in Eq (58). The various values for the vibrational partition function may be determined from Table IXX. The intensities, ground energy levels, and line half widths at half heights are given in Table XX.

Table IXX
 Vibrational Partition Functions (Ref 47:4)

Molecule	j	Temperature	175	200	225	250	275	296	325
H ₂ O	1.5		1.000	1.000	1.000	1.000	1.000	1.000	1.001
O ₂	1.0		1.000	1.000	1.000	1.000	1.000	1.000	1.001

Table XX
 Absorption Line Parameters
 (Ref 50)

Wavenumber (cm ⁻¹)	S (cm ⁻¹ /mole cm ⁻²)	α ₀ (cm ⁻¹)	E'' (cm ⁻¹)
9385.570	.109E-24	.051	1255.160
9385.920	.233E-24	.076	586.480
9386.220	.758E-26	.048	81.581
9386.960	.106E-24	.081	224.830
9388.236	.596E-26	.048	79.565
9388.980	.542E-24	.080	885.620
9390.556	.702E-26	.048	130.437
9392.596	.580E-26	.048	128.398
9392.604	.432E-26	.048	16.388
9393.460	.660E-26	.059	1006.120
9394.592	.602E-26	.048	190.775
9396.653	.514E-26	.048	188.713
9398.220	.227E-25	.063	882.930
9398.325	.480E-26	.048	262.583
9400.407	.420E-26	.048	260.501
9401.756	.357E-26	.048	345.850
9401.760	.345E-25	.039	1327.140
9403.175	.453E-26	.048	42.224
9403.460	.104E-25	.038	1327.140
9403.857	.319E-26	.048	343.749
9404.882	.249E-26	.048	440.565
9407.002	.225E-26	.048	438.444
9407.701	.163E-26	.048	546.712
9409.070	.541E-24	.061	586.260
9409.840	.149E-26	.048	544.572
9410.210	.998E-27	.048	664.275
9411.540	.954E-26	.065	744.090
9412.340	.331E-26	.041	1033.510
9412.368	.921E-27	.048	662.118
9412.407	.576E-27	.048	793.239
9412.820	.417E-24	.069	704.220

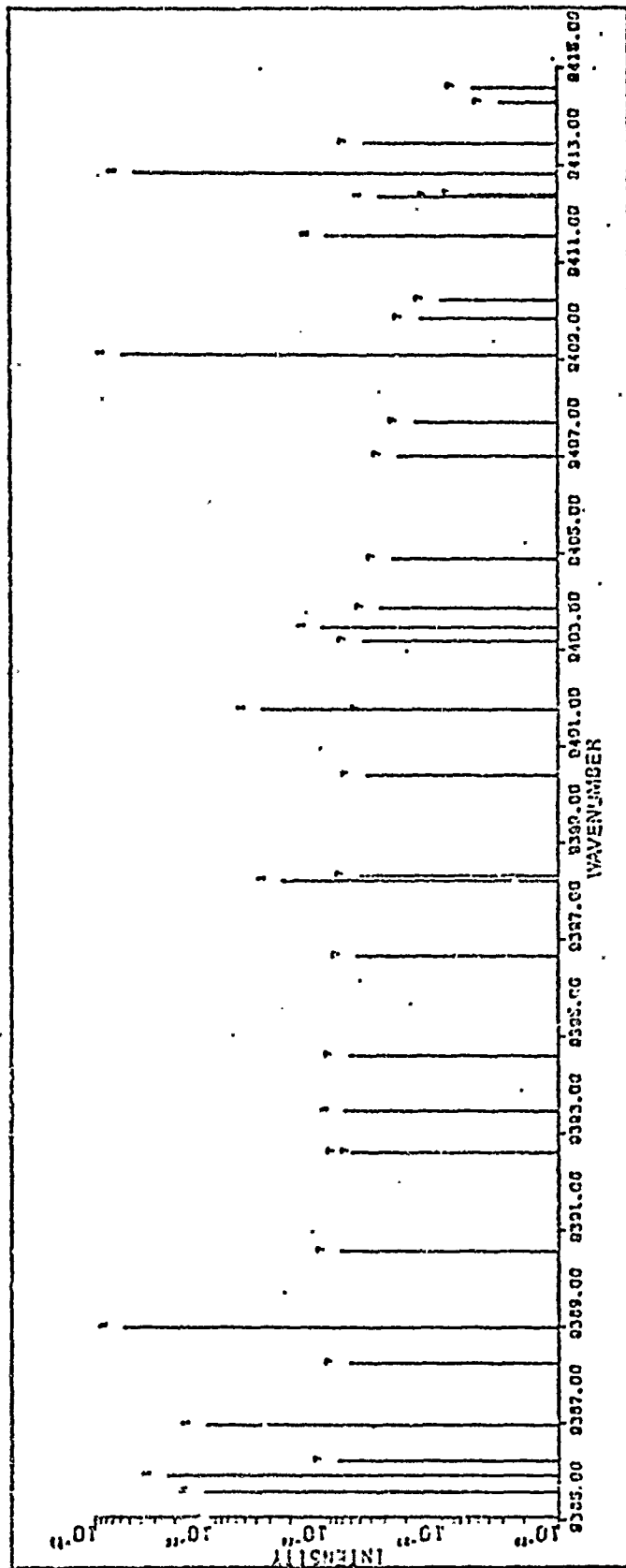


Fig. 23. Absorption Line Intensities 9385 cm^{-1} to 9415 cm^{-1} . Index 1 indicates Water Vapor Line; Index 7 indicates Oxygen.

Absorption Lines

All the absorption lines with intensities greater than 1.0×10^{-27} ($\text{cm}^{-1}/\text{molecules cm}^{-2}$) are shown in Figure 23. The number one on the line indicates water vapor; a seven represents oxygen.

Absorption Coefficient Tables

Tables XXI through XXVII show the absorption coefficients (in km^{-1}) for the different altitudes and model atmospheres for seven wavenumbers. Tables XXI through XXV are for wavenumbers in the spectral region of interest. Table XXVI and Table XXVII are for wavenumbers outside the spectral region.

The following relationship between wavenumber, k , and wavelength, λ , is given for convenience of the reader:

$$\lambda = 10^4/k$$

where λ is expressed in microns ($1 \times 10^{-6}\text{m}$)

and k is expressed in cm^{-1}

Table XXI

Molecular Absorption Coefficients
for $K = 9389.6714$ Wavenumbers

Altitude (Km)	Atmosphere Models		U.S. Standard
	Midlat. Summer	Midlat. Winter	Spring Fall
0	1.480E-03	4.210E-04	6.700E-04
0 - 1	1.179E-03	3.518E-04	5.494E-04
1 - 2	6.908E-04	2.378E-04	3.503E-04
2 - 3	3.834E-04	1.610E-04	2.183E-04
3 - 4	2.062E-04	1.057E-04	1.341E-04
4 - 5	1.166E-04	6.966E-05	8.529E-05
5 - 6	7.005E-05	4.879E-05	5.669E-05
6 - 7	4.668E-05	3.508E-05	3.956E-05
7 - 8	3.233E-05	2.585E-05	2.857E-05

Table XXII

Molecular Absorption Coefficients
for $K = 9398.220$ Wavenumbers

Altitude (Km)	Atmosphere Models		U.S. Standard
	Midlat. Summer	Midlat. Winter	Spring Fall
0	8.188E-03	4.177E-03	5.054E-03
0 - 1	7.187E-03	3.777E-03	4.542E-03
1 - 2	5.364E-03	3.047E-03	3.599E-03
2 - 3	3.841E-03	2.426E-03	2.784E-03
3 - 4	2.695E-03	1.875E-03	2.111E-03
4 - 5	1.920E-03	1.426E-03	1.595E-03
5 - 6	1.393E-03	1.090E-03	1.204E-03
6 - 7	1.047E-03	8.232E-04	9.096E-04
7 - 8	7.833E-04	6.177E-04	6.850E-04

Table XXIII

Molecular Absorption Coefficients
for K = 9398.4962 Wavenumbers

Altitude (Km)	Atmosphere Models		U.S. Standard
	Midlat. Summer	Midlat. Winter	Spring Fall
0	1.532E-03	1.432E-03	1.393E-03
0 - 1	1.358E-03	1.284E-03	1.255E-03
1 - 2	1.054E-03	1.017E-03	1.005E-03
2 - 3	8.212E-04	8.023E-04	8.012E-04
3 - 4	6.432E-04	6.312E-04	6.353E-04
4 - 5	5.078E-04	4.961E-04	5.021E-04
5 - 6	4.011E-04	3.878E-04	3.949E-04
6 - 7	3.158E-04	3.011E-04	3.087E-04
7 - 8	2.475E-04	2.320E-04	2.396E-04

Table XXIV

Molecular Absorption Coefficients
for K = 9401.760 Wavenumbers

Altitude (Km)	Atmosphere Models		U.S. Standard
	Midlat. Summer	Midlat. Winter	Spring Fall
0 - 1	2.498E-02	1.406E-02	1.700E-02
1 - 2	2.298E-02	1.376E-02	1.624E-02
2 - 3	1.939E-02	1.323E-02	1.489E-02
3 - 4	1.649E-02	1.277E-02	1.378E-02
4 - 5	1.444E-02	1.228E-02	1.290E-02
5 - 6	1.319E-02	1.183E-02	1.227E-02
6 - 7	1.241E-02	1.148E-02	1.180E-02
7 - 8	1.192E-02	1.115E-02	1.141E-02
	1.150E-02	1.083E-02	1.105E-02

Table XXV

Molecular Absorption Coefficients
for $K = 9403.857$ Wavenumbers

Altitude (Km)	Atmosphere Models		U.S. Standard Spring Fall
	Midlat. Summer	Midlat. Winter	
0	1.116E-02	1.092E-02	1.108E-02
0 - 1	1.112E-02	1.088E-02	1.103E-02
1 - 2	1.104E-02	1.080E-02	1.094E-02
2 - 3	1.096E-02	1.073E-02	1.084E-02
3 - 4	1.088E-02	1.063E-02	1.074E-02
4 - 5	1.079E-02	1.051E-02	1.062E-02
5 - 6	1.069E-02	1.038E-02	1.050E-02
6 - 7	1.059E-02	1.024E-02	1.036E-02
7 - 8	1.046E-02	1.008E-02	1.020E-02

Table XXVI

Molecular Absorption Coefficients
for $K = 9388.98$ Wavenumbers
(Outside Spectral Region)

Altitude (km)	Atmosphere Models		U.S. Standard Spring Fall
	Midlat. Summer	Midlat. Winter	
0	9.892E-02	1.891E-02	3.901E-02
0 - 1	8.470E-02	1.676E-02	3.397E-02
1 - 2	5.893E-02	1.299E-02	2.485E-02
2 - 3	3.759E-02	9.792E-03	1.710E-02
3 - 4	2.226E-02	6.464E-03	1.096E-02
4 - 5	1.297E-02	3.779E-03	6.819E-03
5 - 6	7.536E-03	2.238E-03	4.140E-03
6 - 7	4.790E-03	1.170E-03	2.475E-03
7 - 8	2.940E-03	5.054E-04	1.430E-03

Table XXVII

Molecular Absorption Coefficients
for $K = 9407.07$ Wavenumbers
(Outside Spectral Region)

Altitude (Km)	Midlat. Summer	Midlat. Winter	U.S. Standard Spring Fall
0	1.306E-01	2.792E-02	5.298E-02
0 - 1	1.138E-01	2.406E-02	4.082E-02
1 - 2	8.021E-02	1.975E-02	3.545E-02
2 - 3	5.258E-02	1.520E-02	2.526E-02
3 - 4	3.218E-02	1.029E-02	1.6815E-02
4 - 5	1.937E-02	6.237E-03	1.087E-02
5 - 6	1.167E-02	3.830E-03	6.869E-03
6 - 7	7.692E-03	2.064E-03	4.277E-03
7 - 8	4.910E-03	9.113E-04	2.579E-03

APPENDIX B

Summary of Mie Theory and Calculation:

Outline of Mie Theory

In 1908, Gustov Mie solved the problem of a monochromatic plane wave incident on a homogeneous, isotropic *sphere* of radius r surrounded by a transparent homogeneous and isotropic medium. The incident wave causes oscillations of the free and bound charges in phase with the applied radiation. These oscillating charges (dipole) in turn create secondary electric and magnetic fields. These fields, both inside and outside the sphere, are expressed by Maxwell's Equations and a formal solution of the problem involves solving these equations with the appropriate boundary conditions.

An abbreviated derivation of the fields inside and outside the sphere is presented in Van de Hulst, Chapter 9. Basically, the field outside the sphere is composed of the scattered wave and the incident wave. Applying the boundary conditions and the conditions to be satisfied at infinity, then the outside scattered and incident waves are solved in terms of Legendre Polynomials and Bessel Functions. Likewise, the waves inside the particle are represented by Legendre Polynomials and Bessel Functions, due to the geometry of the problem. Matching the boundary conditions of the two functions now completes the solution. The field at any point inside or outside the sphere may be expressed in terms of known functions.

The intensity of the scattered radiation at any point that is a great distance, R , from the center of the sphere where θ is the scattering angle is given by

$$I = \frac{I_0}{R^2} \frac{\lambda^2}{8\pi^2} \left[i_1(m, x, \theta) + i_2(m, x, \theta) \right] \quad (59)$$

where m = complex refractive index of the sphere with respect to the medium

$x = 2\pi r/\lambda$, the dimensionless size parameter

r = radius of the sphere

θ = angle between the incident and scattered radiation

I_0 = Intensity of the incident radiation (Ref 68:83).

The intensity functions of the scattered light, i_1 and i_2 , are respectively the components perpendicular and parallel to the plane formed by the incident and scattered beams. The determination of the intensity by Mie Theory is generally then the computation of the intensity functions:

$$i_1 = |S_1(\theta)|^2 \quad (60)$$

$$i_2 = |S_2(\theta)|^2$$

where $S_1(\theta)$ and $S_2(\theta)$ are the amplitude functions.

The field components are directly proportional to these amplitude functions. The amplitudes are given by

$$S_1(\theta) = \sum_{n=1}^{\infty} \frac{2n+1}{n(n+1)} \left| a_n \pi_n(\cos \theta) + b_n \tau_n(\cos \theta) \right| \quad (61)$$

$$S_2(\theta) = \sum_{n=1}^{\infty} \frac{2n+1}{n(n+1)} \left| b_n \pi_n(\cos \theta) + a_n \tau_n(\cos \theta) \right|$$

where a_n and b_n are Riccati-Bessel functions, which may be written in terms of spherical Bessel functions, and where π_n and τ_n are scattering angle functions. These scattering angle functions are the result of the derivation of the tangential field components. These functions are written

$$\begin{aligned}\pi_n(\cos\theta) &= \frac{1}{\sin\theta} P_n'(\cos\theta) \\ \tau_n(\cos\theta) &= \frac{d}{d\theta} P_n'(\cos\theta)\end{aligned}\tag{62}$$

where P_n are associated Legendre Polynomials.

The efficiency factor is defined by Van de Hulst as the ratio of the outgoing flux to the incident flux per unit geometrical cross-sectional area of the sphere. These factors are given in Chapter 9 of Reference 62 as:

$$\begin{aligned}Q_{sca} &= \frac{2}{x^2} \sum_{n=1}^{\infty} (2n+1) \{ |a_n|^2 + |b_n|^2 \} \\ Q_{ext} &= \frac{2}{x^2} \sum_{n=1}^{\infty} (2n+1) \operatorname{Re}(a_n + b_n) \\ Q_{abs} &= Q_{ext} - Q_{sca}\end{aligned}\tag{63}$$

where Q_{sca} = Scattering efficiency factor

Q_{ext} = Extinction efficiency factor, and

Q_{abs} = Absorption efficiency factor

These are the efficiency factors for one particle of unit size, $x = 2\pi r/\lambda$. The foregoing expressions now define the Mie parameters

from which all other parameters needed to describe intensity and polarization produced by a single sphere can be derived.

The scattering due to N particles of radius r in a volume is then

$$\beta = N\pi r^2 Q_{sca} \quad (64)$$

where the area is πr^2 .

Generally, however, there are many-sized particles in a volume and the scattering coefficient, β , for a volume of polydisperse spheres is

$$\beta = \pi \int_{r_1}^{r_2} Q_{sca}(r) n(r) r^2 dr \quad (65)$$

where $n(r)$ = the size distribution of spheres,

$Q(r)$ = scattering efficiency at radius r .

This scattering coefficient is generally written in terms of the size parameter, $x = 2\pi r/\lambda$. Then Eq (65) becomes

$$\beta = \frac{\lambda^3}{8\pi^2} \int_{x_1}^{x_2} x^2 n(x) Q_{sca}(x) dx \quad (66)$$

The size distribution function $n(x)$ can be of any form. For aerosol, rain and fog distributions, the function $n(x)$ is a smoothly varying function such as the log-normal, modified gamma or power law distribution or it may be a discontinuous distribution. These distributions are discussed in Chapter 5. The scattering efficiency function, Q_{sca} , on the other hand, is an oscillatory function which is

dependent on the complex index of refraction and the size parameter, x . Figure 24 shows this function for various indices of refraction as a function of the size parameter.

Mie Theory is an exact computation of the scattering of a plane wave incident on a sphere. There are two approximations to exact Mie Theory: Rayleigh scattering and Geometric scattering. The Rayleigh is an approximation to Mie Theory for the case $r \ll \lambda$; that is the radius of the particle is much smaller than the wavelength of the incident radiation. The basis of this approximation is that the contribution of the efficiency factor Q_{sca} is small in this region so that the contribution to the total scattering is small regardless of the magnitude of $n(x)$. The other approximation is the Geometrical approximation, valid for the region $r \gg \lambda$. In this region, the scattering efficiency factor Q_{sca} approaches a constant value as shown in Figure 24.

Description of Program

The computer program used for calculations in this report was originally designed by Major Paul D. Try of Headquarters, Air Weather Service for use in the visible spectral region. The program was converted for use on the CDC 6600 at Air Force Institute of Technology by this author and modified for use in the near infrared as well as the visible spectral region. A program listing is not included in this document. A complete program is on file, however, at the Department of Physics (ENP), Air Force Institute of Technology, Wright-Patterson Air Force Base, Ohio. A short description of this

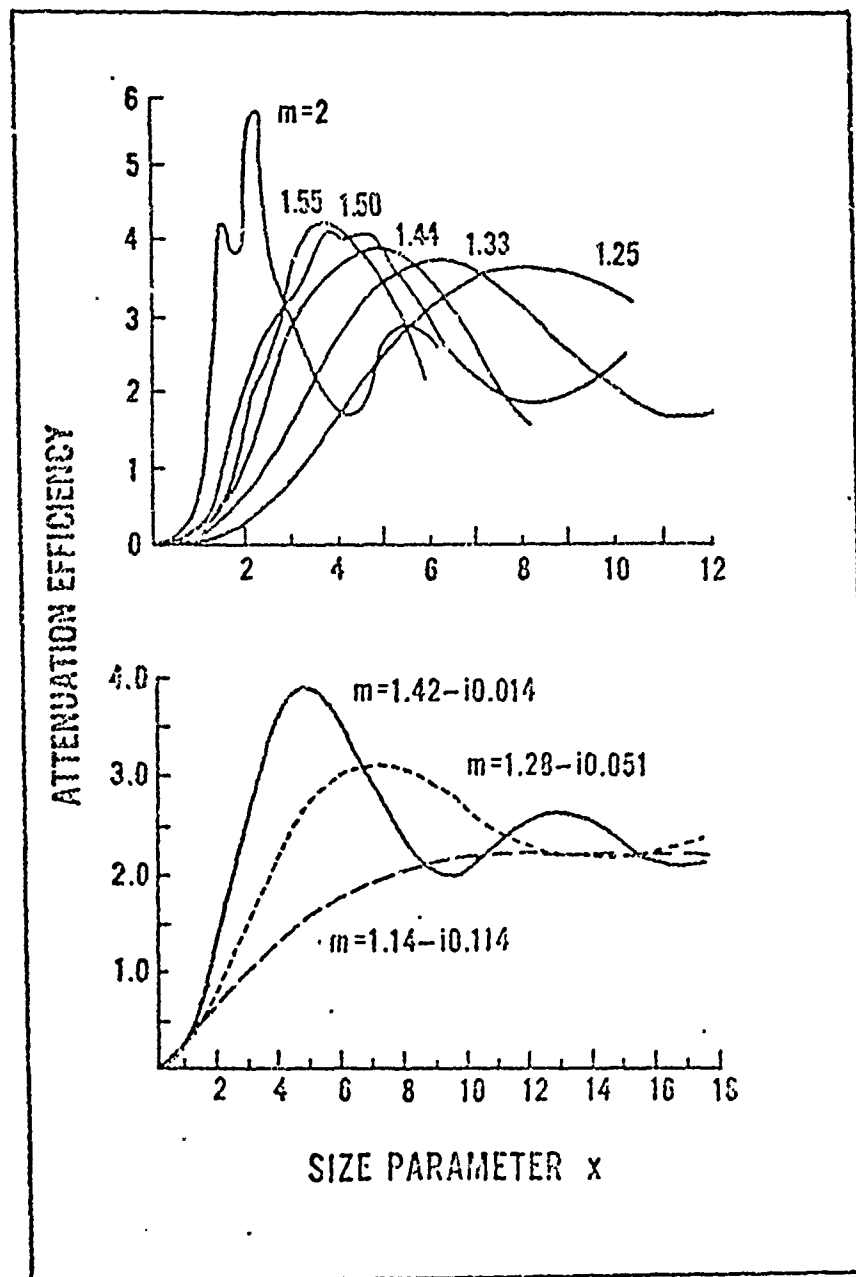


Fig. 24. Efficiency Factor as a Function of the Size Parameter for Different Indices of Refraction (Ref 63:91)

program follows.

The program contains two subroutines. One of the subroutines does exact Mie theory calculations. This subroutine was originally developed by J. V. Dave in IBM Report No. 360D-17.4.002 and is based on Mie theory as explained in Reference 62. The other subroutine is an approximation method to the exact Mie calculations which was programmed by this author based on articles by John A. Hodges (Ref 38:2510) and by D. Deirmendjian (Ref 17:29,30). This approximation scheme is specifically designed to limit lengthy machine calculations. The main program uses the Romberg Integration technique to integrate over the particle size distribution.

APPENDIX C

Use of the Model

In order to determine the lock-on range of the laser target designator system receiver, the geometry of the problem must be described. Once the problem geometry is described then solution of the problem is reduced to a two-step process: (1) determination of the total atmospheric attenuation coefficients based on atmospheric conditions (observables), and (2) substitution of these coefficients into the laser lock-on range equation

$$R_r^2 e^{\sigma_{tr}} = (6.7 \times 10^9 \text{m}^2) e^{-\sigma_{td}} \quad (67)$$

which is a simplification of Eq (12) and where σ_{tr} is the total optical depth (attenuation coefficient times path length) from target to receiver and σ_{td} is the total optical depth from designator to target.

The first step is the subject of this work, and therefore once the problem is reduced to Eq (67) the problem will be considered solved. At that point, the remaining transcendental equation may be solved with the aid of the computer.

Before illustrating the use of the model the following important rules for determining the total attenuation coefficient are reiterated:

(1) In rain, the total attenuation coefficient is the sum of the molecular absorption coefficient, the aerosol attenuation coefficient, and the rain attenuation coefficient;

(2) In fogs, the total attenuation coefficient is the sum of the molecular absorption coefficient and the fog attenuation coefficient;

(3) In clouds, the total attenuation coefficient is the sum of the molecular absorption coefficient and the cloud attenuation coefficient; and

(4) In air with no precipitation falling, the total attenuation coefficient is the sum of the molecular absorption coefficient and the aerosol attenuation coefficient.

The following summary of important tables and equations is also provided:

(1) Table XXIV provides the molecular absorption coefficients;

(2) Table XXVIII provides the aerosol attenuation coefficients for the background air mass;

(3) Eq (45) provides the aerosol attenuation coefficient for the boundary layer;

(4) Table XVI provides the attenuation coefficients for rain as a function of source mechanisms and reported rain category.

(5) The attenuation coefficient of fog is calculated from Eq (56) or determined from Table XVII; and

(6) The attenuation coefficient of clouds is found in Table XVII.

Consider now the following example: The laser designator is at an altitude of 2 km at a look angle of 30° . The designator is

Table XXVIII
 Aerosol Attenuation Coefficients
 for 1.0636 Micron Radiation
 for Vertical Clear Air
 Profile (Meteorological Range
 of 40 KM at Ground Level)

Altitude (km)	Attenuation Coefficient (km ⁻¹)
0	.0523
0 - 1	.0493
1 - 2	.0435*
2 - 3	.0383
3 - 4	.0338
4 - 5	.0299
5 - 6	.0263
6 - 7	.0232
7 - 8	.0205

*Average Attenuation Coefficient from 1.5 km to 2 km is .0421 km⁻¹.
 However, since the value is used for only 1/2 km then the value to
 be used in the vertical summation is .0211 km.

illuminating the target through a summer afternoon haze where the reported visibility is 5 km. The boundary layer extends from ground level to 1.5 km. The receiver is located at an altitude of 6 km and at a 40° look angle where the term look angle refers to the angle between the vertical (zenith) and line of vision connecting target to receiver or designator.

First, let us calculate the atmospheric transmission for the designator. Table XXIV yields the vertical molecular absorption optical path (for summer) of .04237. Caution should be exercised when summing coefficients from the tables so that the zero altitude value is not included in the sum. Next, the boundary layer aerosol attenuation is given by Eq (45) as $.3165 \text{ km}^{-1}$. This value times the extent of the boundary layer of 1.5 km plus the average clear air value from 1.5 km to 2 km yields the vertical aerosol optical path of 0.4959. Since there are no clouds or precipitation then the optical depth of the designator becomes .5382 times secant (30°). Then the right hand side (R.H.S.) of the laser range equation becomes

$$\text{R.H.S.} = (6.7 \times 10^9 \text{m}^2) e^{-.6215} \quad (68)$$

The receiver optical depth is computed in like manner. The vertical molecular absorption optical depth is .0989. The vertical aerosol attenuation optical depth is .62415. The total vertical optical depth is then .72305 and the total receiver optical depth becomes .72305 times secant (40°). The left hand side of the laser range equation becomes

$$\text{L.H.S.} = (7832.4m)^2 e^{.9439} \quad (69)$$

Since the laser range equation is a transcendental equation then these values must be checked to ascertain if this is a solution or if the receiver is outside range. This can best be done with the aid of a computer.